



UNIVERSITÀ DEGLI STUDI DI PAVIA
DOTTORATO IN SCIENZE CHIMICHE
E FARMACEUTICHE
XXX CICLO

Coordinatore: Chiar.mo Prof. Mauro Freccero

TECHNOLOGICAL PLATFORMS
CONTAINING NATURAL
COMPOUNDS TO MAINTAIN AND
RESTORE TISSUE INTEGRITY

Tutore

Chiar.ma Prof. ssa Giuseppina Sandri

Co-tutore

Chiar.ma Prof. ssa Maria Cristina Bonferoni

Tesi di Dottorato di

FRANCESCA SAPORITO

a.a. 2016- 2017

SUMMARY

Premise	1
Introduction-part I.....	7
1 WOUNDS.....	8
1.1 Wound infections	8
1.2 Bleeding	9
2 WOUND HEALING	9
2.1 Hemostasis	10
2.2 Inflammation.....	11
2.3 Proliferation	11
2.4 Remodeling.....	12
3 WOUND MANAGEMENT	12
3.1 Wound dressings.....	12
3.1.1 Traditional systems	13
3.1.2 Modern wound systems.....	13
4 REFERENCES	15
Chapter 1	17
1.1 ABSTRACT	18
1.2 INTRODUCTION.....	19
1.3 EXPERIMENTAL PART	22
1.3.1 Materials.....	22
1.3.2 Methods.....	22
1.3.2.1 Sponge-like dressing preparation	22
1.3.2.2 Sponge-like dressing characterization.....	24
1.3.2.2.1 Penetrometry measurements.....	24
1.3.2.2.2 Hydration measurements	24
1.3.2.2.3 Bioadhesion measurements	24
1.3.2.2.4 Morphology	26
1.3.2.2.5 FT-IR measurements	26
1.3.2.2.6 TA release measurements.....	26
1.3.2.2.7 In vitro dynamic whole-blood clotting	27
1.3.2.2.8 In vitro biocompatibility and proliferation	28
1.3.2.2.9 Ex vivo proliferation on human skin biopsy	29

1.3.2.2.10 Statistical analysis	30
1.4 RESULTS AND DISCUSSION.....	31
1.4.1 Sponge-like dressing technological properties	31
1.4.1.1 Mechanical properties	31
1.4.1.2 Hydration properties.....	33
1.4.1.3 Bioadhesion properties	37
1.4.1.4 Morphology	40
1.4.1.5 FT-IR analysis	43
1.4.1.6 In vitro drug release properties.....	44
1.4.2 Sponge-like dressing biopharmaceutical properties	46
1.4.2.1 In vitro dynamic whole-blood clotting.....	46
1.4.2.2. In vitro biocompatibility and proliferation.....	48
1.5 CONCLUSIONS	51
1.6 REFERENCES	53
Chapter 2	59
2.1 ABSTRACT	60
2.2 INTRODUCTION	61
2.3 EXPERIMENTAL PART	64
2.3.1 Materials	64
2.3.2 Methods	64
2.3.2.1 Lipid nanoparticle preparation	64
2.3.2.2 Lipid nanoparticle characterization.....	65
2.3.2.2.1 Physical-chemical properties	65
2.3.2.2.2 Eucalyptus essential oil assay.....	66
2.3.2.2.3 Bioadhesion measurements	66
2.3.2.3 In vitro biocompatibility	67
2.3.2.3.1 Cytotoxicity test.....	67
2.3.2.3.2 Proliferation test	68
2.3.2.3.3 Cell migration/proliferation assay for wound healing	69
2.3.2.4 Antimicrobial properties	70
2.3.2.5 In vivo wound healing efficacy in rat model.....	71
2.3.2.6 Histological analysis	71
2.3.2.7 Statistical analysis	72
2.4 RESULTS AND DISCUSSION.....	73
2.4.1 Physical-chemical characterization of nanoparticles	73

2.4.2 Bioadhesion properties	74
2.4.3 In vitro biocompatibility properties	76
2.4.4 Proliferation properties	77
2.4.5 Cell migration/proliferation properties in an <i>in vitro</i> wound healing test	78
2.4.6 In vitro characterization of NLCo/e	82
2.4.7 In vivo wound healing efficacy of NLC o/e	83
2.5 CONCLUSIONS	87
2.6 REFERENCES	88
Introduction-part II	92
1 THE HEART	93
2. MYOCARDIAL INFARCTION	94
2.1 Pathophysiology.....	95
2.2 Tissue repair after MI.....	96
3. MYOCARDIAL TISSUE ENGINEERING	98
3.1 Cell therapy.....	100
3.1.1 Cell types used in myocardial tissue engineering	101
3.2 Polymers used in cardiac tissue repair	102
3.3 Strategies for tissue engineering cardiac constructs	104
3.3.1 Preformed scaffolds.....	104
3.3.2 Scaffoldless cell sheets.....	105
3.3.3 Injectable hydrogels	106
4 ELECTROSPINNING TECNIQUE	107
4.1 Effecting parameters on electrospinning process	108
4.1.1 Solution parameters.....	108
4.1.1.1 Concentration	108
4.1.1.2 Molecular weight.....	108
4.1.1.3 Viscosity	108
4.1.1.4 Surface tension	109
4.1.1.5 Conductivity	109
4.1.2 Processing parameters	109
4.1.2.1 Applied voltage	109
4.1.2.2 Feed rate/flow rate	110
4.1.2.3 Distance between needle and collector.....	110
Chapter 3	118
3.1 ABSTRACT	119

3.2 INTRODUCTION	120
3.3 EXPERIMENTAL PART	123
3.3.1 Materials	123
3.3.2 Methods	123
3.3.2.1 Preparation of polymeric solutions	123
3.3.2.2 Determination of the gelation properties.....	124
3.3.2.2.1 Rheological measurements	124
3.3.2.2.2 Penetrometry.....	124
3.3.2.2.3 Injectability properties	125
3.3.2.3 In vitro tests.....	125
3.3.2.3.1 Fetal cardiomyocytes and cardiac fibroblasts isolation.....	125
3.3.2.3.2 Biocompatibility properties of the formulations	126
3.3.2.3.3 Evaluation of the optimal conditions to simulate the oxidative damage. 126	
3.3.2.3.4 Evaluation of cardiac cell survival after oxidative damage and treatment with formulations.....	127
3.3.2.3.5 Live dead assay.....	127
3.3.2.3.6 Fluorescence microscopy analysis of the cell substrates.....	128
3.3.2.3.7 Statistical analysis	129
3.4 RESULTS AND DISCUSSION	130
3.4.1 Gelation properties of the systems.....	130
3.4.2 Injectability properties	132
3.4.3 In vitro tests	133
3.4.3.1 Biocompatibility properties of the formulations	133
3.4.3.2 Oxidative damage.....	138
3.4.3.3 Cardiac cell survival after oxidative damage and treatment with formulations	139
3.5 CONCLUSIONS	145
3.6 REFERENCES	146
Chapter 4	149
4.1 ABSTRACT	150
4.2 INTRODUCTION	151
4.3 EXPERIMENTAL PART	154
4.3.1 Materials	154
4.3.2 Methods	154
4.3.2.1 Preparation of polymeric solutions	154

4.3.2.2 Rheological measurements.....	155
4.3.2.3 Physical properties of the solutions.....	155
4.3.2.3.1 Surface tension	155
4.3.2.3.2 Conductivity	155
4.3.2.4 Preparation of electrospun scaffolds	155
4.3.2.5 Nanofibers characterizations	156
4.3.2.5.1 SEM analysis	156
4.3.2.5.2 FT-IR analysis	156
4.3.2.5.3 Mechanical properties	156
4.3.2.6 In vitro adhesion and proliferation assay: fibroblasts and endothelial cells ..	157
4.3.2.6.1 MTT test	157
4.3.2.6.2 SEM analysis	158
4.3.2.6.3 CLSM analysis	158
4.3.2.7 In vitro adhesion and proliferation assay: cardiac cells	158
4.3.2.7.1 CLSM analysis	159
4.3.2.8 Statistical analysis	160
4.4 RESULTS AND DISCUSSION.....	161
4.4.1 Characterization of polymeric solutions	161
4.4.2 Characterization of nanofibrous scaffolds	163
4.4.3 In vitro adhesion and proliferation assay: fibroblasts and endothelial cells	168
4.4.4 In vitro adhesion and proliferation assay: cardiac cells	172
4.5 CONCLUSIONS	177
4.6 REFERENCES	179
Conclusions	183
Acknowledgements	186

Premise

Premise

Tissue-repairing is one of the most important challenge of these years. Many studies aimed to understand how to improve tissue healing after traumatic, infective and degenerative diseases, have been conducted. Healing is usually a result of the combination between regeneration and scar formation. When the balance between collagen deposition and degradation on the scar is altered, fibrosis and chronic inflammation occur. In order to restore the physiologic function of damaged tissues and the orchestrated process of wound healing, new therapeutic approaches have been developed all over the years [Caramella et. al, 2016].

The aim of this PhD research project was the development of multifunctional therapeutic platforms to restore tissue integrity. Two different targets were considered as topics: 1) skin: acute wounds with massive bleeding and non-healing cutaneous lesions as chronic wounds and severe burns, 2) heart: myocardial infarction.

Chapter 1 focuses on the development of chitosan (CH) – glycosaminoglycan (GAG, Hyaluronic acid, HA; Chondroitin sulfate, CS) based dressings loaded Tranexamic acid (TA), to be used in case of massive bleeding. TA is an antifibrinolytic drug analog of the aminoacid lysine, which explains its function by blocking lysine sites on plasminogen molecules [Ker et al., 2012]. CH is a polysaccharide able to enhance coagulation and stabilize the clot structure [Hoemann et al., 2007]. The association of CH with TA allowed to obtain a synergic effect to speed up clotting formation. Dressings were prepared by freeze-drying, by adding mannitol or glycerol as lyoprotectant agents, and characterized in terms of mechanical and biopharmaceutical properties. Penetrometry measurements showed that the presence of HA in the dressings caused an increment in the mechanical resistance, while CS did not significantly influence stiffness of the dressings, probably for the interaction between CS, negatively charged, and CH.

The formation of a polyelectrolyte complex between CH and GAG decreased hydration properties of the systems, probably due to CH gelation, while enhanced dressing bioadhesive properties, important to favor a prolonged contact between wound dressing and lesion. TA release study showed a fast viability of the drug to allow procoagulant functions as quickly as possible. The hemostatic performance of the dressings, evaluated by means of a dynamic whole-blood clotting test, reported a

faster clot formation in presence of all the dressings loaded TA than that of the only blood. In vitro evaluation on fibroblasts and ex-vivo studies on human skin evidenced that the developed dressings are promising to enhance cell proliferation.

Chapter 2 focuses on the development of solid lipid nanoparticles (SLN) and nanostructured lipid carriers (NLC) based on cocoa butter, as solid lipid, and olive oil or sesame oil, as liquid lipids, loaded with eucalyptus or rosemary oils as medical devices to enhance wound healing of chronic wounds and severe burns by preventing resistant microbial infections. The systems were prepared by means of high shear homogenization and ultrasound method. Nanoparticles particle size ranged from 220 and 300 nm and remained stable up to 3 months storage. NLC showed higher bioadhesive properties than SLN, probably due to their higher flexibility that allowed a bioadhesive joint formation. Cytotoxicity and proliferation assays towards normal human dermal fibroblasts (NHDFs) reported a higher cell proliferation for NLC based on olive oil and loaded eucalyptus essential oil. These results were confirmed by an in vitro wound healing test, associated to a Bromodeoxyuridine assay, that showed as NLC based on olive oil and eucalyptus essential oil allowed a complete gap closure within 48 h, presenting a higher cell density if compared to standard growth conditions (only growth medium). Finally, the in vivo murine burn model allowed to obtain a proof of concept of efficacy and safety of NLC based on olive oil and eucalyptus oil.

Chapter 3 focuses on the development of injectable hydrogel scaffolds based on in situ gelling systems to release Platelet lysate (PL) in the treatment of myocardial infarction. PL is a hemoderivative derived from platelet lysis rich in growth factors (PDGF, TGF- β , platelet derived epidermal growth factor, epidermal growth factor, VEGF, FGF, IGF, IL-8, TNF- α) involved in tissue regeneration [Sandri et al., 2014; Rossi et al., 2015].

In situ thermosensitive gelling systems were prepared by using Poloxamer 407 (P407), a copolymer having a transition temperature between 30 and 37 °C [Dumortier et al., 2006]. In situ ion-dependent gelling systems were prepared by using Sodium alginate (Alg), that undergoes gelation in presence of divalent cations, such as Ca²⁺ [Van Tomme et al., 2008]. Both polymers were associated to

Chondroitin sulfate (CS), a sulfate negatively charged polymer able to interact with positively charged molecules, such as growth factors. Formulations were characterized in terms of mechanical properties, by means of penetrometry and siringability tests. Rheological measurements allowed to evaluate gelation temperature of the formulations, that resulted optimal for obtaining handle systems characterized by low viscosity values before the administration and that go through gelation once into the infarcted site. Furthermore, *in vitro* assays towards cardiomyocytes (CMCs) and cardiac fibroblasts (CFs) isolated from heart fetal rats were performed to evaluate the ability of the developed systems to improve CMCs survival after infarction. To reproduce the oxidative damage that usually occurs after an infarcted event, cardiac cells were put in contact with two different (0.05 and 0.25 mM) H₂O₂ concentrations for different times (30-45-90 minutes). A live/dead assay allowed to choose the right H₂O₂ concentration and contact time able to induce 50% cell viability. Cell survival was evaluated after oxidative damage simulation and treatment with the developed formulations.

Chapter 4 focuses on the development of nanofibrous membranes based on gelatin or gelatin in association with Chondroitin sulfate (CS) for the treatment of myocardial infarction, obtained by means of electrospinning technique. Citric acid was added to the formulations to allow polymer cross-linking by heating at 150°C for 2 h to obtain insoluble membranes in physiologic fluids. Scaffolds were characterized by a homogeneous and bead-free structure, as shown by SEM (Scanning Electron Microscope) microphotographs, with fiber diameter ranging from 150 nm to 450 nm, depending on the dried or hydrated state. The contractile function and alignment of cardiac cells depends on the elasticity of the substrate and for this reason mechanical properties of the fiber membranes were evaluated: scaffolds appeared quite stiff in their dried state but highly elastic after hydration. *In vitro* adhesion and proliferation properties of the cells growth onto the supports were evaluated towards two different cell lines, NHDFs (Normal human dermal fibroblasts) and HUVEC (Human umbilical vein endothelial cells). Furthermore, as proof of concept, cardiac cells (cardiomyocytes and cardiac fibroblasts) were isolated from fetus rats. Nanofibrous membranes, in particular gelatin in association with CS based systems, resulted an

optimal substrate for allowing either NHDFs and HUVEC growth and proliferation, as reported by MTT test, SEM and CLSM analysis. Furthermore, gelatin-CS based membranes embedded with platelet lysate allowed mainly cardiomyocytes adhesion and proliferation rather than cardiac fibroblasts one. This should reduce in vivo collagen deposition by fibroblasts and the consequent formation of an extended non contractile scar tissue around the infarcted area which leads to the development of cardiomyopathies.

REFERENCES

- Caramella, C., Conti, B., Modena, T., Ferrari, F., Bonferoni, M. C., Genta, I., Rossi, S., Torre, M. L., Sandri, G., Sorrenti, M., Catenacci, L., Dorati, R., Tripodo, G. (2016). Controlled delivery systems for tissue repair and regeneration. *Journal of Drug Delivery Science and Technology*, 378, 206-228.
- Dumortier, G., Grossiord, G. L., Agnely, F., Chaumeil, J. C. (2006). A Review of Poloxamer 407 Pharmaceutical and Pharmacological Characteristics, *Pharmaceutical Research*, 23, 2709-2728.
- Hoemann, C.D., Sun, J., McKee, M. D., Chevrier, A., Rossomacha, E., Rivard, G. E., Hurtig, M., Buschmann M. D. (2007). Chitosan-glycerol phosphate/blood implants elicit hyaline cartilage repair integrated with porous subchondral bone in microdrilled rabbit defects. *Osteoarthritis Cartilage*, 15, 78-89.
- Ker, K., Edwards, P., Rerei, P., Shakur, H., Roberts, I. (2012). Effect of tranexamic acid on surgical bleeding: systematic review and cumulative meta-analysis. *British Medical Journal*, 17, 344 e 3054.
- Rossi, S., Ferrari, F., Sandri, G., Bonferoni, M.C., Del Fante, C., Perotti, C., Caramella, C. (2015). Wound healing: biopolymers and hemoderivatives, *In: Mshram M (Ed), Encyclopedia of Biomedical Polymers and Biomaterials* 1st ed., vol. 11. *Taylor & Francis*, 8280-8298.
- Sandri, G., Bonferoni, M. C., Rossi, S., Ferrari, F., Mori, M., Cervio, M., Riva, F., Liakos, I, Athanassiou, A., Saporito, F., Marini L. & Caramella, C. (2014). Platelet lysate embedded scaffolds for skin regeneration. *Expert Opinion Drug Delivery*, 12 525-545.
- Van Tomme, S. R., Storm, G., Hennink, W. E. (2008). In situ gelling hydrogels for pharmaceutical and biomedical applications, *International Journal of Pharmaceutics*, 355, 1-18.

Introduction-part I

1 WOUNDS

Although different approaches have been considered to treat lesions, in many cases wounds remain a crucial problem that could lead to early and late complications, causing morbidity and even mortality [Natarajan et al., 2000].

A wound consists of a damage of the normal structure and function of an organ or a tissue [Velnar et al., 2009]. It can derive from pathological processes or from accidental events that result in a disease process.

Depending on different parameters, different wound classifications have been made. Indeed, on the basis of the time of the repair process, acute or chronic wounds can be distinguished. Acute wounds include all tissue injuries that repair by an ordered healing process within 12 weeks. They can include mechanical injuries, caused by the contact between skin and hard surfaces, or can derive from surgical procedures [Robson et al., 2001].

A failure in the normal repairing process, due to infections, excess of exudate and inflammation cytokines, or repeated trauma to the lesion area, leads to chronic wounds. This kind of inflammatory wounds do not heal within 12 weeks and often reoccur [Gurtner et al., 2008].

On the basis of the number of skin layers and area of skin involved, wounds can be classified as: a) superficial (I grade), when the injury is localized to the epidermal surface; b) partial thickness wound, when both epidermis and dermal layers, including blood vessels, gland and hair follicles are involved in the injury; c) full thickness wound, when the damage concerns the subcutaneous fat or deeper tissues [Krasner et al., 1993].

1.1 Wound infections

In most of the open wounds, infections caused by one or more micro-organisms, such as bacteria or fungi, usually occur. Among the most common bacteria affecting wounds and slow down wound healing, there are *Staphylococcus aureus*, *Pseudomonas aeruginosa*, *Streptococcus pyogenes* and some *Clostridium* species

[Bowler et al., 2001]. The presence of micro-organisms into the injured site causes many local and systemic problems: formation of purulent exudate and painful erythema [White et al., 2006]. The importance to speed up wound accelerate healing by means of different strategies is due to the high microbial bioburden that usually appears in chronic wounds. Factors that promote wound infections are hypoxia, ischemia, tissue necrosis and some immunodeficiency [Bowler et al., 2001].

1.2 Bleeding

A severe loss of blood can derive from particular wounds in trauma patients. Uncontrolled bleedings are still one of the main causes of death after trauma [Kauvar et al., 2006] and the control of bleeding represents the most critical step in the management of the injured patients.

The blood coagulation process consists of a series of reactions having as final step the cleavage of prothrombin into thrombin, which leads to the production of fibrin monomer which then polymerizes to form insoluble fibrin. Furthermore, thrombin activates factor XIII which brings to the formation of a resistant clot by means of the formation of covalent bonds between fibrin molecules.

On the contrary, fibrinolysis starts with the activation of plasminogen that binds to lysine residues on the surface of fibrin and is converted in plasmin.

2 WOUND HEALING

Wound healing is a complex dynamic process including various intracellular and intercellular pathways leading to tissue regeneration. Four main interdependent stages are involved in tissue repair: hemostasis, inflammation, proliferation and remodeling [Boateng et al., 2008] (Figure 1).

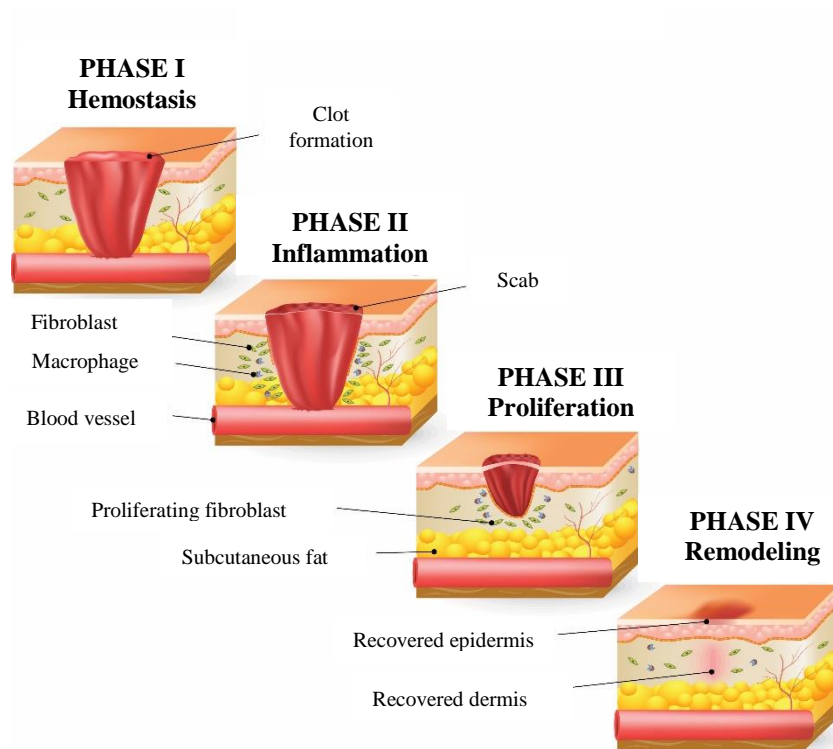


Figure 1: the 4 main stages of wound healing [Maynard, 2015].

2.1 Hemostasis

When a skin injury occurs, bleeding usually takes place in order to remove bacteria and antigens from the wound. Immediately after injury, coagulation and hemostasis occur in the wound [Broughton et al., 2006]. This phase plays an important role during wound healing, since it leads to the formation of a clot in the wound, blocking bleeding and contributing to successful wound healing [Martin, 1997]. The contact between blood components, platelets and exposed collagen brings to the clot formation, composed of fibrin, fibronectin, and other factors [Robson et al., 2001].

An important role in wound healing is played by platelets, containing different growth factors such as platelet derived growth factor (PDGF), transforming growth factor- β (TGF- β), epidermal growth factors and insulin-like growth factors, acting as chemotactic agents. Indeed, these factors activate and attract neutrophils, macrophages, endothelial cells and fibroblasts, resulting in the following inflammatory phase [Richardson, 2004].

2.2 Inflammation

The inflammatory phase takes place almost simultaneously with hemostasis and can be distinguished into two phases: early and late inflammatory response [Hart, 2002]. Within 24-36 h after injury, neutrophils start to be attracted to the injury site and show their phagocytosis ability, aiming to remove bacteria and damaged tissue, therefore to prevent infections [Broughton et al, 2006]. Once the bacteria have been removed from the injury site, neutrophil activity starts to change until they are eliminated from the wound, in order to proceed with the next wound healing phase. Approximately 48-72 h after injury, the phagocytosis process is continued by macrophages that invade wound site and secrete chemokines and cytokines [Attinger et al., 2006].

Finally, the last cells to invade the wound site during the late inflammatory phase are lymphocytes, attracted by interleukin-1 (IL-1) and immunoglobulin G (IgG) products, necessary for collagenase regulation.

2.3 Proliferation

The proliferative phase occurs between 3-15 days after injury and provide the formation of abundant granulation tissue. Different processes occur during this phase. Fibroblasts migrate into the wound, attracted by growth factors, and there they start to proliferate in order to produce matrix proteins. Hyaluronan, fibronectin, proteoglycans and procollagen lead to the formation of extracellular matrix, an important support for cell migration [Ramasastry et al., 2005]. One of the most important component of the extracellular matrix is collagen, produced by fibroblasts, which plays a key role during the proliferative and remodeling phases of wound healing [Baum and Arpey, 2005].

Angiogenesis, the new blood vessels formation, takes place during all phases of the reparative process, promoted by different angiogenic factors secreted during hemostatic stage. Growth and proliferation of endothelial cells are stimulated by molecules secreted under hypoxic conditions.

2.4 Remodeling

Remodeling phase of wound healing involves the development of new tissue and the final scar formation. During this phase, the tensile strength of the wound increases by the replacement of collagen type III with type I, more resistant. A continuous remodeling between collagen deposition and degradation takes place during the remodeling phase, until an equilibrium is reached about 3 weeks after injury [Clark, 1993]. At this step, fibroblasts and macrophages density is reduced, the growth of capillaries decreases and the formation of a stiff scar, poor either in cell number and in blood vessels occurs [O’Kane, 2002].

3 WOUND MANAGEMENT

Several precautions are necessary for achieve a successful wound healing, the removal of necrotic tissue and other material from the injured area is one of this. This process is named debridement and is necessary to reduce the risk of infection and the duration time of the inflammatory phase. Wound debridement can be obtained by surgical removal, autolytic or enzymatic removal, using dressings.

3.1 Wound dressings

Many wound dressings have been developed all over the years, starting from the simple use of medical herbs to the use of engineered constructs. They were firstly developed as protection against wound contamination and nowadays they can act as platforms to deliver biomolecules to the injured site [Jones et al., 2006].

Different classifications of wound dressings can be obtained considering their function (antibacterial, absorbent, occlusive, debridement), the type of material used for their production (alginate, collagen, hydrocolloid), and their physical form [Eccleston, 2007]. Another classification includes traditional and modern wound dressings.

3.1.1 Traditional systems

Category of traditional systems include liquid (solutions, suspensions ad emulsions) and semi-solid (creams) preparations, as well as traditional dressings. Liquid solutions are usually applied onto the wounds in the initial stage of wound healing in order to reduce bacterial contamination, or as debriding agents. Typical liquid traditional formulations are silver, as antimicrobial agent, or saline solution, used to wet dry wounds during dressing changes. The problem connected to the use of topical agents in the form of liquid or semi-solid systems is the short residence time on the wound site. For this reason, they have been substituted by dressings.

Traditional dressings are usually made from woven and nonwoven fibers of cotton, polyester or a combination of the two materials. They are used as sterile gauzes to protect open wounds from bacterial contamination and to absorb exudate. They need to be changed systematically to avoid laceration of the tissue [Harding et al., 2000]. One of the disadvantages of gauze dressings is that they become more adherent while the exudate decreases, causing pain to the patient during the dressing removal. This is also due to the moisture evaporation caused by their occlusion properties. [Chang et al., 1998].

3.1.2 Modern wound systems

To overcome the problems related to the traditional dressings, modern systems have been developed. They have the ability to preserve the moisture into the wound allowing wound healing. The main characterization of modern dressings is based on the materials selected for their production: hydrocolloids, alginates and hydrogels.

Hydrocolloid dressings

Hydrocolloidal dressings include the systems obtained from the combination between colloidal agents and other materials such as elastomers. Among these we can find gelatin and carboxymethylcellulose. When applied onto the wounds, hydrocolloid

dressings are impermeable to water and change their physical state becoming a gel permeable to water after the absorption of wound exudate. One of the advantages of hydrocolloid dressings is that they do not cause pain during the removal, therefore they result particularly useful for the management of both acute and chronic wounds [Thomas, 1992].

Alginate dressings

Alginic acid is a polysaccharide composed by mannuronic and glucuronic acid units. The formation of gels on the wounds starting from the sodium salt of alginic acid is due to the crosslinking with the calcium ions present in exudate and blood. The resulting strong hydrophilic gel allows a high exudate absorption, with the consequent reduction in wound secretion and bacterial contamination. Furthermore, alginate gels could stay on the wound longer than the hydrocolloids, also helping fibroblasts proliferation and migration. The main disadvantage of alginate dressings is that they need moisture to explain their function, therefore they cannot be used for dry wounds [Boateng et al., 2008].

Hydrogel dressings

Hydrogels represent a good choice for enhancing wound healing. They are hydrophilic insoluble material, applied either as a gel or as solid sheet or film, able to absorb high volumes of water after the application on the wound. If applied as gels, they need to be protected with a gauze. They are non-irritant, permeable to metabolites and allow the moisture of the wound; all of these advantages increase patient compliance [Boateng et al., 2008].

4 REFERENCES

- Attinger, C. E., Janis, J. E., Steinberg, J. (2006). Clinical approach to wounds: debridement and wound bed preparation including the use of dressings and wound-healing adjuvants. *Plastic Reconstruction Surgery* 117, 72S–109S.
- Baum, C. L., Arpey, C. J. (2005). Normal cutaneous wound healing: clinical correlation with cellular and molecular events. *Dermatologic Surgery*, 31, 674–686.
- Boateng, J. S., Matthewes, K. H., Stevens, H. N. E., Eccleston, G. M. (2008). Wound Healing Dressings and Drug Delivery Systems: A Review. *Journal of Pharmaceutical Sciences*, 97, 2892–2923.
- Bowler, P. G., Duerden, B. I., Armstrong, D. G. (2001). Wound microbiology and associated approaches to wound management. *Clinical Microbiology Reviews* 14, 244–269.
- Broughton, G., Janis, J. E., Attinger, C. E. (2006). The basic science of wound healing. *Plastic Reconstruction Surgery*, 117, 12S–34S.
- Chang, K. W., Alagoof, S., Ong, K. T., Sim, P. H. (1998). Pressure ulcers—randomised controlled trial comparing hydrocolloid and saline gauze dressings. *Medical Journal Malaysia*, 53, 428–431.
- Clark, R. A. Regulation of fibroplasia in cutaneous wound repair. (1993). *The American Journal of the Medical Sciences*, 306, 2–48.
- Eccleston, G. M. (2007). Wound dressings. In: Aulton ME, editor. *Pharmaceutics: The science of dosage form design*. 3rd edition. UK: Churchill Livingstone. 264–271.
- Gurtner, G. C., Werner, S., Barrandon, Y., Longaker, M. T. (2008). Wound repair and regeneration. *Nature*, 453, 314–321.
- Harding, K., Cutting, K., Price, P. (2000). The cost effectiveness of wound management protocols of care. *British Journal of Nursing*, 9, S6–S10.
- Hart, J: (2002). Inflammation. 1: its role in the healing of acute wounds. *Journal of Wound Care*; 11, 205 – 209.
- Jones, V., Grey, J. E., Harding, K. G. (2006). Wound dressings. *British Medical Journal*, 332, 777–780.

- Kauvar, D. S., Lefering, R., Wade, C. E. (2006). Impact of hemorrhage on trauma outcome: an overview of epidemiology, clinical presentations, and therapeutic considerations. *Journal Trauma*, 60, S3eS11.
- Krasner, D., Kennedy, K. L., Rolstad, B. S., Roma, A.W. (1993). The ABCs of wound care dressings. *Ostomy Wound Manage* 39, 66, 68–69, 72 passim.
- Martin, P. (1997). Wound healing—Aiming for perfect skin regeneration. *Science* 276, 75–81.
- Maynard, J (2015) How wounds heal: the 4 main phases of wound healing. *Shield health care*. Wound community.
- Natarajan, S., Williamson D., Stiltz, A. J., Harding, K. (2000). Advances in wound care and healing technology. *American Journal of Clinical Dermatology*, 1, 269-275.
- O’Kane, S. (2002). Wound remodelling and scarring. *Journal of Wound Care*, 11, 296–299.
- Ramasasthy, S. S. (2005). Acute wounds. *Clinics in Plastic Surgery*, 32, 195–208.
- Richardson, M. (2004). Acute wounds: an overview of the physiological healing process. *Nursing Times*; 100, 50–53.
- Robson, M. C., Steed, D. L., Franz, M. G. (2001). Wound healing: biologic features and approaches to maximize healing trajectories. *Current Problems in Surgery*, 38, 72–140.
- Thomas, S. (1992). Hydrocolloids. *Journal of Wound Care*, 1, 27–30.
- Velnar, T., Bailey, T., Smrkolj, V. (2009). The wound healing process: An overview of the cellular and molecular mechanisms. *Journal of International Medical Research*, 37, 1528–1542.
- White, R. J., Cutting, K., Kingsley, A. (2006). Topical antimicrobials in the control of wound bioburden. *Ostomy Wound Manage*, 52, 26–58.

Chapter 1

Freeze dried chitosan acetate dressings with glycosaminoglycans and tranexamic acid

*Saporito, F., Sandri, G., Rossi, S., Bonferoni, M.C., Riva, F., Caramella, C.,
Ferrari, F.*

Carbohydrate Polymers (2018), 184, 408-417

Corresponding author: Giuseppina Sandri

1.1 ABSTRACT

Bleeding control plays an important role to increase survival in the early phase after a traumatic event.

The aim of the present work was the development of hemostatic sponge-like dressings based on chitosan, in association with glycosaminoglycans (GAG as chondroitin sulfate or hyaluronic acid) and the improvement of their hemostatic performance by loading tranexamic acid (TA). The dressings were prepared by lyophilization and were characterized for mechanical, hydration, bioadhesion properties and morphology. Moreover, FTIR analysis was performed to understand the interactions between the different polyelectrolytes present in the dressing. Clotting was investigated *in vitro* by using rat whole blood. Moreover *in vitro* biocompatibility and proliferation were evaluated towards fibroblasts. *Ex vivo* proliferation properties were assessed by using human skin.

All the dressings were characterized by mechanical, hydration and bioadhesion properties suitable to be applied on bleeding wounds and to absorb bleeding or wound exudate, avoiding tissue dehydration. TA release was fast, and TA and chitosan showed a synergic effect to speed up clotting. The dressings were biocompatible and able to sustain cell proliferation *in vitro* and *ex vivo* in human epidermis. In conclusion, sponge-like dressings based on chitosan and GAG and loaded with TA are an effective tool to enhance hemostasis and healing in bleeding wounds.

1.2 INTRODUCTION

Since 2001 (at the beginning of Afghanistan and Iraq military conflicts), many medical advances in military trauma care have been made to decrease morbidity and mortality and in particular, efforts have been made to control internal and external hemorrhage. However massive bleeding remains the leading cause of combat death and the second leading cause of death after traumatic brain injury in the civilian sector (Bennet, 2017; Champion, Bellamy, Roberts and Leppaniemi, 2003). Moreover, in surgery, the reduction of bleeding can positively influence patient's prognosis (Li et al., 2016). Thus, bleeding control plays an important role not only to increase survival but also to prevent the development of multiple organ failure in the early phase after a traumatic event (Shields and Crowley, 2014).

Advanced topical hemostatic devices (including bandages, fibrin glue, liquids, powders, gels, and scaffolds – generally referred to as dressings) have been developed to control hemorrhages, to reduce mortality and prevent further complications (Seon, Lee, Kwon, Kim, et al., 2017). These dressings can be grouped into three classes by mechanism of action: including blood factor concentrators, which concentrate blood cellular and protein components to promote clot formation, bioadhesive agents having strong adherence to tissues and, procoagulant supplementary, which provide local concentration of procoagulat blood factors (Granville-Chapman, Jacobs, and Midwinter, 2011). Furthermore, dressings cover wounds preventing risk of infections (Seon et al., 2017).

Many types of natural polysaccharides have proposed as dressing biomaterials. In particular, chitosan (CH), a linear cationic polysaccharide based on glucosamine and N-acetyl glucosamine, obtained by partial chitin deacetylation, is well known as hemostatic agent. CH is able to enhance coagulation, by both hemagglutination and promoting platelet activation. In presence of blood, CH forms a solid clot due to thrombin and platelet activation, fibrin polymerization and fibrin fibers cross linking by FXIIIa (Marchand, Rivard, Sun, and Hoemann; 2009; Iliescu, Hoemann, Shive, Chenite et al., 2008) and CH is able to stabilize clot structure preventing its lysis (Hoemann et al., 2007). Moreover, it possesses other crucial properties fundamental

in wound healing: it is biodegradable and characterized by antimicrobial properties. Furthermore, CH supports extracellular matrix regeneration stimulating granulation tissue formation, activating fibroblasts (Francesko and Tzanov, 2011) and enhancing their proliferation and migration (Sandri et al., 2011) in the early phases of healing. Moreover, it is able to enhance remodeling process increasing also angiogenesis.

Glycosaminoglycans (GAGs) play a crucial role in different stages of skin tissue regeneration and maturation, being important components of its extracellular matrix (ECM). Moreover, GAGs are able to bind proteins including several chemokines and growth factors. The polysaccharidic structure of glycosaminoglycans as well as the presence, position and number of sulfate groups within the polymer chain plays an important role on these GAG-protein interactions. Among glycosaminoglycans, chondroitin sulfate (CS) and hyaluronic acid (HA), are naturally present in mammals and have an important role in the healing process.

CS is a sulfated polysaccharide based on N-acetylgalactosamine-glucuronic acid disaccharide units. It is able to interact with different important positively charged biological molecules, such as growth factors, chemokines, cytokines and adhesion molecules, involved in tissue healing and it prolongs their activities by charge-charge interactions, avoiding their enzymatic degradation (Silbert and Sugumaran, 2002; Yamada and Sugahara, 2008). HA is a linear polysaccharide composed of a dimeric repeating unit of D-glucuronic acid and N-acetyl-D-glucosamine and, during the tissue injuries, it takes part to the wound healing and coagulation process forming, together with fibrin, a matrix support for fibroblast migration and proliferation (Chen and Abatangelo, 1999; Jiang, Liang and Noble, 2007).

The polysaccharides based systems should be more biocompatible rather than protein ones. In particular Collagen, one of the major components of ECM seems the best candidate to obtain dressings/scaffolds for wound reparation but in literature it is reported as immunogenic material due to possible helical- recognition by antibodies, due to 3D intact triple helix conformation, peculiar aminoacid sequence able to start antibody recognition, presence of non-helical terminal regions (telopeptides) (Lynn, Yannas and Bonfield, 2004; Olsen, Yang, Bodo, Chang et al., 2003). Moreover, it

could have concerns of species-to-species transmissible diseases (xenozoonoses) (Cataldo, Ursini, Lilla and Angelini, 2008).

Given these premises, the aim of the present work was the development of hemostatic sponge-like dressings based on chitosan (CH), in association with chondroitin sulfate (CS) and hyaluronic acid (HA) and loaded with tranexamic acid (TA), to be used in case of massive bleeding.

Tranexamic acid (TA) is a synthetic derivative of the aminoacid lysine and acts as antifibrinolytic agent by reversibly blocking lysine sites on plasminogen molecules (Dunn and Goa, 1999). In particular, TA is able to inhibit fibrinolysis by displacing plasminogen from fibrin and by avoiding its degradation (Ker, Edwards, Rerei, Shakur and Roberts, 2012).

Sponge-like dressings should have advantages in application with respect to powdery hemostatic agents, especially in the treatment of intra-abdominal solid organ bleedings or injuries: if hemostatic agents are based on granules (microparticles) can leave residue in the lumen of the vessel and may occlude distal arterial flow. Moreover, intraluminal dissemination of the clot, resulting in distal thrombosis, may occur (Khoshmohabat, Paydar, Kazemi and Dalfardi, 2016).

TA loaded sponge-like dressings were prepared by freeze-drying and were characterized by hydration, mechanical, bioadhesion properties and morphology. Moreover, FTIR analysis was performed to understand the interactions between the different polyelectrolytes present in the dressing. The release profile of TA was evaluated in isotonic solution (NaCl 0.9%) by using Franz diffusion cells. The hemostatic performance of the systems was evaluated by means of a dynamic whole-blood clotting test. Furthermore, *in vitro* cytocompatibility and proliferation tests were assessed by using NHDFs (normal human dermal fibroblasts from juvenile foreskin). Finally, proliferation properties of TA loaded sponge-like dressings were evaluated by means of an *ex-vivo* test on human skin.

1.3 EXPERIMENTAL PART

1.3.1 Materials

The following materials were used: Chitosan (CH) low MW 251000 Da, deacetylation degree 98%, maximum charge density: number of positively charged functional groups per repeated unit: 0.98 (ChitoClear, Siiiglufjordur-Iceland); Hyaluronic Acid (HA) low MW 212000 Da; maximum charge density: number of negatively charged functional groups per repeated unit: 0.5 (Bioiberica, Barenz, Italy); Chondroitin sodium sulfate bovine 100 EP (CS) low MW 14000 Da, mixture of A (chondroitin 4 sulfate) and C (chondroitin 6 sulfate); maximum charge density: number of negatively charged functional groups per repeated unit: 1 (Bioiberica, Barenz, Italy); Trans-4 (amino-methyl) cyclohexanecarboxylic acid (Sigma Aldrich, Milan-Italy); Glycerol (g) 30° Be (Carlo Erba, Italy); D-Mannitol (Fluka, France).

1.3.2 Methods

1.3.2.1 Sponge-like dressing preparation

CH was hydrated in acetic acid 1% w/w (glacial acetic acid, Sigma Aldrich, Italy) under gentle stirring at room temperature. Acetate was used as counterion to obtain chitosan salification in mild pH conditions and it was preferred to hydrochloric acid because chitosan fragmentation could occur in HCl environment also at low molarity (Sabnis, Block, 2000).

HA and CS were hydrated in distilled water under gentle stirring at room temperature. The two polymeric solutions were mixed 1:1 weight ratio to obtain polymeric mixtures. Systems containing CH alone were mixed 1:1 weight ratio with bidistilled water. Final acetic acid concentration in the polymeric systems was 0.5% (w/w). CH 1 - HA and CH 1 - CS mixtures and CH 1, were subjected to zeta potential evaluation. Measurements were carried out at 25°C by means of a Malvern Zetasizer Nano ZS90 (Malvern Ltd., UK). HA and CS solutions, prepared in the same concentrations used for CH 1 - HA and CH 1 - CS mixtures but without CH were also tested.

In two series of preparations CH 1 - HA and CH 1 - CS mixtures and CH 1, glycerol or mannitol were added as lyoprotectants. Polymeric solutions appeared transparent without visible precipitate. In Table 1 mixture compositions are reported. As for TA loaded systems drug was added to the polymeric mixture at 0.75% (w/w). Two ml of each mixture were poured into each well of 12-well plate (well area 3.8 cm²). In the TA loaded systems the drug was 4 mg/cm². All the polymeric solutions were frozen at -40°C overnight and freeze-dried (Heto 15, Analitica De Mori, I) for 24 h. All the dressings prepared were 5 mm thick (sd ± 0.52). Dressings were re-solubilized in distilled water to check the eventual residues of acetic acid (2 g of distilled water per each dressing). pH of each sample was measured by means of a pHmeter (pH 210 Microprocessor, Hanna Instruments, Italy) and the acetic acid excess was titrated by means of acid-base titration by using phenolphthalein as indicator and NaOH 0.1 M (Carlo Erba, Italy).

Table 1: quali-quantitative composition of polymeric mixture (% w/w) used to prepare sponge-like dressings and their composition (amount/dressing area (mg/cm²)).

	Concentration of polymeric mixture % w/w					Amount/dressing area (mg/cm ²)				
	CH	HA	CS	lyoprotectant		CH	HA	CS	lyoprotectant	
				mannitol	glycerol				mannitol	glycerol
CH 1	1					5				
CH 2	2					10				
CH 1 - m	1			2		5			10.5	
CH 2 - m	2			2		10			10.5	
CH 1 - g	1				0.25	5				1.3
CH 2 - g	2				0.25	10				1.3
CH 1 - HA	1	1				5	5			
CH 1 - CS	1		1			5		5		
CH 1 -HA-m	1	1		2		5	5		10.5	
CH 1 - CS -m	1		1	2		5		5	10.5	
CH 1 - HA - g	1	1			0.25	5	5			1.3
CH 1 - CS - g	1		1		0.25	5		5		1.3

1.3.2.2 Sponge-like dressing characterization

1.3.2.2.1 Penetrometry measurements

Sponge-like dressings were subjected to penetrometry measurements by means of a texture analyzer (TA.XT plus, Stable Microsystems, ENCO, Spinea, I), equipped with a cylinder probe (10 mm, P10), to evaluate the resistance to compression. Each dressing was placed onto the apparatus base and the probe was lowered at 1 mm/s speed. Maximum force of resistance to compression (F_{max}) was determined as the maximum force required to penetrate into the sponge up to 2.5 mm.

1.3.2.2.2 Hydration measurements

Dressings were placed on a 0.45 μm membrane (HA, Millipore, I) that covered a container filled with pH 7.2 phosphate buffer (USP), simulating wound exudate. The liquid could freely cross the membrane dependently of the capability of each system to absorb liquid. At dry state (before the beginning of the hydration test) and at prefixed times during hydration (after the contact between each dressing and the membrane), the dressings were weighted, and the amount of liquid absorbed was normalized by the weight of the dried dressing.

1.3.2.2.3 Bioadhesion measurements

Bioadhesion measurements were performed using texture analyzer (TA.XT plus, Stable Microsystems, ENCO, Spinea, I) equipped with a 1 kg load cell, a cylinder probe having a diameter of 10 mm (P10) and the measuring system A/MUC (mucoadhesion test system) (Sandri, Bonferoni, D'Autilia, Rossi et al., 2013; Szucs, Sandri, Bonferoni, Caramella et al., 2008) (Figure 1). The measuring system A/MUC consists of a support in which a biological substrate can be fixed. In this case, the biological substrate was egg shell membrane (Tao, Lu, Sun, Gu et al., 2009), chosen to mimic damaged skin, wetted with 100 μl of isotonic saline (NaCl 0.9% w/v). To obtain the membrane, the egg shell was placed in a 0.5 M HCl solution for 1h. Sponge

like dressings, having diameter of 10 mm, were stuck with cyanoacrylate glue to the cylinder probe and hydrated with 100 μ l of pH 7.2 phosphate buffer (USP). The sample and the biological substrate were put in contact under a preload of 0.02 N for 3 min. The cylinder probe was then moved upward at a prefixed speed of 2.5 mm/s up to the complete separation of the bioadhesive interface (egg shell membrane-sample). The maximum force of detachment (F_{max}) was recorded as a function of displacement.

Blank measurements were performed by using a filter paper disc wetted with 100 μ l of isotonic saline solution (NaCl 0.9% w/v) instead of biological substrate: this allowed to evaluate cohesive properties of the sample. As comparison, two physical mixtures (CH-HApm and CH-CSpm) having the same polymer composition than sponge-like dressings were evaluate. Moreover, the bioadhesion of CS and HA as powders (CSp and HAp) were compared to understand the contribution of GAG to bioadhesion. In these latter cases, the same experimental conditions (hydration and sample weight) were used.

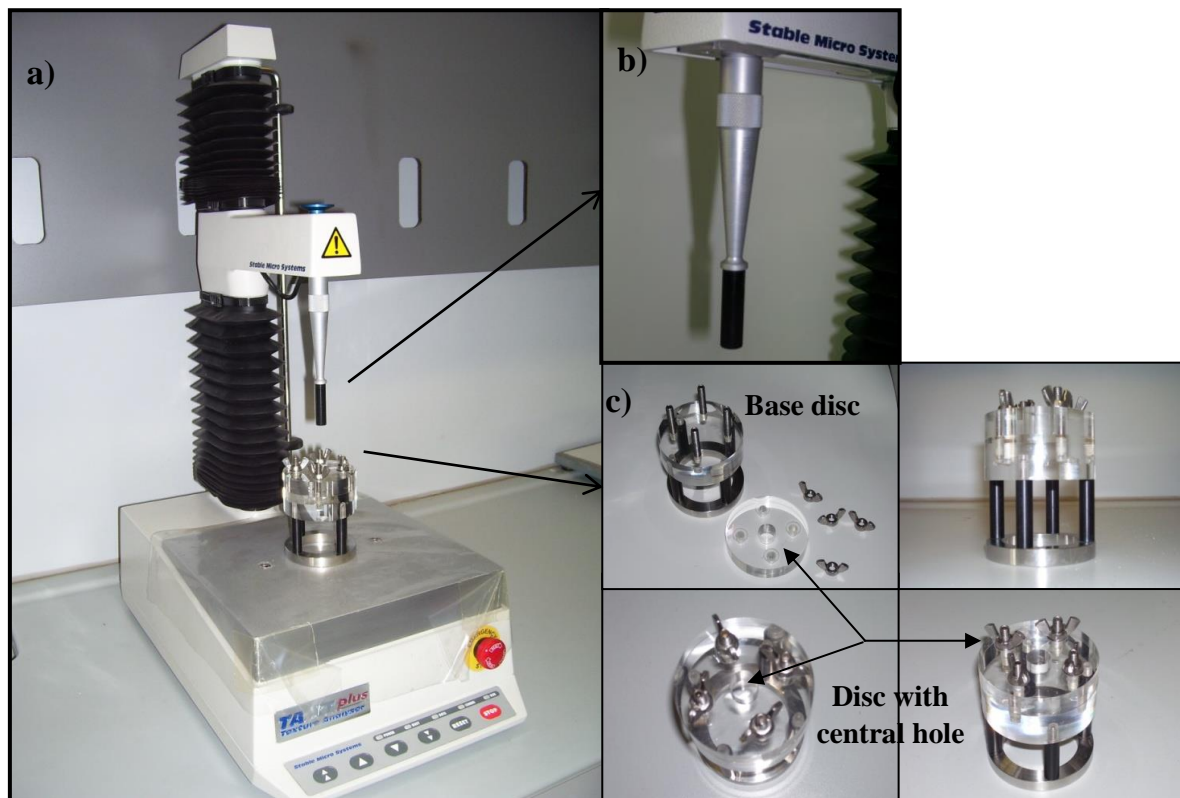


Figure 1: Picture of texture analyzer apparatus (a), consisting of probe (b) and measuring system A/MUC (c) (Sandri, Rossi, Bonferoni, Ferrari et al., 2012, with permission).

1.3.2.2.4 Morphology

Dressing morphology was analyzed by means of scanning electron microscopy (SEM, Tescan, Mira3XMU, ARVEDI Center, University of Pavia). Samples were sputtered by means of graphite deposition under vacuum.

1.3.2.2.5 FT-IR measurements

FT-IR spectra were obtained using a Nicolet FT-IR iS10 Spectrometer (Nicolet, Madison, WI, USA) equipped with ATR (Attenuated Total Reflectance) sampling accessory (Smart iTR with ZnSe plate) by co-adding 256 scans in the 4000–650 cm⁻¹ range at 4 cm⁻¹ resolution.

1.3.2.2.6 TA release measurements

TA release measurements were performed *in vitro* by using Franz cells (vertical glass diffusion cell, orifice diameter 20 mm, PermeGear Inc., USA). A cellulose acetate membrane (pore size 0.45 μm, diameter 25 mm) was placed between the donor and the receptor chambers. The cells were thermostated at 32°C by means of a water jacket. Isotonic solution (NaCl 0.9% w/v) was used as receiving phase. Each dressing was placed in the donor chamber and wetted with 100 μl of isotonic solution. At prefixed times, 500 μl of receiving phase were collected and the amount of drug released was assayed by means of a spectrophotometric method (Ansari, Raza, and Rehman, 2005). This method is based on the colorimetric detection of the Ruhemann's purple resulting from ninhydrin and TA reaction via oxidation deamination of TA primary amino group, followed by the condensation of the reduced ninhydrin in the basic medium at pH 8.0. TA stock solution was prepared in NaCl 0.9 % w/v at 1 mg/ml concentration and a calibration curve was prepared with TA concentrations ranging from 1 mg/ml to 0.1 mg/ml. 1 ml of ninhydrin reagent (0.2 % w/w ninhydrin (Carlo Erba, Milan, I) in methanol) and 0.5 ml of 20 mM phosphate buffer at pH 8.0 were added to 200 μl of each sample. Each sample was heated at 90 °C for 20 min in a shaking bath, subsequently they were cooled at room temperature and their

absorbance was read at 565 nm wavelength (Lamba 25, Perkin Elmer, I). The method was linear in the concentration range from 1 mg/ml to 0.1 mg/ml with R^2 higher than 0.995.

1.3.2.2.7 In vitro dynamic whole-blood clotting

The hemostatic activity of sponge-like dressings was evaluated using rat whole blood pooled from 6 male rats (Wistar 200–250 g). All animal experiments were carried out in full compliance with the standard international ethical guidelines (European Communities Council Directive 86/609/EEC) and approved by Italian Health Ministry (D.L. 116/92). The study protocol was approved by the Local Institutional Ethics Committee of the University of Pavia for the use of animals. The whole blood was supplemented with 10% v/v of acid-citrate-dextrose (ACDC, 38 mM citric acid/75 mM trisodium citrate /100 mM dextrose) to avoid the coagulation during the storage at 4°C (Quan, Lia, Luana, Yuana, et al., 2015; Ong, Wu, Moochhala, Tan, et al., 2008; Sudheesh Kumar, Lakshmanan, Anilkumar, Ramya, et al., 2012). Just before experiments, the anticoagulant activity of ACDC was inhibited by adding 100 μ l of saturated CaCl_2 solution to 50 μ l of blood.

50 μ l volume of fresh blood was dropped onto unloaded and TA loaded sponge dressings (5 mm in diameter) placed in 50 ml glass beaker. After prefixed contact times, 10 ml distilled water was slowly poured in beaker without disturbing the clotted blood. The beaker was gently shaken for 2 minutes to suspend free red blood cells, not entrapped in the clot. The absorbance of each resulting sample, was assayed by means of spectrophotometric detection at 542 nm wavelength (Lamba 25, Perkin Elmer, I). As reference, fresh blood was considered.

The content of hemoglobin was quantified by the following equation:

$$\text{Hemoglobin absorbance} = I_s/I_r \times 100\%$$

where I_s is the absorbance of the resulting sample, and I_r is the absorbance of the reference value (blood or blood/TA (Ong, Wu, Moochhala, Tan, et al., 2008; Sudheesh Kumar, Lakshmanan, Anilkumar, Ramya, et al., 2012).

1.3.2.2.8 In vitro biocompatibility and proliferation

NHDFs (normal human dermal fibroblasts from juvenile foreskin, Promocell GmbH, Heidelberg, G) were used between the 2nd and 5th passage, for all the experiments.

Fibroblasts were grown in presence of Dulbecco's modified Eagle medium (Sigma, I) and supplemented with 10% fetal calf serum (FCS, Euroclone, I) with 200 IU/ml penicillin, and with 0.2 mg/ml streptomycin (Sigma, I) and kept at 37° C in a 5% CO₂ atmosphere with 95% relative humidity (RH).

Fibroblasts were seeded in each well of 96-well plates (area 0.34 cm²) at a seeding density of 10⁵ cells/cm². Cells were grown 24 h to obtain sub-confluence.

3.5 x 10⁴ cells/well (area 0.34 cm²) were seeded in a 96-well plate and grown to confluence for 24 h.

After 24 h cells were washed with saline solution and placed in contact with 200 µl of CH, CH-CS and CH-HA polymeric mixtures (prepared as reported in the section 1.3.2.1) at 1:20 (CH, CS or HA at 500 µg/ml, solubilized in cell growth medium) and 1:50 dilution with growth medium (GM) (CH, CS or HA at 200 µg/ml). After dilution, all the samples were transparent without visible precipitate. TA having the same concentration as in the loaded polymeric mixtures and GM were used as control. Cell substrates were incubated for 3 h (biocompatibility test) and for 24 h (proliferation test) with the samples, then the medium was removed and the MTT test was performed. Briefly, MTT test is based on the activity of mitochondrial dehydrogenases of vital cells that convert MTT in formazan (Sandri, Aguzzi, Rossi, Bonferoni et al., 2017). At this purpose, 50 µl of MTT solution (Sigma Aldrich, I) at 2.5 mg/ml concentration in HBSS (Hank's Buffered Salt Solution) pH 7.4 was put in contact with each cell substrate for 3 h. The reagent was removed from each well, and the substrates were washed with 200 µl of PBS. After the removal of PBS, 100 µl of DMSO was put in each well, and the absorbance was assayed at 570 nm by means of an ELISA plate reader (Imark Absorbance Reader, Biorad, I), with a reference wavelength of 690 nm. Cell viability was calculated as % ratio between the absorbance of each sample and the absorbance of cell substrate maintained in contact with growth medium.

1.3.2.2.9 Ex vivo proliferation on human skin biopsy

To analyze the effects of dressings on wound healing, an ex vivo human skin model was used to reproduce in vivo physiological conditions (Mori, Rossi, Ferrari, Bonferoni et al., 2016). Adult healthy human skin biopsies were clinically obtained from surgery for breast reduction of different age donors (range 35-60 years old), after obtaining informed consent. Surgical biopsy (about 4x8 cm) was cut into smaller fragments (about 0.6x0.6 cm) and a skin circular portion (including epidermis and dermis) was centrally removed with aseptic circular punch (diameter: 3 mm). Each fragment was placed into Transwell[®] inserts (growing area: 0.33 cm², Corning[®] Costar[®], Sigma, I) in 24-well-plate (membrane pore size: 0.4 µm) and circular portions of each dressing, having the same diameter of punch, were applied in correspondence of skin lesion.

The samples were maintained in culture in presence of Dulbecco's modified Eagle medium (Sigma, I) and supplemented with 10% fetal calf serum (FCS, Euroclone, I) with 200 IU/ml penicillin, and with 0.2 mg/ml streptomycin (Sigma, I) and kept at 37° C in a 5% CO₂ atmosphere with 95% relative humidity (RH).

The medium (900 µl/each well) was added into well basal compartment to maintain skin viability, avoiding skin dehydration and ensuring an adequate supply of nutrients through hypodermis. After different times (24 and 72 h and 7 days) of culture, the biopsies were fixed with 4% paraformaldehyde in 0.1 M phosphate buffer, pH 7.4, for 24 h, and processed for histological analysis (Riva, Casasco, Nespoli, Icaro Cornaglia, et al., 2007). Briefly, the fragments were dehydrated through graded concentrations of ethanol and embedded in paraffin. 8 µm sections were obtained by means of a microtome (Leitz, G), rehydrated and processed for immunohistochemical reactions for bromodeoxyuridine (BrdU) incorporation. The sections were incubated with primary antibody anti-BrdU (Ge Healthcare, UK) overnight at appropriate dilution (1:100), the primary antibody anti-BrdU was reacted by using MACH 1 Universal HRP-Polymer Detection kit (Biocare Medical, USA). At this purpose the sections were reacted with MACH 1 Mouse probe for 15 min and subsequently with HRP-Polymer (horseradish peroxidase polymer) for 30 min and finally with Biocare's

Betazoid DAB for 5 min. At the end the sections were dehydrated and mounted with DPX mounting medium (a mixture of distyrene, a plasticizer, dissolved in toluene-xylene, Sigma, I).

Skin sections obtained in the middle of the lesions were observed at the magnification of 20X under a light microscope Axiophot (Zeiss, G) equipped with a digital camera. Image J program was used to analyze images, counting cell nuclear positivity in a section area larger 2 mm at right and left side than the lesions.

1.3.2.2.10 Statistical analysis

Statistical differences were evaluated by means of a non-parametric test: Mann Whitney (Wilcolxon) W test, (Stat Graphics 5.0, Statistical Graphics Corporation, MD, USA). Differences were considered significant at $p < 0.05$; only significant differences are reported in the captions of the relevant figures as asterisks.

1.4 RESULTS AND DISCUSSION

1.4.1 Sponge-like dressing technological properties

1.4.1.1 Mechanical properties

Figure 2 reports the results of mechanical resistance as maximum force of penetration of the dressings without lyoprotectant and with glycerol or mannitol as lyoprotectants.

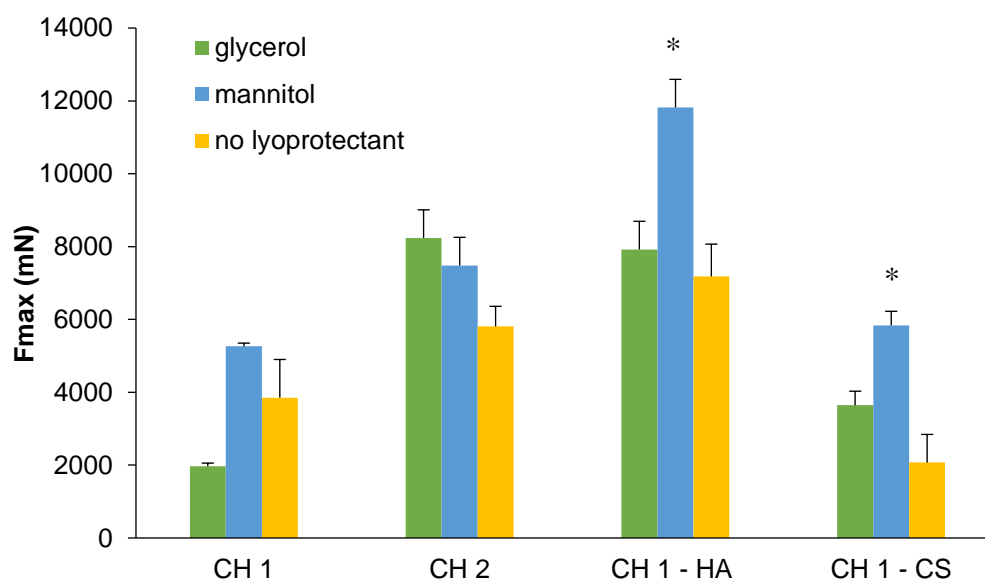


Figure 2: mechanical resistance as maximum force of penetration (F_{max} , mN) of the dressings without lyoprotectant and with glycerol or mannitol as lyoprotectants (mean values \pm sd; n=6).

The increase of chitosan amounts in the dressings increased the mechanical resistance of the formulations: stiffness was significantly greater when lyoprotectants (glycerol or mannitol) were included in the formulations. The presence of HA in the dressings caused a significantly increase in the mechanical resistance and HA based formulation with mannitol as lyoprotectant was characterized by the higher F_{max} value to indicate a more rigid structure. This behavior could probably due to the high

molecular weight of HA, with respect to CS, that could dramatically strengthen the tridimensional network of the system. It is conceivable that HA interacted with chitosan during the preparation procedure, forming a polyelectrolyte complex (PEC) between chitosan and hyaluronate. Since both CH and HA have similar molecular weight the interaction between the two polymers should be able to form a highly crosslinked structure.

On the contrary, the presence of CS in the formulation did not significantly change the stiffness of the dressings. This is probably due to the resulting PEC formed by an interaction between CS and CH: CS is characterized by a molecular weight 18 folds lower than that of CH, moreover sulfate groups of CS (more acid with respect to carboxylic group) could cause a coiled structure less prone to polymer chain entanglements. This probably rendered the dressing structure less stiff.

As reported in literature, structure and stability of PECs strongly depend on different parameters such as concentrations of each polyelectrolyte, charge molar ratio, charge density, molar masses and chain flexibility but depend also on extrinsic parameters as pH, ionic strength and/or temperature (Kabanov, 2005; Feng, Leduc, and Pelton, 2008; Le Cerf, D., Pepin, A. S., Niang, P.M., Cristea et al., 2014).

According to all these parameters, mixing oppositely charged polyelectrolytes could give two types of PECs dependently of charge stoichiometry: soluble PECs, leading to stable and transparent solutions, and insoluble PECs, with or without precipitation. The soluble PECs are obtained with an excess of anionic or cationic charges (Feng, Leduc, and Pelton, 2008; Kabanov and Zezin, 1984; Schatz, Domard, Viton, Pichot, et al., 2004) and this was the case of CH-HA and CH-CS. In fact, charge density (positive) is 0.006 mole/g for chitosan, 0.0013 mole/g for HA (negative) and 0.002 mole/g for CS (negative) with a clear excess of positive charges, in both cases. The charge molar ratio of CH – HA was 4.6 while that of CH – CS was 3.

Moreover Denunziere, Ferrier, and Domard (1996) reported interaction between CS and CH was independent of CS sulfate substitution on 4 or 6 carbons.

This was confirmed by zeta potential evaluation. CH 1 had a positive zeta potential of 53.2 ± 1.9 (mean value \pm sd; n=3) while HA and CS as solutions showed negative zeta potentials of -27.9 ± 0.9 and -16.8 ± 1.2 , respectively (mean value \pm sd; n=3). CH 1

– HA and CH 1 – CS were characterized by positive zeta potentials of 39.3 ± 0.3 and 25.3 ± 0.8 , respectively (mean value \pm sd; n=3). These results supported that the interaction between CH and GAGs did not cause a neutralization of the two polyelectrolytes mixed (CH and HA or CS) and an excess of positive charges was present.

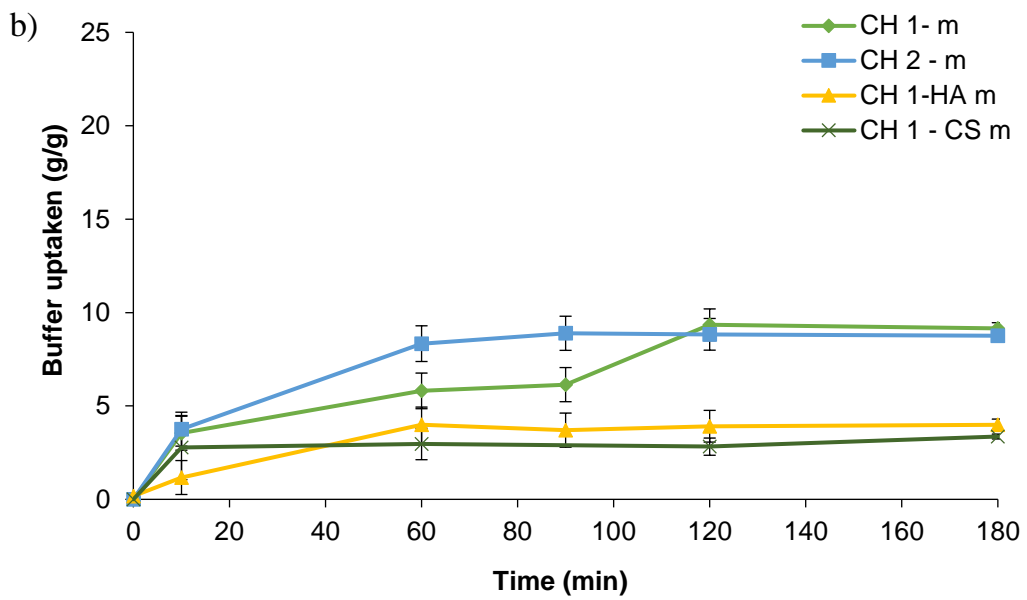
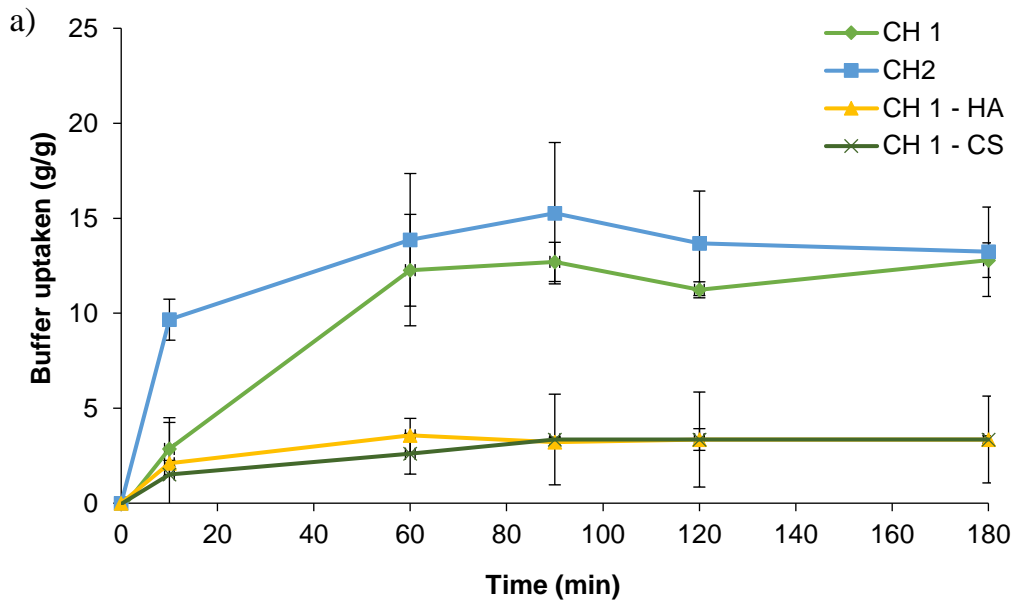
Moreover, lyophilization caused acetic acid evaporation. In particular, acetic acid was added, to form chitosan acetate, in excess: 350 μ moli of acetic acid were added to 110 μ moli of chitosan per each dressing prepared, starting from chitosan at 1% w/w. The titration of acetic acid residues after lyophilization revealed that there was a residue of 5 ± 1 μ moli per each system independently of the addition of HA or CS. This is conceivably due to the almost total removal of acetic acid in excess (not involved in chitosan salification).

1.4.1.2 Hydration properties

Figure 3 reports buffer (pH 7.2 phosphate buffer, to mimic wound exudates) taken up a function of time for all the dressings prepared: a) without lyoprotectant, b) with glycerol and c) with mannitol as lyoprotectants.

Considering all the compositions with and without lyoprotectants, chitosan based dressings were characterized by higher buffer taken up vs time profile with respect to those of chitosan and GAG systems; moreover, chitosan dressings based on higher CH amounts, showed higher hydration profile even not significantly different from hydration capability of dressing based on lower CH amounts. Dressings based on chitosan and GAG were characterized by significantly lower hydration profiles, independently of both the presence and type of lyoprotectants. All the systems showed a high hydration capacity in the first hour: it is conceivable that chitosan was likely to create a lower pH environment at the dressing/liquid interface and this caused a high liquid absorption probably due chitosan gelation. Subsequently, chitosan poor solubility at neutral pH (pKa 6.5) prevailed over its buffering properties and liquid absorption stopped. The presence of GAG further decreased system

hydration probably due to the interpolymer interaction between chitosan and hyaluronic acid or chondroitin sulfate.



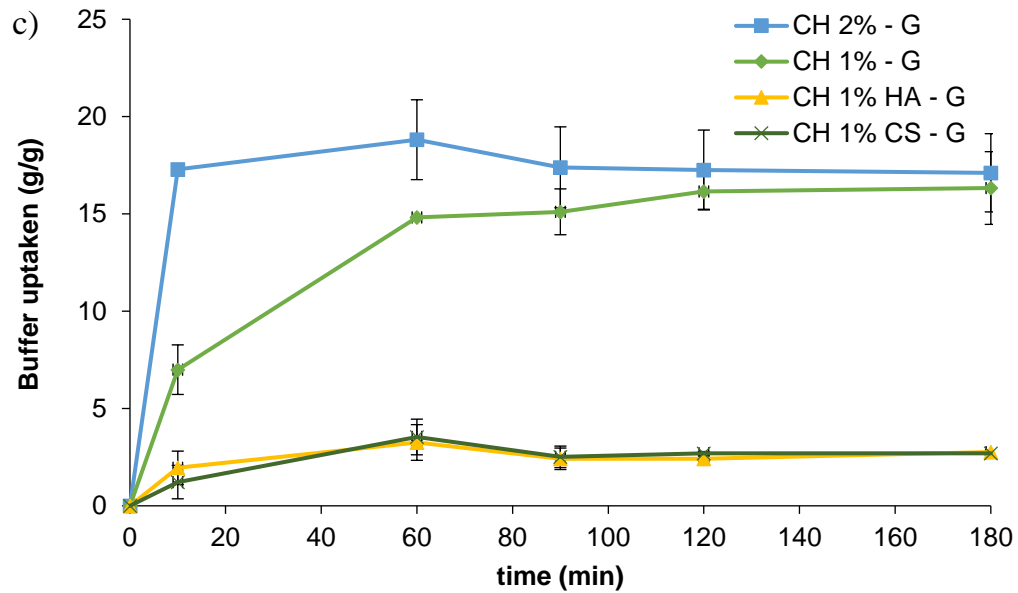


Figure 3: liquid taken up (pH 7.2 phosphate buffer) as function of time for all the dressings prepared: a) without lyoprotectant, b) with mannitol and c) with glycerol as lyoprotectans (mean values \pm sd; n=6).

Glycerol did not markedly change the hydration properties of CH and CH in association with GAG. On the contrary, mannitol substantially decreased the hydration capacity of the systems: this could be related to stiff structure of the dressings, which could slow down and impair liquid penetration into the dressings. Hydration behavior is a crucial point in dressings to ensure hemostasis, to absorb wound exudate and to avoid wound bed dehydration, enhancing granulation phase and healing.

1.4.1.3 Bioadhesion properties

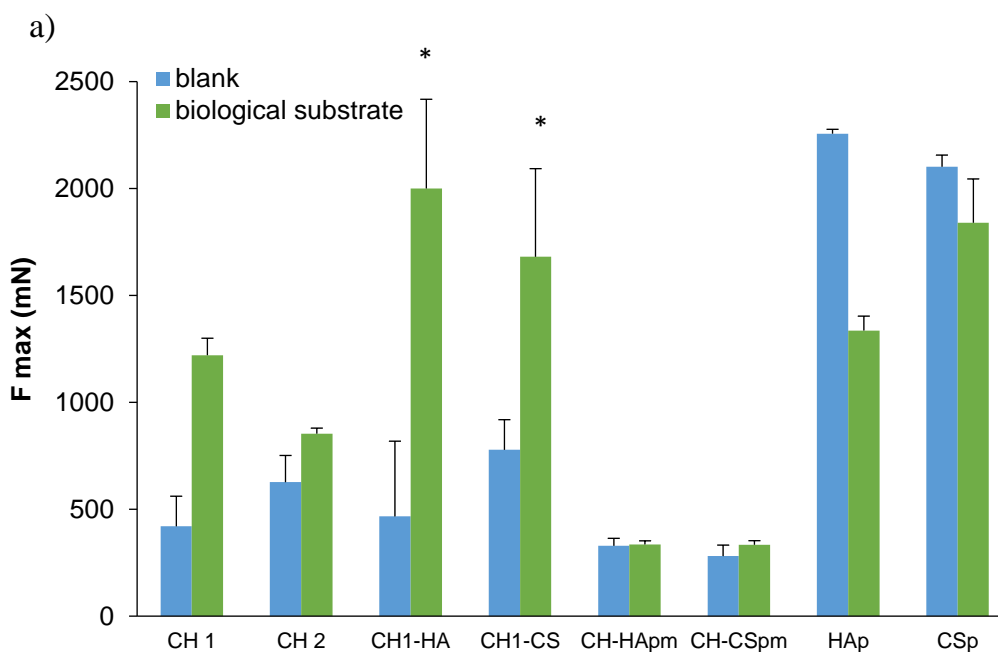
Figure 4 reports maximum force of bioadhesion (mN) all the dressings prepared: a) without lyoprotectant, b) with glycerol and c) with mannitol as lyoprotectants.

As for dressings without lyoprotectants (Fig. 4 a), chitosan concentration influenced bioadhesive behavior: CH 2 sponge-like dressing (containing higher chitosan amount) did not show bioadhesive propensity (F_{max} measured without biological substrate was not significantly different with respect to the value in presence of biological substrate – egg shell membrane) while CH 1 dressing (containing chitosan at lower amount) was characterized by good bioadhesive properties. Such a behavior is probably due to a different degree of entanglement between chitosan polymeric chains. In particular, the lowest chitosan concentration the lowest the entanglement and the highest the capability to form a bioadhesive joint with the biological substrate (Rossi, Ferrari, Bonferoni, Caramella, 2001).

Since zeta potential analysis confirmed that there was not a complete neutralization of CH with GAGs and both CH-HA and CH-CS had positive zeta potentials, the presence of GAG in dressings significantly enhanced the bioadhesive properties. The interaction between chitosan and GAG probably assisted bioadhesive joint consolidation, considering a higher concentration of carboxylic and OH residues in these systems with respect to that of CH 1. The highest presence of these groups able to form hydrogen bonds could consolidate bioadhesive properties of chitosan, that are mainly due to its positive charge density. Chitosan and GAG physical mixtures (CH-HA_{pm}, and CH-CS_{pm}) did not show bioadhesive properties: these are easily inferred by the negligible solubility properties of chitosan at pH 7.2 phosphate buffer (hydration medium chosen to mimic wound bed exudate). Moreover, CS or HA, as powders, were also considered and they showed a lack of bioadhesion in those conditions: this was probably due to the slower hydration of HA during the test with respect to the lyophilized dressings and to the poor bioadhesive strenght of CS mainly caused by its low molecular weight.

In presence of lyoprotectants, both mannitol and glycerol (Fig. 4 b and c, respectively), the bioadhesive properties were less pronounced and were significant only for HA

and CS dressings with mannitol. The presence of lyoprotectants, especially of mannitol, that increased system stiffness and probably decreased polymer chain mobility, could impair polymer capability to interact with the biological substrate. Also, bioadhesion is a crucial characteristic that should favor an intimate and prolonged contact between wound dressings and lesion, favoring blood absorption and avoiding formulation detachment to increase the hemostatic potential.



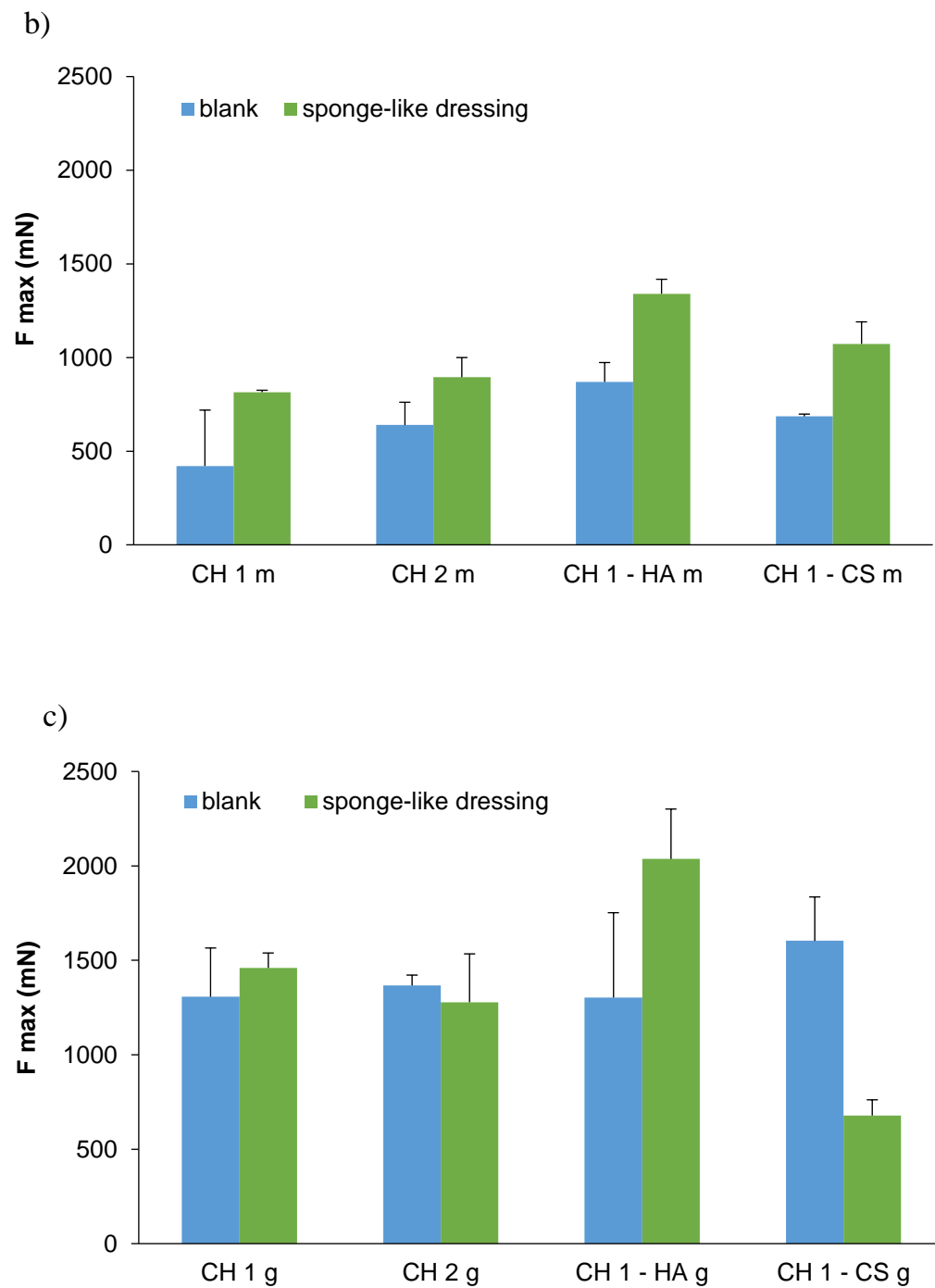


Figure 4: maximum force of bioadhesion, F_{max} (mN) of all the dressings prepared: a) without lyoprotectant, b) with glycerol and c) with mannitol as lyoprotectants (mean values \pm sd; n=6).

1.4.1.4 Morphology

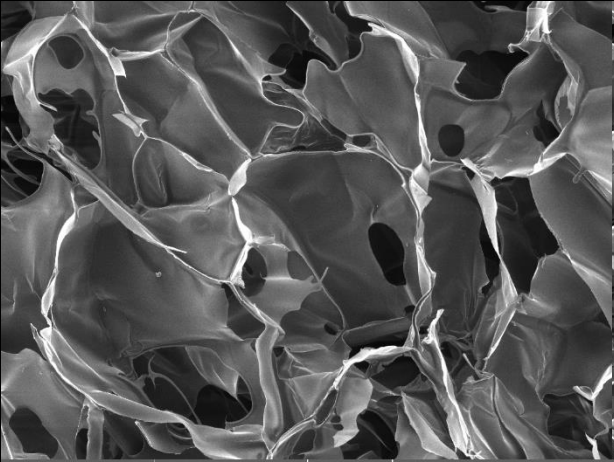
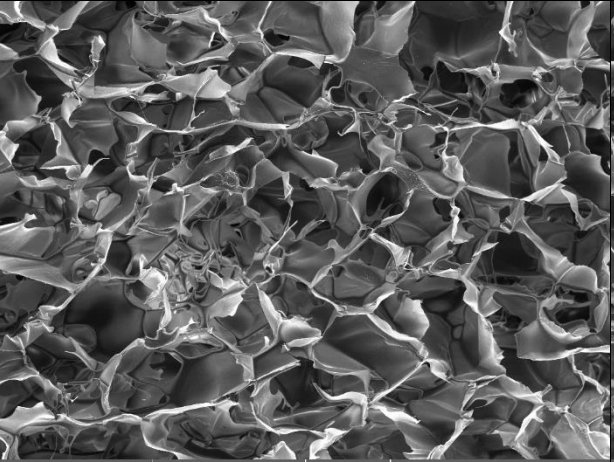
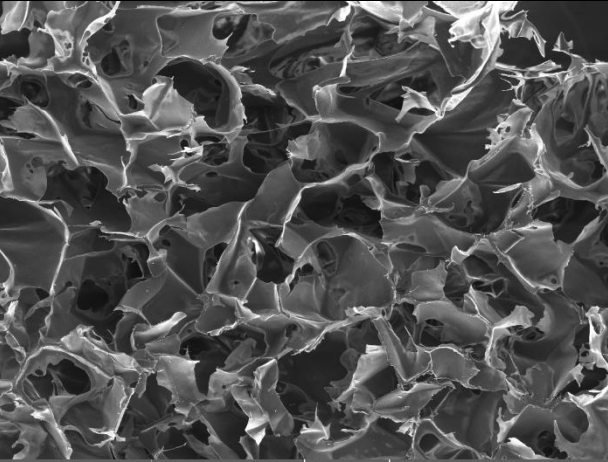
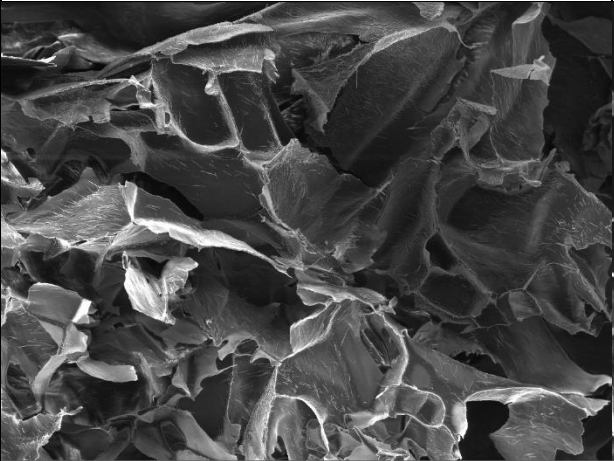
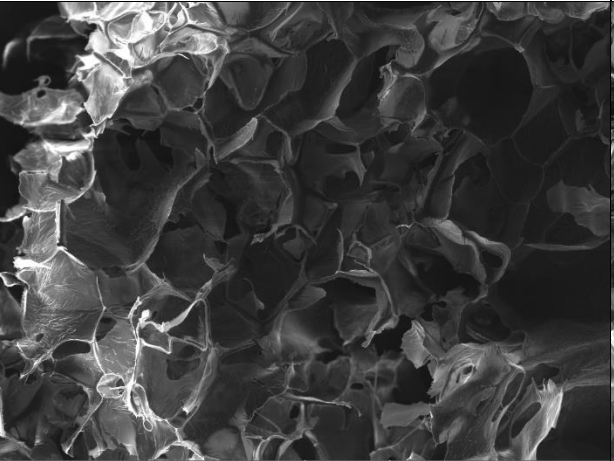
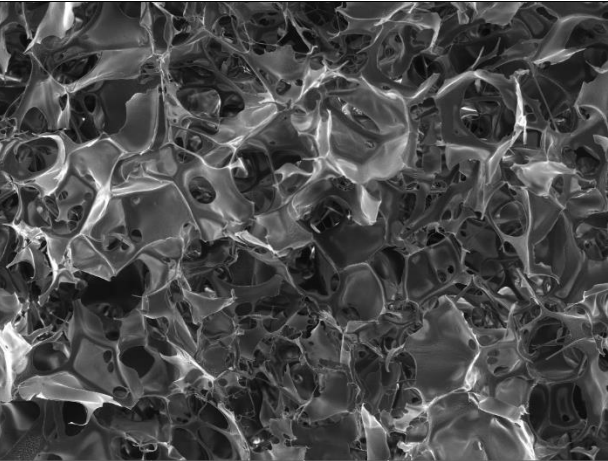
To understand if the system tridimensional networks could affect hydration and bioadhesion properties, morphology was assessed.

Figure 5 reports SEM images of transversal sections of CH 1, CH 1- HA and CH 1 – CS unloaded dressings and TA loaded dressings without lyoprotectans, and CH 1, CH 1- HA and CH 1 – CS dressings with glycerol and with mannitol.

CH 1 dressing showed a beehive structure with polyhedric cavities interconnected by pores having oval or round shapes. The cavities had dimensions of about 500 μm while the pores ranged from 50 to 200 μm . The presence of GAG did not change the system morphology while it markedly decreased the cavity dimensions that were around 200-300 μm and furthermore the pore diameters that were of about 50 μm . This difference in system porosity conceivably contributed to their hydration behavior. The TA loading did not modify the structure of the dressings.

The presence of glycerol as lyoprotectant did not substantially change dressing structure while the presence of mannitol caused a partially loss of polyhedric cavities and the structure resembled much more randomly organized sheets without marked modifications of the porosity. This modification could be responsible to the system behavior upon hydration and bioadhesion.

Since lyoprotectans did not markedly improve the technological properties of the dressings and considering mechanical, hydration and bioadhesive properties, lyoprotectant free systems prepared using chitosan at 1% w/w were considered for the further characterizations.

	CH 1	CH 1 - HA	CH1 - CS
No lyoprotectant			
	SEM HV: 8.0 kV WD: 10.12 mm MIRA3 TESCAN SEM MAG: 200 x Det: SE 200 µm BI: 10.00 Date(m/d/y): 11/07/17	SEM HV: 8.0 kV WD: 10.67 mm MIRA3 TESCAN SEM MAG: 200 x Det: SE 200 µm BI: 10.00 Date(m/d/y): 11/07/17	SEM HV: 8.0 kV WD: 10.08 mm MIRA3 TESCAN SEM MAG: 200 x Det: SE 200 µm BI: 10.00 Date(m/d/y): 11/07/17
TA loaded dressing without lyoprotectant			
	SEM HV: 8.0 kV WD: 9.96 mm MIRA3 TESCAN SEM MAG: 200 x Det: SE 200 µm BI: 10.00 Date(m/d/y): 11/02/17	SEM HV: 8.0 kV WD: 9.36 mm MIRA3 TESCAN SEM MAG: 200 x Det: SE 200 µm BI: 10.00 Date(m/d/y): 11/02/17	SEM HV: 8.0 kV WD: 9.36 mm MIRA3 TESCAN SEM MAG: 199 x Det: SE 200 µm BI: 10.00 Date(m/d/y): 11/02/17

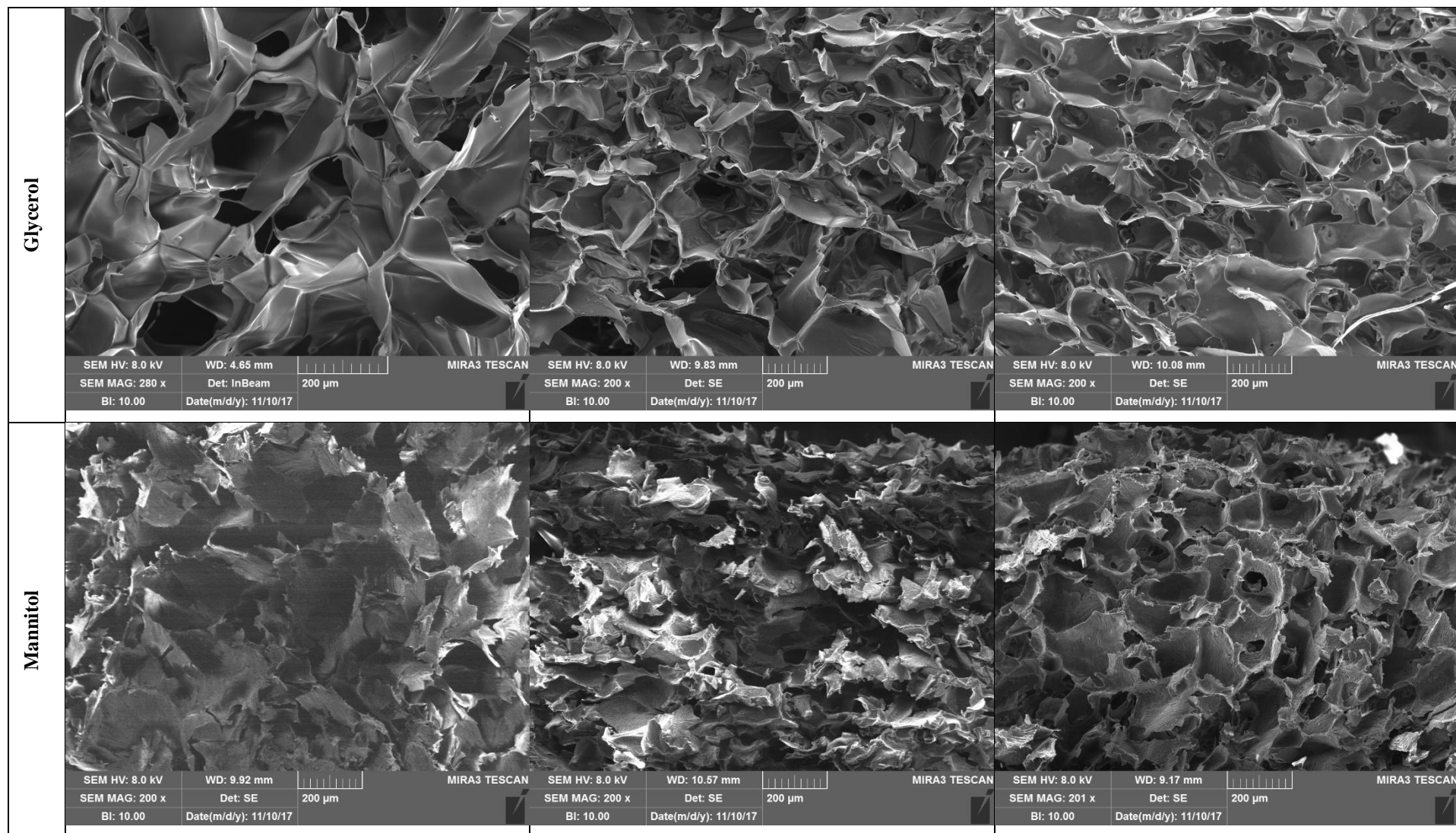


Figure 5: SEM microphotographs of transversal sections of CH 1, CH 1- HA and CH 1 – CS unloaded dressings and TA loaded dressings without lyoprotectants, dressings with glycerol and with mannitol.

1.4.1.5 FT-IR analysis

Figure 6 reports the FT-IR spectra of CH 1, CH 1 – HA and CH 1 – CS HA and CH+CS dressings and of CH powder (in the inset) as comparison.

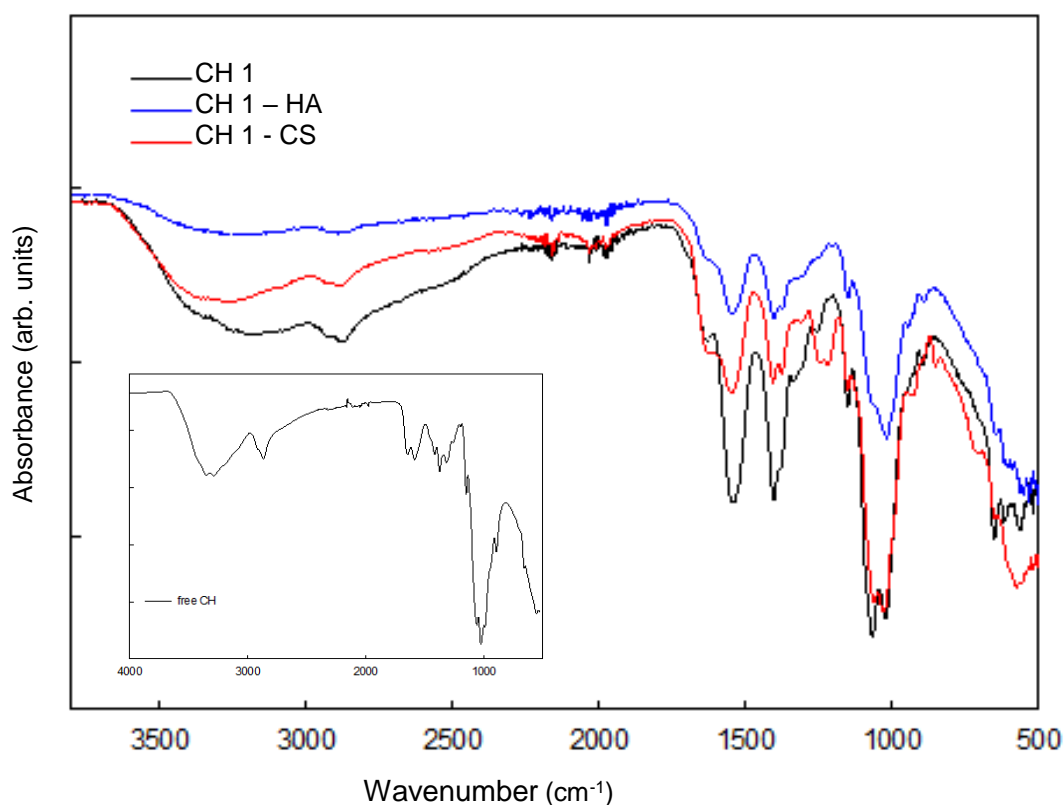


Figure 6: FT-IR spectra of CH 1, CH 1 – HA and CH 1 – CS HA and CH+CS dressings. In the inset the FTIR spectrum of CH powder (free CH) is reported as comparison.

The three spectra shared many common features both in the number and position of the peaks and seemed to be dominated by the FT-IR pattern of CH (free CH as powder), where the region around 1630 and 1540 cm^{-1} is typical of the amide I and amide II stretching and bending modes (Radhakumary, Antony, Sreenivasan, 2011; Jayakumar, Prabhakaran, Nair, Tamura, 2010). Interestingly, the position of these peaks shifted to lower frequency with respect to free CH (i.e. not interacting with acetate ions) shown Figure 1 inset. In particular, the $-\text{C}=\text{O}$ stretching of the amide I in free CH moved from 1652 to 1634 cm^{-1} when it interacted with acetate ions and it remained in the same

position even in the CH 1 - HA and CH 1 - CS systems. Moreover, a new peak around 1404 cm^{-1} (correlated to the -C-H- bending) appeared in the spectra of CH 1 dressing with respect to free CH and was found also in the spectra of CH 1 - HA and CH 1 - CS. The two mentioned spectral features have been correlated to charge-charge neutralization (salification) which most probably occurred between CH and acetate ions and dominated the spectra of all the three systems shown in Figure 1 (Shanti Krishna, Radhakumary, Sreenivasan, 2015).

This suggests that, in presence of acetate ions, the charge-charge interaction, involving chitosan amino groups, was preferentially between CH and acetate and therefore the further addition of HA and CS mostly interact with chitosan through less strong bonding such as polar interactions. Such results are in agreement with zeta potential values determined.

1.4.1.6 In vitro drug release properties

Figure 7 reports TA release profiles as function of time obtained for TA loaded dressings without lyoprotectans.

All the dressings were characterized by the same release behavior. TA is a water- soluble drug (167 mg/ml) and considering the experimental conditions, the maximum concentration reached in the receiving phase was 1 mg/ml. In these conditions, TA release from all the dressings was relatively fast: the 50% of TA was released in about 30 min and reached quantitative and plateau value within about 3 h. The fast release of TA should be due by the presence of drug crystals onto cavity walls of the dressings, which rendered it prone to a prompt dissolution. This behaviour should deliver TA at the application site, in the wounded bleeding lesion, to perform its procoagulant function as quickly as possible and moreover to sustain hemostatic activity for prolonged time to stabilize clot formation.

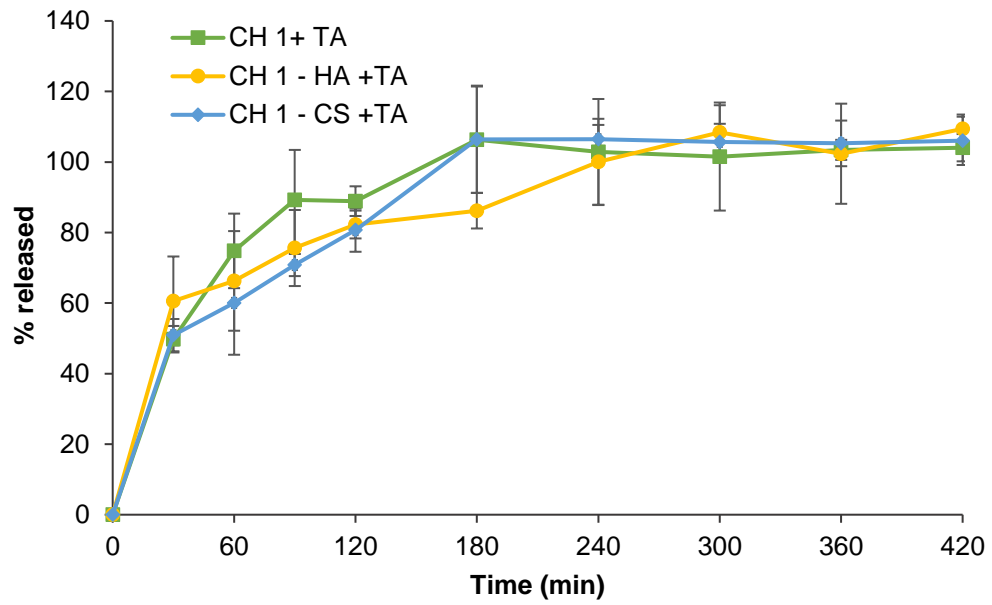


Figure 7: TA release profiles as function of time obtained for TA loaded dressings without lyoprotectants (mean values \pm sd; n=6).

1.4.2 Sponge-like dressing biopharmaceutical properties

1.4.2.1 In vitro dynamic whole-blood clotting

Figure 8 shows % hemoglobin absorbance profiles as function of time evaluated for a) unloaded dressings and b) TA loaded formulations.

A higher degree of hemoglobin absorbance indicates a slower clot formation rate.

Whole blood clotting formation was relatively slow, and the hemoglobin absorbance reached the minimum level after about 420 s. A faster clot formation occurred in presence of all the dressings and 30 s immediately after the contact between blood and formulations the % of free hemoglobin was around 20-50%. The minimum level of hemoglobin absorbance was reached after about 300 s. Chitosan capability to bind and aggregate platelets causing agglutination of erythrocytes and activation of hemostasis was predominant in all the formulation considered also in presence of GAG.

TA is a synthetic analogue of lysine and its antifibrinolytic activity is related to reversible bindings with four to five lysine receptor sites on plasminogen or plasmin: this prevents plasmin from binding to and degrading fibrin and preserves clot structure. TA showed a synergic activity with chitosan in enhancing clot formation: all the formulations reached the minimum in hemoglobin absorbance in about 180 s, presenting a better clotting performance with respect to unloaded dressings.

TA CH 1 dressing allowed to maintain a % of hemoglobin at 420 s not significantly different from initial value, while CH 1 dressing determined a significant increase in % of hemoglobin comparing the initial value with respect to the final one (at 420 s). TA CH1 –HA and TA CH1- CS dressings proved to maintain clot integrity stable from the beginning up to 420 s, while the same compositions unloaded showed a partial clot modification at 90 s with a sharp increase in % of hemoglobin.

The presence of GAG slightly decreased the procoagulant activity of the dressings. In fact, HA and CS are reported in literature as anticoagulant materials. Fragments of HA having a molecular weight lower than 500 kDa, as it is the case, cause clot structure susceptible to mechanical deformations and softening (Komorowicz, Balazs, Varga, Szabo, et al., 2016). CS is a sulfated glycosaminoglycan with heparin-

like activity (Pandolfi, M., Hedner, U., 1984). On this basis, the procoagulant activity of the systems seems exclusively due to chitosan and its synergic effect with TA.

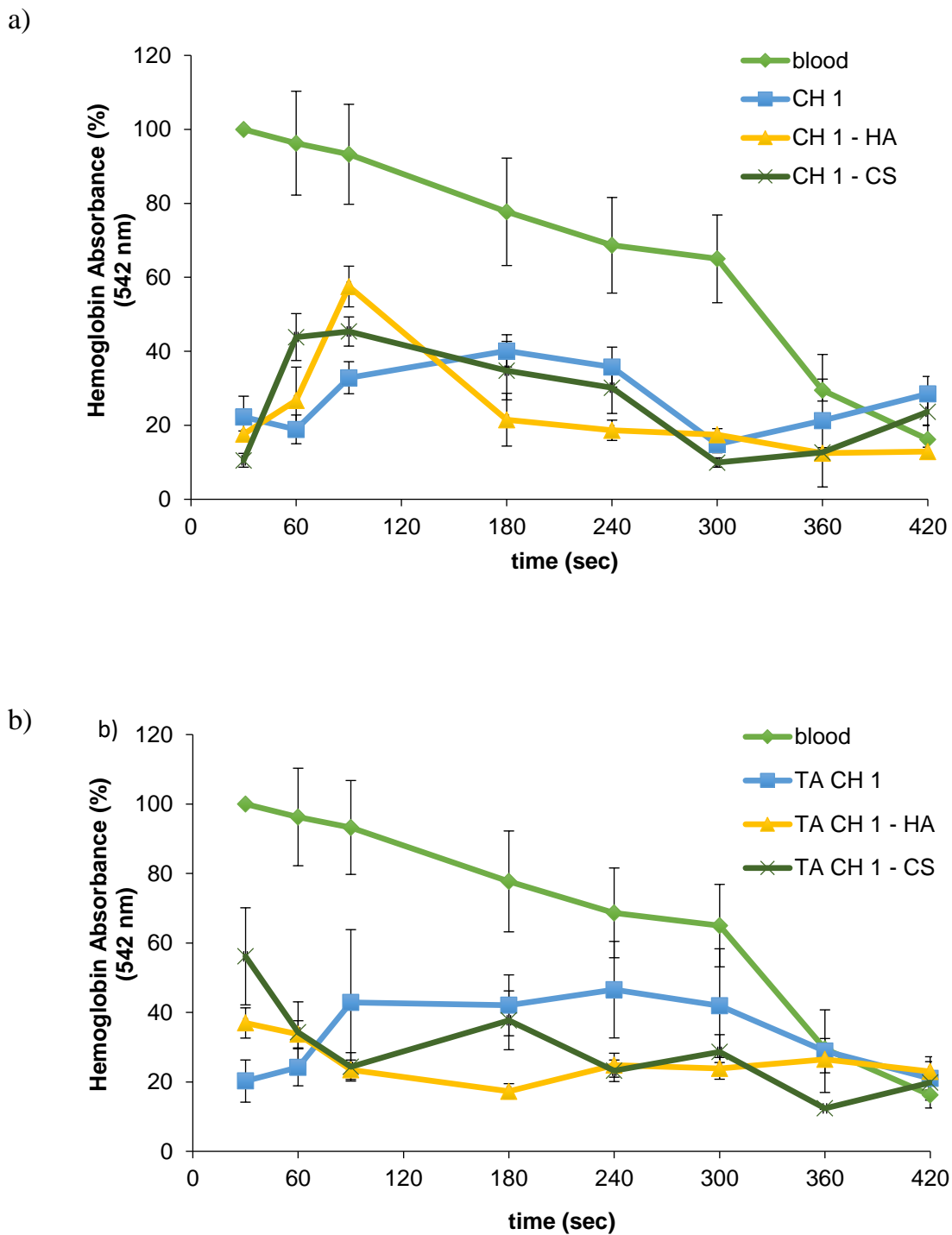


Figure 8: % hemoglobin absorbance profiles as function of time evaluated for a) unloaded dressings and b) TA loaded formulations (mean values \pm sd; n=6).

1.4.2.2. In vitro biocompatibility and proliferation

Figure 9 reports % biocompatibility (a) and % of proliferation (b) of all unloaded or TA loaded dressings (polymeric mixtures used to prepare dressings) towards fibroblasts (NHDF) for 3 and 24 h of contact time, respectively, and the amounts of proliferating nuclei/area (c) (positively stained for BrdU) counted for all the unloaded and TA loaded dressings.

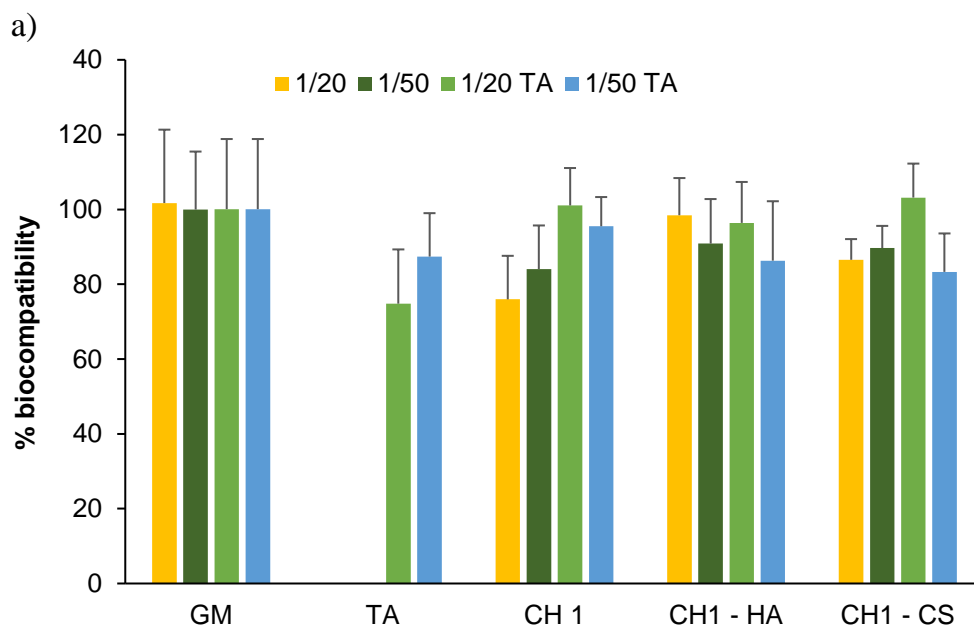
Independently of the concentrations considered, all the dressings were characterized by good biocompatibility properties towards fibroblasts also in presence of TA and the cell availability was not significantly different from those obtained with growth medium (GM, standard growth conditions).

Similarly, after 24 h the lower dressing concentrations determined the higher proliferation properties that becomes more evident in presence of tranexamic acid.

These results put in evidence that the presence of the hemostatic drug, TA, did not interfere with cell growth in the experimental conditions considered. Similar results were observed by Cholewinski et al. (2009): carotid artery derived cells maintained their morphology with toxic reaction in presence of TA.

Ex vivo skin cell proliferation (GM) was maximum in the first 24 h and decreased after 72 h and 7 days, except for CS based system that had constant activity (Figure 9 (c)). Unloaded dressings were able to sustain cell proliferation up to 7 days demonstrating a capability to enhance cell proliferation after tissue damage. TA loaded dressings were characterized by the same proliferating properties as unloaded one, considering CH 1 and CH1 - HA dressings. As for CH1 - CS dressing the presence of TA significantly increased the system proliferation properties after 24 h and 7 days and allowed to obtain the better performance, with a prolonged effect up to one week. This probably was caused by the synergic effect of TA and CS on cell growth: CS was reported as able to enhance fibroblasts and endothelial cells proliferation (Sandri, Bonferoni, Rossi, Ferrari et al., 2015) while TA could stabilize fibrin clot without impairment of cell growth and proliferation (Cholewinski, Dietrich, Flanagan, Schmitz-Rode et al., 2009). At this purpose fibrin clot was conceivably formed just after skin biopsies and it could retain growth factors released

by platelets during normal physiological process, on this perspective TA, as fibrinolytic drug, could preserve the clot integrity assisting cell proliferation (Wolberg and Campbell, 2008).



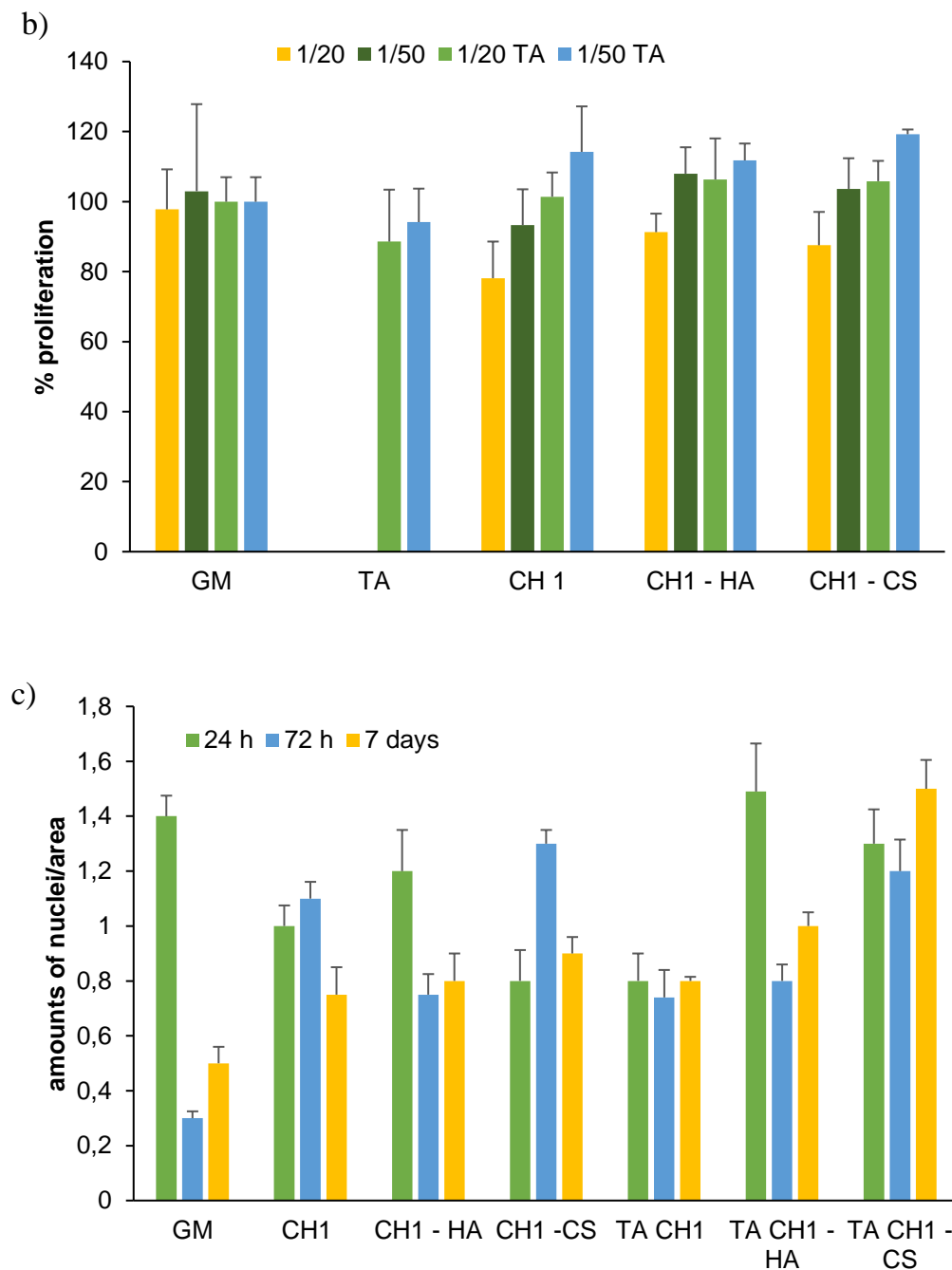


Figure 9: % biocompatibility (a) and % proliferation (b) of all unloaded or TA loaded dressings (polymeric mixtures used to prepare dressings) towards fibroblasts (NHDF) for 3 and 24 h of contact time, respectively; amounts of proliferating nuclei (c) (positively stained for BrdU) for all the unloaded and TA loaded dressings after 24 and 72 h and 7 days of contact time (mean values \pm sd; n=8).

1.5 CONCLUSIONS

Sponge-like dressings based on chitosan and chondroitin sulfate or hyaluronic acid were prepared by lyophilization and loaded with tranexamic acid. The presence of GAG conceivably caused the occurrence of either chitosan and hyaluronic acid or chitosan and chondroitin sulfate interactions. The presence of glycosaminoglycans decreased hydration properties of the systems in a buffer simulating wound exudate – pH 7.2) and this was primarily due to dressing morphology. Chitosan based dressings had a beehive structure with polyhedral cavities of about 500 μm , interconnected by pores having oval or round shapes (50 to 200 μm) while dressings based on chitosan in association with GAG markedly decreased the cavity dimensions (200-300 μm) and with smaller pore diameters (about 50 μm). Liquid absorption is a key point in dressings to ensure hemostasis, to control wound bed hydration enhancing granulation phase and healing.

The presence of GAG in dressings significantly enhanced dressing bioadhesive properties considering as biological substrate egg-shell membrane to mimic wound bed. The association of chitosan with GAG allowed the consolidation of bioadhesive joint probably via hydrogen bonds that strengthen chitosan bioadhesion behavior, mainly due to charge-charge interaction between chitosan and the biological substrate. This is a functional property since bioadhesion is fundamental to favor an intimate and prolonged contact between wound dressings and lesion, avoiding formulation detachment and increasing hemostatic potential.

TA release was fast to allow procoagulant function as quickly as possible and moreover to sustain hemostatic activity for prolonged time, to stabilize clot, moreover TA presented a synergic effect with chitosan to speed up clotting formation.

In vitro and ex vivo evaluations on fibroblasts and human skin, respectively, evidenced that the developed dressings enhanced cell proliferation.

Bartley (2013) suggested that the association of chitosan with TA should improve hemostatic control and should lead to improved clinical outcomes in internal surgical wounds. In this paper, sponge-like dressings based on chitosan and GAG and loaded with TA demonstrated to combine both hemostasis and proliferation properties and it

seemed promising in control bleeding and healing in wounds as well as in abdominal surgery.

Acknowledgment

Dr. F Saporito wishes to thank ABOCA Società Agricola S.p.A. for her PhD grant. The authors wish to thank Prof. Boselli (Department of Drug Science, University of Pavia, I) for the rat blood collection, Prof. Nicoletti (Plastic and Reconstructive Surgery Unit, Department of Clinical Surgical Diagnostic and Pediatric Sciences, University of Pavia, Salvatore Maugeri Research and Care Institute, Pavia, Italy for the human skin biopsy, Dr. I. Tredici (Centro Arvedi, University of Pavia) for SEM measurements.

1.6 REFERENCES

- Ansari, T. M., Raza, A., Rehman, A. (2005). Spectrophotometric determination of Tranexamic acid in pharmaceutical bulk and dosage forms. *Analytical Sciences*, 21, 1133-1135.
- Bartley, J. (2013). Should chitosan and traxenamic acid be combined for improved hemostasis after sinus surgery? *Medical Hypothesis*, 81, 1036-1038.
- Bennet, B.L. (2017). Bleeding control using hemostatic dressings: lessons learned. *Wilderness and Environmental Medicine*, 28, S39-S49.
- Cataldo, F., Ursini, O., Lilla, E., Angelini, G. (2008). Radiation-induced crosslinking of collagen gelatin into a stable hydrogel. *J. Radioanal. Nucl. Che.* 275, 125-131
- Champion, H. R., Bellamy, R. F., Roberts, C. P., Leppaniemi, A. (2003). A profile combat injury. *Journal of Trauma*, 54, S13-S19.
- Chen, W. Y. J, Abatangelo, G. (1999). Functions of hyaluronan in wound repair. *Wound Repair and Regeneration*, 7, 79-89.
- Cholewinsski, E., Dietrich, M., Flanagan, T.C., Schmitz-Rode, T., Jockenhoevel, S. (2009). Traxenamic acid – an alternative to aprotinin in fibrin-based cardiovascular tissue engineering. *Tissue Engineering part A*. 15, 3645-3653
- Denunziere, A., Ferrier, D., and Domard, A. (1996). Chitosan-chondroitin sulfate and chitosan-hyaluronate polyelectrolyte complexes. Physico-chemical aspects. *Carbohydrate Polymers*. 29, 317-323
- Dunn, C. J., Goa, K. (1999). Tranexamic acid, a review of its use in surgery and other indications. *Drugs*, 57, 1005-1032.
- Feng, X., Leduc, M., Pelton, R. (2008). Polyelectrolyte complex characterization with isothermal titration calorimetry and colloid titration. *Colloids and Surfaces A: Physicochemical and Engineering Aspect*, 317, 535–542.
- Francesko, A., Tzanov, T. (2011). Chitin, chitosan and derivatives for wound healing and tissue engineering. *Advances in Biochemical Engineering/Biotechnology*, 125, 1–27.

- Granville-Chapman, J., Jacobs, N., Midwinter, M. J. (2011). Pre-hospital haemostatic dressings: a systematic review. *Injury-International of the Care of the Injured*, 42, 447–59.
- Hoemann, C.D., Sun, J., McKee, M. D., Chevrier, A., Rossomacha, E., Rivard, G. E., Hurtig, M., Buschmann M.D. (2007). Chitosan-glycerol phosphate/blood implants elicit hyaline cartilage repair integrated with porous subchondral bone in microdrilled rabbit defects. *Osteoarthritis Cartilage*, 15, 78-89.
- Iliescu, M., Hoemann, C. D., Shive, M. S., Chenite, A., Buschmann, M.D. (2008). Ultrastructure of hybrid chitosan-glycerol phosphate blood clots by environmental scanning electron microscopy. *Microscopy Research Technique*, 71, :236-47.
- Jayakumar, R., Prabhakaran, M., Nair, S.V., Tamura, H. (2010). Novel chitin and chitosan nanofibers in biomedical applications. *Biotechnology Advances*, 28, 142-150.
- Jiang, D., Liang, J., Noble, P. W. (2007). Hyaluronan in tissue injury and repair, *Annual Review of Cell and Developmental Biology*, 23, 435-461.
- Kabanov, V. A. (2005). Polyelectrolyte complexes in solution and in bulk. *Russian Chemical Reviews*, 74, 3–20.
- Kabanov, V. A., Zezin, A. B. (1984). Soluble interpolymeric complexes as a new class of synthetic polyelectrolytes. *Pure Appl. Chem.*, 56, 343-354
- Ker, K., Edwards, P., Rerei, P., Shakur, H., Roberts, I. (2012). Effect of tranexamic acid on surgical bleeding: systematic review and cumulative meta-analysis. *British Medical Journal*, 17, 344 e 3054.
- Khoshmohabat, H., Paydar, S., Kazemi, H. M., Dalfardi, B. (2016). Overview of Agents Used for Emergency Hemostasis. *Trauma Monthly*. 21, e26023.
- Komorowicz, E., Balazs, N., Varga, Z., Szabo, L., Bota, A., Kolev, K. (2017). Hyaluronic acid decreased the mechanical stability, but increases the lytic resistance of fibrin matrices, *Matrix Biol.* 63, 55-68
- Le Cerf, D., Pepin, A. S., Niang, P.M., Cristea, M., Karakasyan-Dia, C., Picton, L. (2014). Formation of polyelectrolyte complexes with diethylaminoethyl-dextran: Charge ratio and molar mass effect. *Carbohydrate Polymers*, 113, 217–224

- Li, T.-T., Lou, C.-W., Chen, A.-P., Lee, M.-C., Ho, T.-F., Chen, Y.-S., Lin, J.-H. (2016). Highly absorbent antibacterial hemostatic dressing for healing severe hemorrhagic wounds, *Materials*, 9, 793.
- Lynn, A. K., Yannas, L.V., Bonfield, W. (2004). Antigenicity and Immunogenicity of Collagen. *J. Biomed. Mater. Res. B Appl. Biomater.*, 71, 343-354
- Marchand, C., Rivard, G. E., Sun, J., Hoemann, C.D. (2009). Solidification mechanisms of chitosan-glycerol phosphate/blood implant for articular cartilage repair. *Osteoarthritis Cartilage*, 17, 953-60.
- Olsen, D., Yang, C., Bodo, M., Chang, R., Leigh, S., Baez, J., Carmichael, D., Perala, M., Hamalainen, E.R., Jarvinen, M., Polarek, J. (2003). Recombinant collagen and gelatin for drug delivery. *Adv. Drug Deliv. Rev.* 55, 1547-1567.
- Ong, S.-Y., Wu, J., Moochhala, S. M., Tan, M.-H., Lu, J. (2008). Development of a chitosan-based wound dressing with improved hemostatic and antimicrobial properties. *Biomaterials*, 29, 4323.
- Pandolfi, M., Hedner, U. (1984). The Effect of Sodium Hyaluronate and Sodium Chondroitin Sulfate on the Coagulation System In Vitro. *Ophthalmology*, 91, 864-866.
- Quan, K., Guofeng, L., Luana, D., Yuana, Q., Taob, L., Wanga, X. (2015). Black hemostatic sponge based on facile prepared cross-linked graphene. *Colloids and Surfaces B: Biointerfaces*, 132, 27-33.
- Riva, F., Casasco, A., Nespoli, E., Icaro Cornaglia, A., Casasco, M., Faga, A., Scevola, S., Mazzini, G., Calligaro, A. (2007). Generation of Human Epidermal Constructs on a Collagen Layer Alone, *Tissue Engineering*, 13, 2769-2779.
- Rossi, S., Ferrari, F., Bonferoni, M.C., Caramella, C. (2001). Characterization of chitosan hydrochloride–mucin rheological interaction: influence of polymer concentration and polymer:mucin weight ratio, *European Journal of Pharmaceutical Sciences*, 12, 479–485
- Rossi, S., Sandri, G., Ferrari, F., Bonferoni, M.C., Caramella, C. (2003). Buccal delivery of acyclovir from films based on chitosan and polyacrylic acid, *Pharmaceutical Development and Technology*, 8, 199 – 208.

- Rossi, S., Sandri, G., Ferrari, F., Bonferoni, M.C., Caramella, C. (2003b). Development of films and matrices based on chitosan and polyacrylic acid for vaginal delivery of acyclovir, *STP Pharma Sci.* 13, 181 – 190.
- Sabnis, S., Block L. H. (2000) Chitosan as an enabling excipient for drug delivery systems I. Molecular modifications. *International Journal of Biological Macromolecules*, 27, 181 – 186.
- Sandri, G., Aguzzi, C., Rossi, S., Bonferoni, M.C., Bruni, G., Boselli, C., Cornaglia, A.I., Riva, F., Viseras, C., Caramella, C., Ferrari, F. (2017). Halloysite and chitosan oligosaccharide nanocomposite for wound healing, *Acta Biomaterialia*, 57, 2016-224.
- Sandri, G., Bonferoni, M. C., D'Autilia, F., Rossi, S., Ferrari, F., Grisoli, P., Sorrenti, M., Catenacci, L., Del Fante, C., Perotti, C., Caramella, C. (2013). Wound dressings based on silver sulfadiazine SLN for tissue repairing, *European Journal of Pharmaceutics and Biopharmaceutics*, 84, 84-90
- Sandri, G., Bonferoni, M.C, Rossi, S., Ferrari, F., Mori, M., Del Fante, C., Perotti, C., Scudeller, L., Caramella, C., (2011). Platelet lysate formulations based on mucoadhesive polymers for the treatment of corneal lesions. *Journal of Pharmacy and Pharmacology*, 63, 189–219.
- Sandri, G., Bonferoni, M.C., Rossi, S., Ferrari, F., Mori, M., Cervio, M., Riva, F., Liakos, I., Athanassiou, A., Saporito, F., Marini, L., Caramella C. (2015) Platelet lysate embedded scaffolds for skin regeneration. *Expert Opin. Drug Del.* 12, 525-54
- Sandri, G., Rossi, S., Bonferoni, M. C., Ferrari, F., Mori, M., Caramella, C. (2012) The role of chitosan as a mucoadhesive agent in mucosal drug delivery. *Journal of Drug Delivery Science and Technology*, 21, 275-284
- Schatz, C., Domard, A., Viton, C., Pichot, C., Delair, T. (2004). Versatile and Efficient Formation of Colloids of Biopolymer-Based Polyelectrolyte Complexes. *Biomacromolecules*, 5, 1882-1892
- Seon, G. M., Lee, M. H., Kwon, B.-J., Kim, M. S., Koo, M.-A., Kim, D., Seomun, Y., Kim, J.-T., Park, J.-C-. (2017). Functional improvement of hemostatic dressing by addition of recombinant baxotropin, *Acta Biomaterialia*, 48, 175-185.

- Shanti Krishna, A., Radhakumary, C., Sreenivasan, K. (2015). Calcium ion modulates protein release from chitosan-hyaluronic acid poly electrolyte gel. *Polymer Engineering and Science*. 55, 2089-2097 (2007). *Journal of Materials Science: Materials in Medicine*, 42, 1719.
- Shields, D. W., Crowley, T. P. (2014). Current concepts, which effect outcome following major hemorrhage. *Journal of emergencies trauma and shock*, 7, 20-24.
- Silbert, J. E., Sugumaran, G. (2002). Biosynthesis of chondroitin/dermatan sulfate, *Iubmb Life*, 54, 177-186,
- Sudheesh Kumar, P. T., Lakshmanan, V. K., Anilkumar, T. V., Ramya, C., Reshmi, P., Unnikrishnan, A. G., Nair, S. V, Jayakumar, R. (2012). Flexible and Microporous Chitosan Hydrogel/Nano ZnO Composite Bandages for Wound Dressing: In Vitro and In Vivo Evaluation. *ACS Applied Materials & Interfaces*, 4, 2618-2629.
- Szucs, M., Sandri, G., Bonferoni, M. C., Caramella, C., Vaghi, P., Szabó-Révész, P., Eros, I. (2008). Mucoadhesive behaviour of emulsion containing polymeric emulsifier. *European. Journal of Pharmaceutical Sciences*, 34, 226–235.
- Tao, Y, Lu, Y., Sun, Y., Gu, B, Lu, W., Pan, J. (2009). Development of mucoadhesive microspheres of acyclovir with enhanced bioavailability. *International Journal of Pharmaceutics*, 378, 30–36.
- Wolberg, A.S., Campbell, R.A. (2008). Thrombin generation, fibrin clot formation and hemostasis, *Transfusion and Apheresis Science*, 38, 15–23
- Yamada, S., Sugahara, K. (2008). Potential therapeutic application of chondroitin sulfate/dermatan sulfate, *Current Drug Discovery. Technologies*, 5, 289-301.

This work was objected of 2 conference presentations:

Saporito, F., Sandri, G., Bonferoni, M.C., Rossi, S., Boselli, C., Caramella, C., Ferrari, F.

Hemostatic dressings loaded tranexamic acid in the treatment of bleeding, 11th AItUN Annual Meeting “Clinical experience and technological innovation in pain therapy: from traditional APIs to cannabinoids”, Padua, Italy, May 11th-12th, 2017 (poster presentation).

Saporito, F., Sandri, G., Bonferoni, M.C., Rossi, S., Boselli, C., Caramella, C., Ferrari, F.

Chitosan/Glycosaminoglycans based dressings as hemostatic systems, 13th International Conference of the European Chitin Society, 8th Symposium of the Iberoamerican Chitin Society, Seville, Spain, May 31st-June 3rd, 2017 (oral presentation).

Chapter 2

Essential oil-loaded lipid nanoparticles for wound healing

Saporito, F., Sandri, G., Bonferoni, M. C., Rossi S., Boselli, C., Icaro Cornaglia, A., Mannucci, B., Grisoli, P., Vigani, B., Ferrari F.

International journal of Nanomedicine (2018), 13, 175-186

Corresponding author: Giuseppina Sandri

2.1 ABSTRACT

Chronic wounds and severe burns are diseases responsible for severe morbidity and even death. Wound repair is a crucial process and tissue regeneration enhancement and infection prevention are key factors to minimize pain, discomfort, and scar formation. The aim of this work was the development of lipid nanoparticles (solid lipid nanoparticles and nanostructured lipid carriers [NLC]), to be loaded with eucalyptus or rosemary essential oils and to be used, as medical devices, to enhance healing of skin wounds. Lipid nanoparticles were based on natural lipids: cocoa butter, as solid lipid, and olive oil or sesame oil, as liquid lipids. Lecithin was chosen as surfactant to stabilize nanoparticles and to prevent their aggregation. The systems were prepared by high shear homogenization followed by ultrasound application. Nanoparticles were characterized for physical–chemical properties, bioadhesion, cytocompatibility, in vitro proliferation enhancement, and wound healing properties toward normal human dermal fibroblasts. Antimicrobial activity of nanoparticles was evaluated against two reference microbial strains, one of *Staphylococcus aureus*, the other of *Streptococcus pyogenes*. Finally, the capability of nanoparticles to promote wound healing in vivo was evaluated on a rat burn model. NLC based on olive oil and loaded with eucalyptus oil showed appropriate physical–chemical properties, good bioadhesion, cytocompatibility, in vitro proliferation enhancement, and wound healing properties toward fibroblasts, associated to antimicrobial properties. Moreover, the in vivo results evidenced the capability of these NLC to enhance the healing process. Olive oil, which is characterized by a high content of oleic acid, proved to exert a synergic effect with eucalyptus oil with respect to antimicrobial activity and wound repair promotion.

2.2 INTRODUCTION

Wound repair is one of the most complex physiological process, involving a multitude of different cell types, the contribution of which is tightly regulated over time. The breakdown of such a complex path could result in wound healing failure, leading to non-healing wounds. The typical path of wound repair includes overlapping stages of inflammation, new tissue generation, and subsequent remodelling of neofomed tissue. These stages take place over dramatically different timescales, lasting from minutes (initial clotting and coagulation) to several months or even years.^{1, 2}

Chronic wounds (including venous leg ulcers, diabetic foot ulcers, arterial insufficiency and pressure ulcers) determine severe morbidity and even mortality especially in older individuals, in particular those affected from diabetes mellitus and vascular diseases. In addition, surgery, more common in older population, presents risk of wound complication. In general, chronic wounds deeply affect quality of life and wound care requires high costs of therapy.³

Resident cells are less proliferating in chronic wounds and possess a morphology similar to that of senescent cells. In particular, fibroblasts of chronic wounds (long-lasting vascular leg ulcers) are characterized by a poorer response to PDGF (platelet derived growth factor), altered capability of transforming beta growth factor (TGF- β) type II receptor expression, and abnormal phosphorylation of critical signal transduction proteins. Such features are typical of cells exposed to low oxygen tension, suggesting that chronic wounds are hypoxic.³

The effect of microbial burden on healing of chronic wound is not completely understood and it is probably underestimated.² The presence of a biofilm was indicated as a critical factor and a correlation between depth and duration of the lesion and the presence of *Staphylococcus* strains was demonstrated.⁴ Moreover, microbial wound colonization (typically due to *Staphylococcus aureus*, *Pseudomonas aeruginosa*, *Streptococcus pyogenes*, and some *Clostridium* strains) was proved responsible for a further delay in wound recovery.⁵ Burns are skin wounds that can

affect a significant portion of the body. Prevention of microbial infection and scar formation are key factors for wound healing.⁶

Many efforts to enhance the effectiveness of wound healing process have been focused on boosting the antimicrobial activity of topically applied devices, preventing infections, promoting tissue regeneration, and minimizing pain, discomfort, and scar formation.

In the last decades, the occurrence of multiresistant bacteria poses a serious problem worldwide, making a challenge the choice of appropriate treatment for patients affected with infected lesions.⁷ Natural products including β -glucans, aloe, honey and especially essential oils have been proposed as antibacterial agents.⁸ In particular, essential oils (EOs) are known to possess antimicrobial effect against multi-resistant bacteria, thanks to a broad spectrum of biological and antimicrobial activity.⁹

EOs are volatile products produced by the secondary metabolism of plants, are extracted from non-woody part (flowers, seeds, leaves, fruits, and roots) and are mainly composed by terpenes and terpenoids and aromatic and aliphatic constituents.¹⁰

Eucalyptus leaf extracts (essential oil from Eucalyptus tree, belonging to the family of Myrtaceae) demonstrated various biological effects, such as antibacterial, antifungal, antiseptic, anti-hyperglycemic and antioxidant activities; 1,8-cineole or eucalyptol is the most important component, responsible for bioactive properties.¹¹

Rosemary essential oil (from *Rosmarinus officinalis*, belonging to the Family of Lamiaceae), which is mainly composed of camphor, 1,8-cineole and borneol, verbenone, α -pinene and camphene, has been historically used as antibacterial, antifungal, and antioxidant.¹²⁻¹⁴

All EOs are unstable volatile compounds and are easily degradable (by oxidation, volatilization, heating, and light): encapsulation in nanosystems should, therefore, represent a useful tool to enhance their stability and improve antibacterial activity.¹⁵

Giving these premises, the aim of this work was the development of lipid nanoparticles, solid lipid nanoparticles (SLN) and nanostructured lipid carriers (NLC), to be loaded with eucalyptus or rosemary essential oils and to be used, as medical devices, to enhance healing of skin wounds.

Lipid nanoparticles were based on natural lipids: cocoa butter, as solid lipid, and olive oil or sesame oil, as liquid lipids. Lecithin was chosen as surfactant to stabilize nanoparticles and to prevent their aggregation. The systems were prepared by high shear homogenization followed by ultrasound application.

Nanoparticles were characterized for physical-chemical properties, bioadhesion, cytocompatibility, *in vitro* proliferation enhancement and wound healing properties towards normal human dermal fibroblasts. Antimicrobial activity of nanoparticles was evaluated against two reference microbial strains, one of *Staphylococcus aureus*, the other of *Streptococcus pyogenes*. Finally, the capability of nanoparticles to promote wound healing *in vivo* was evaluated on a rat burn model.

2.3 EXPERIMENTAL PART

2.3.1 Materials

Lipid nanoparticles (solid lipid nanoparticles, SLN, or nanostructured lipid carriers, NLC), were prepared by using cocoa butter (Aboca S.p.a., Sanspolcro, Italy) as solid lipid, olive oil (o) (Ph. Eur) (Sigma-Aldrich, Milan, Italy) or sesame oil (s) (Sigma-Aldrich) as liquid lipids, L- α -Phosphatidylcholine (L- α -lecithin) from soybean (Sigma-Aldrich) as surfactant, and eucalyptus globulus oil (e) (Janousek, Milan, Italy, Aboca S.p.a., Italy) or rosemary oil (r) (Sigma-Aldrich) as essential oils. Pullulan (pull) (food grade, Hayashibara, Japan, Giusto Faravelli, Milan, Italy) was used as viscosifying agent.

2.3.2 Methods

2.3.2.1 Lipid nanoparticle preparation

Lipid nanoparticles were prepared by high shear homogenization followed by ultrasound application to avoid agglomeration during cooling.¹⁶⁻¹⁷

Cocoa butter (225 mg) was used as lipid phase for SLNs, whereas NLCs were based on a lipid phase made of cocoa butter (150 mg) mixed with olive oil (75 mg) or sesame oil (75 mg).

Each lipid phase was melted at 40°C and eucalyptus or rosemary essential oil (75 mg) was added. The total amounts of lipid components were the same for SLN and NLC. An aqueous phase (12.5 ml) containing lecithin (150 mg) was heated to 40 °C and poured into the lipid phase under homogenization at 24000 rpm for 5 min with an UltraTurrax equipment (T25, IKA, Labortechnik, Denmark). The resulting emulsion was cooled by diluting with distilled water (12 ml) at 2-8 °C and subjected to ultrasounds (ultrasound frequency 37 kHz) (Elmasonic S80 H, Elma Hans Schmidbauer GmbH & Co, Germany) for 10 min, to avoid agglomeration.

The resulting lipid nanoparticle suspension was characterized as such or after addition of pullulan (pull) to obtain 5% w/w as final pullulan concentration in the lipid

nanoparticle suspension. The quali-quantitative composition of all the nanosystems is reported in Table 1.

Table 1: quali-quantitative compositions of the systems prepared.

	Lecithin (mg)	Cocoa butter (mg)	Olive oil (mg)	Sesame oil (mg)	Eucalyptus oil (mg)	Rosemary oil (mg)
SLN b	150	225	-	-	-	-
SLN e	150	225	-	-	75	-
SLN r	150	225	-	-	-	75
NLC o/b	150	150	75	-	-	-
NLC s/b	150	150	-	75	-	-
NLC o/e	150	150	75	-	75	
NLC o/r	150	150	75	-	-	75
NLC s/b	150	150	-	75	-	-
NLC s/e	150	150	-	75	75	-
NLC s/r	150	150	-	75	-	75

2.3.2.2 Lipid nanoparticle characterization

2.3.2.2.1 Physical-chemical properties

Particle size (PS) and polydispersity index (PI) of all developed nanosystems were assessed at 25°C by PCS (photon correlation spectroscopy) at an angle of 90° (Beckman Coulter N5, Instrumentation Laboratory, Italy) after suitable dilution of samples with bidistilled and filtered water (0.22 µm, HA Millipore, Italy).

Physical stability of nanoparticles was evaluated up to 90 days of storage at 2-8°C.

Zeta potential of the more promising formulation was measured at 25 °C (Nano ZSP, Malvern Instruments, Italy).

These nanosystems were also analyzed by a transmission electron microscope TEM (Jeol JEM-1200 EX II, JP) equipped with a TEM CCD camera (Mega View III, Jeol, JP), after sample deposition on copper grids (Formavar/Carbon 300 mesh, Agar Scientific, UK).

2.3.2.2.2 Eucalyptus essential oil assay

Loading of eucalyptus essential oil in lipid carriers was determined by means of Head Space Solid Phase Microextraction (HSSPME) coupled with gas chromatography-mass spectrometry (according to Eucalyptus oil – 07/2010:0390, Eur Ph. 9.0 Ed monograph). The following HSSPME experimental parameters were used: sample amount, 100 µl; water addition, 10 ml; fiber polydimethylsiloxane (PDMS, 100 µm); extraction temperature, 40 °C; extraction time, 30 min; desorption temperature, 280 °C; desorption time, 5 min.

100µl aliquots of eucalyptus essential oil extracted from lipid nanoparticles and eucalyptus essential oil dispersed in an aqueous lecithin solution at the same concentration of lipid nanoparticles were separately injected.

GC/MS analysis was effected on a Thermo Scientific DSQII single quadrupole GC/MS system (Xcalibur MS Software Version 2.1) equipped with a Restek Rtx-5 MS capillary column (30 m, 0.25 mm i.d., 0.25 µm film thickness), according to the following temperature program: 4 min at 60 °C, then 10 °C/min up to 220 °C, held for 10 min; carrier gas helium, 1.0 ml/min; injector temperature, 280 °C, splitless mode; transfer line temperature 250 °C; run time 30 min. All mass spectra were acquired in electron-impact (EI) mode with ionization voltage equal to 70 eV; ion source temperature 250 °C; acquisition mass range 35-500 Da.

Each sample was analyzed in triplicate. The content percentage of each oil component was computed from the corresponding GC/MS peak area without applying any correction factor.

2.3.2.2.3 Bioadhesion measurements

Bioadhesion measurements were carried out using a texture analyzer apparatus (TA.XT plus, Stable Microsystems, ENCO, Italy) equipped with a 1 kg load cell, a cylinder probe having a diameter of 10 mm (P10) and the A/MUC measuring system.¹⁸⁻¹⁹. The A/MUC measuring system consists of a support in which a biological substrate can be fixed. In this case, the biological substrate chosen to mimic

damaged skin was an egg shell membrane¹⁸, wetted with 100 μ l of isotonic saline (NaCl 0.9% w/v). To recover the membrane, the egg shell was placed in a 0.5 M HCl solution for 1h. The A/MUC system was thermostet at 32°C. 100 μ l of each nanosystem containing 5% w/w of pullulan (pull), and 5%/w pullulan solution, as control, were placed onto the cylinder probe covered by filter paper disc and the sample and the biological substrate were put in contact under a preload of 2.5 N for 3 min.

The cylinder probe was then moved upward at a prefixed speed of 2.5 mm/s up to the complete separation of the bioadhesive interface (egg shell membrane-sample).

The force of detachment was recorded as a function of displacement and the bioadhesion parameter work of adhesion (area under the curve [AUC]) (mN mm, AUC) was calculated as the area under the force vs displacement curve.

The normalized adhesion parameter $\Delta AUC/AUC$ was subsequently calculated according to the following equation:

$$\Delta AUC/AUC = (AUC_{bs} - AUC_{blank})/AUC_{blank}$$

where:

AUC_{bs} = work of adhesion obtained in presence of the biological substrate;

AUC_{blank} = work of adhesion obtained from blank measurements.

Such a normalization should allow comparison of the bioadhesive properties of samples characterized by different cohesive properties (viscosity).²⁰

2.3.2.3 In vitro biocompatibility

2.3.2.3.1 Cytotoxicity test

Normal Human Dermal Fibroblasts (NHDF) from juvenile foreskin (PromoCell GmbH, VWR, Milan, Italy) were used. Cells between the 2nd and 5th passage were employed for all the experiments. As growth medium (GM) Dulbecco's modified Eagle medium (DMEM, Lonza, Milan, Italy), supplemented with 10% fetal calf serum (FCS, Euroclone, Milan, Italy) and 200 IU/ml penicillin-0.2 mg/ml streptomycin (PBI International, Milan, Italy) was used.

Fibroblasts were seeded in each well of 96-well plates (area 0.34 cm²) at a density of 10⁵ cells/cm². Cells were grown 24 h at 37°C in a 95% air/ 5% CO₂ atmosphere with 95% relative humidity to obtain subconfluence.

Then cells were washed with saline solution and subsequently put in contact with 200 µl of each sample. Nanoparticle suspensions, as described in section Lipid nanoparticle preparation, were diluted with GM in a 1/20, 1/40, and 1/100 w/w ratio. In the case of 1/100 dilution nanoparticle suspensions containing 5% w/w pullulan, as described in the section Lipid nanoparticle preparation, were also examined and cytocompatibility was compared with that of 5% w/w pull solution diluted 1/100 with GM. Cells kept in contact with GM were considered as positive control (standard growth conditions). After 3 h contact, an MTT test was performed. This test is based on the activity of mitochondrial dehydrogenases of vital cells, which convert MTT to formazan. 125 µl of MTT solution (Sigma Aldrich, Italy) at 0.25 µg/ml concentration in HBSS (Hank's Buffered Salt Solution) pH 7.4 was put in contact with each sample for 3 h. The reagent was then removed from each well and the cells were washed with PBS (150 µl) to remove the samples and the unreacted MTT solution. After PBS removal, 100 µl of DMSO were put in each well and the absorbance was assayed at 570 nm by means of an ELISA plate reader (Imark Absorbance Reader, Biorad, I), with a reference wavelength set at 655 nm. Cell viability was calculated as % ratio between the absorbance of cells treated with nanoparticle suspension and the absorbance of the cells kept in contact with the control, growth medium (GM).

2.3.2.3.2 Proliferation test

In each well of a 96-well plate, 2x10⁴ fibroblasts/well were seeded and grown 24 h to obtain subconfluence. Afterwards, cell substrates were put in contact with 200 µl of each sample. Nanoparticle suspensions and nanoparticle suspensions containing 5% w/w pullulan, as described in the section Lipid nanoparticle preparation, were diluted with GM in a 1/100 w/w ratio. Cells kept in contact with GM were considered as positive control (standard growth conditions). After 48 h contact, an MTT test was performed as previously described.

2.3.2.3.3 Cell migration/proliferation assay for wound healing

The gap closure cell migration/proliferation assay was performed according to a previously described procedure.^{21,22} The assay employs Petri μ -Dishes (35 mm, Ibidi, Giardini, Italy), which contain a special insert consisting of two cell chambers (growth area: 0.22 cm² each) divided by a septum (500 μ m \pm 50 μ m in width), intended to simulate a cell free gap.

Fibroblasts were seeded in each chamber at 10⁵ cells/cm² concentration and grown at confluence in standard conditions as previously described. After 24h, cells reached confluence and the insert was removed displaying two areas of cell substrates divided by the gap. The cell substrates were put in contact with 200 μ l of each sample. Nanoparticle suspensions and nanoparticle suspensions containing 5% w/w pullulan, as described in the section Lipid nanoparticle preparation, diluted with GM in a 1/100 w/w ratio were tested. Cells kept in contact with GM were considered as control. At prefixed times (0 and 48 h), microphotographs were taken to evaluate cell migration in the gap.

As fibroblasts are migrating cells, a Br deoxyuridine test was associated to in vitro wound healing test to identify cells that were in proliferating phase (S-phase) (positively green and blue stained) and filled the gaps.

In particular, this test enabled identification of cell proliferation properties by assessing 5-Bromo-2'-Deoxyuridine (BrdU) incorporation in DNA synthesis. To this aim, in the last hour of culture, cells were labeled by adding 30 Mm BrdU (Sigma-Aldrich) to the medium; then cells were washed with PBS and fixed in 70% ethanol. The incorporation of BrdU was detected by an immunostaining reaction with anti-BrdU antibody (Amersham Bioscience, Italy) as follows: the substrates were washed with PBS and incubated with HCl 2N for 30 min at room temperature. Cells were neutralized in 0.1 M sodium tetraborate (pH 8.5) for 15 min, washed twice for 5 min in PBS and incubated for 20 min in a blocking solution, consisting of 1% w/v BSA (bovine serum albumin) (Sigma-Aldrich, Italy) and 0.02 % w/v Tween 20 (Sigma-Aldrich, Italy) in PBS. Cells were then incubated for 1 h with mouse anti-BrdU antibody, diluted 1:100 w/v in blocking solution, washed 3 times (10 min each) with

the same solution and then incubated for 30 min in blocking solution containing anti-mouse IgG FITC-antibody (1:100 w/v dilution, Sigma-Aldrich, Italy). Finally, cell substrates were again extensively washed with PBS, counterstained for DNA with 0.5 mg/ml Hoechst 33258 (Sigma-Aldrich, Italy), and mounted in Mowiol (Sigma-Aldrich, Italy). Cells characterized by positive BrdU immunofluorescence were counted by using a fluorescence microscope (Zeiss Axiophot, Carl Zeiss, Germany).

2.3.2.4 Antimicrobial properties

The antimicrobial properties of nanoparticles and eucalyptus essential oil dispersed in lecithin solution at the same concentration of nanoparticles were assessed against the following reference bacterial strains: *Staphylococcus aureus* ATCC 6538 and *Streptococcus pyogenes* ATCC 19615. Before testing, bacteria were grown overnight in Tryptone Soya Broth (Oxoid, UK) at 37 °C and in Todd Hewitt Broth (THB, Oxoid, UK) at 37 °C in the presence of 5% CO₂ in the case of *S. pyogenes*. The cultures were centrifuged at 224 g for 20 min, to separate microorganisms from culture broth and then washed with sterile distilled water. Washed cells were re-suspended in Dulbecco's PBS and optical density (OD) at 650 nm wavelength was adjusted to 0.2, corresponding approximately to 1×10^7 - 1×10^8 colony forming units (CFU)/ml. The antimicrobial activity was determined with the macrodilution broth method, according to Clinical and Laboratory Standards Institute guidelines (2009), with some modifications. The desired sample concentration was achieved through by adding in 15 mm×100 mm test tubes an appropriate sample volume (nanoparticle suspension, as described in the section Lipid nanoparticle preparation) to 1 ml of double-concentrate isoSensitest broth (ISB, Oxoid, UK). Bacterial suspensions were added to the test tubes. The minimum inhibitory concentration (MIC) was evaluated after 24 h incubation at 37°C as the lowest concentration that completely inhibited the formation of visible microbial growth. Control test tubes contained microorganisms in culture broth without nanoparticles. Various concentrations of each sample were tested.

2.3.2.5 In vivo wound healing efficacy in rat model

All experiments on animals were carried out in full compliance with the standard international ethical guidelines (European Communities Council Directive 86/609/EEC), approved by Italian Health Ministry (D.L. 116/92). The study protocol was approved by the Local Institutional Ethics Committee of the University of Pavia for the use of animals. Male rats (Wistar 200–250 g) were anesthetized with equitensine at 3 ml/kg (39 mM pentobarbital, 256 mM chloral hydrate, 86 mM MgSO₄, 10% ethanol v/v, and 39.6% propyleneglycol v/v) and shaved to remove all hair from their backs. Three circular full thickness burns, having a diameter of 4 mm, were produced on the back of the animals by contact with an aluminum rod (105°C for 40 s). 24 h later, the formed blisters were removed using a 4-mm diameter biopsy punch to obtain a full-thickness lesions. Either 20 µl of nanoparticle suspension or 20 µl of nanoparticle suspension containing 5% w/w pullulan, as described in the section Lipid nanoparticle preparation, were applied to the lesions. Lesions treated with 20 µl of saline solution were considered as control. After treatment, each lesion was protected with a sterile gauze and the rat's back was wrapped with a surgery stretch (Safety, Italy). At prefixed times after blister removal (0, 3, 7, 10, 14 and 18 days), photographs of the lesions were taken by a digital camera (Sigma SD 14, Sigma Corporation, Italy) which allowed sizing the lesions and monitoring the healing process. Each treatment was repeated after each photograph. The dimensions of wounded area were determined by an image analysis software (ICY, Institute Pasteur, France).

2.3.2.6 Histological analysis

After 18th day treatment, the animals were sacrificed, full thickness biopsies were made in correspondence of the lesion area and histological analysis of the excised tissues was performed. A biopsy of intact skin was also taken for comparison. Tissue samples were bisected along the widest line of the wound, fixed for 48 h in 4% w/v neutral buffered paraformaldehyde, dehydrated with gradient ethanol series, cleared

in xylene and embedded in paraffin. Sections (8 μm) were obtained using a Leitz microtome (Wetzlar, Germany) and were stained with haematoxylin and eosin (H&E). The slices were examined at 5x magnification under a light microscope (Zeiss Axiophot, Carl Zeiss, Germany), equipped with a digital camera.

2.3.2.7 Statistical analysis

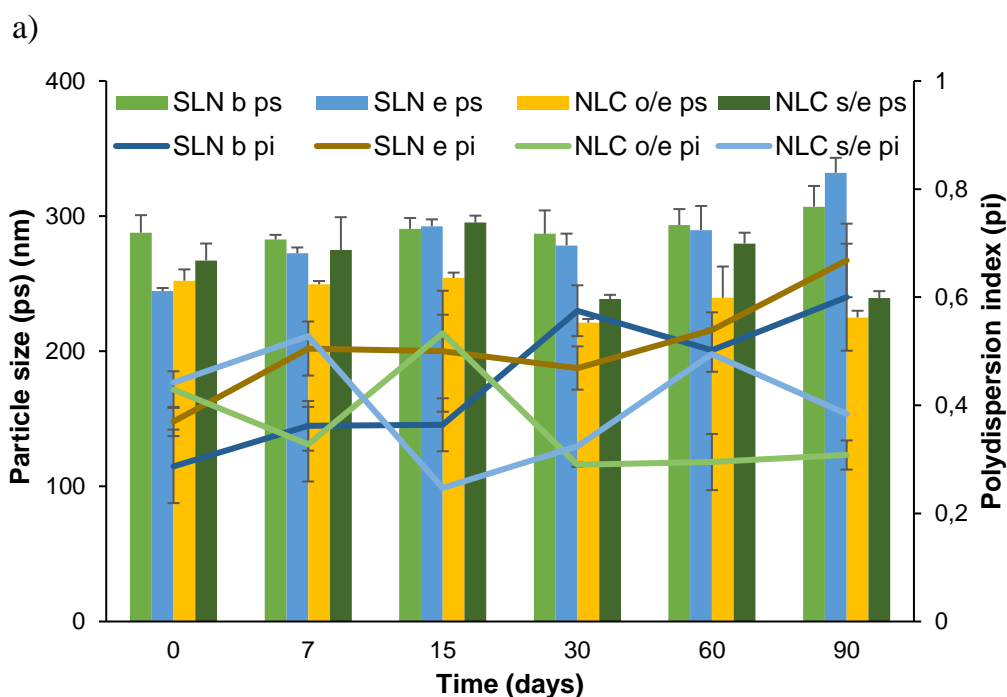
Statistical differences were evaluated by means of one-way Anova followed by multiple range test (Stat Graphics 5.0, Statistical Graphics Corporation, MD, USA). Differences were considered significant at $p < 0.05$ level.

2.4 RESULTS AND DISCUSSION

2.4.1 Physical-chemical characterization of nanoparticles

Figure 1 (a and b) reports the particle size (PS) and polydispersion index (PI) of all lipid nanoparticles developed as a function of storage time (2-8 °C). Figure 1 (a) shows the results of SLN and NLC loaded with eucalyptus oil (e) or rosemary oil (r) and prepared by using olive oil (o), as liquid lipid, while Figure 1 (b) shows the results of analogous nanosystems containing sesame oil (s), as liquid lipid.

Independently of nanoparticle composition, PS ranged from 220 to 300 nm and remained almost constant up to 3 months storage. Similar results were obtained for PI that was close to 0.5, indicating nanoparticle populations characterized by a quite wide particle size distribution, stable up to 3 months.



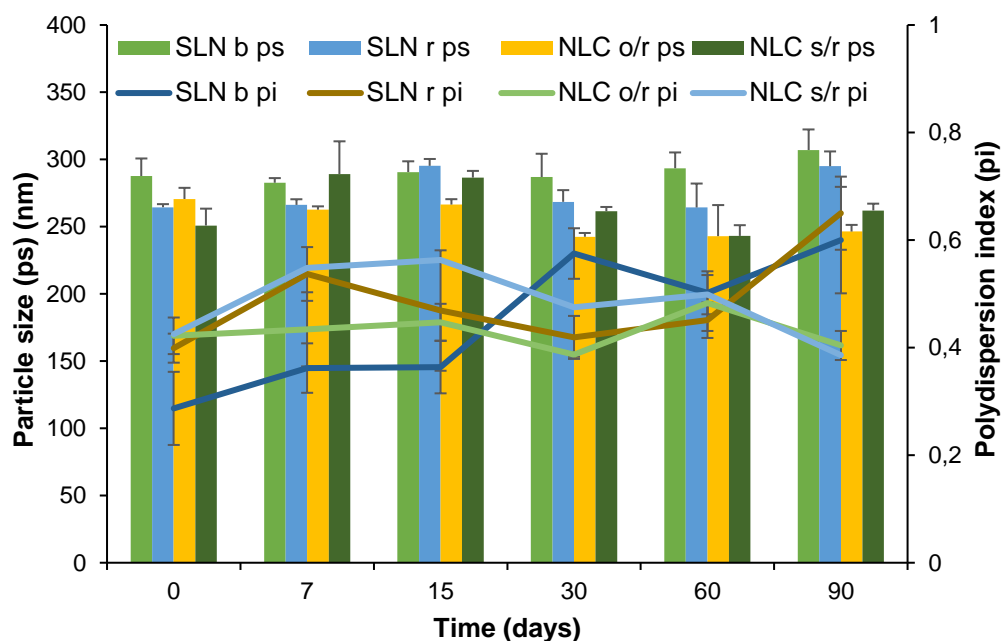


Figure 1: particle size (ps) and polydispersion index (pi) as a function of storage time (2-8 °C): SLN and NLC prepared by using both eucalyptus oil (e) or rosemary oil (r) and a) olive oil (o) or b) sesame oil (s) as liquid lipids (mean values \pm sd; n=6).

2.4.2 Bioadhesion properties

Figure 2 shows the normalized bioadhesion parameter (Δ AUC/AUC) of all the nanosystems developed, nanoparticle suspensions and nanoparticle suspensions containing 5% w/w pullulan.

Pullulan was characterized by good bioadhesive properties. Although all nanoparticles were stabilized lecithin and it is conceivable that their surface was coated by the same lecithin layers, different bioadhesion properties were observed.

Both SLN systems, either loaded with eucalyptus oil or with rosemary oil, were characterized by scarce bioadhesive properties. This result could be attributable to rigid structure of these nanoparticles, which impaired their interaction with the biological substrates, preventing the formation of the bioadhesive joint. On the contrary, all NLC formulations were characterized by good bioadhesive properties.

The systems containing olive oil showed bioadhesion parameters significantly higher than those of the corresponding systems prepared by using sesame oil (one way ANOVA, multiple range test $p < 0.05$).

Olive oil contains 85% of unsaturated fatty acids, in particular 70 % of monounsaturated (mainly oleic and palmitoleic acid) and about 15% of polyunsaturated ones (mainly linoleic and linolenic acid). On the contrary, sesame oil contains about 85 % unsaturated acids; mono- and poly-unsaturated acids, which are present in comparable amounts (41% of polyunsaturated -linoleic acid and 39% of monounsaturated -oleic acid).

These differences in composition could determine a different lipid packaging in nanoparticle core and a consequent modification of NLC flexibility. This could cause a different degree of interaction with the biological substrate and consequently a different strength of the bioadhesive joint.^{23, 24} Bioadhesion is an important property to assure efficacy, since it allows an intimate contact between wounded area and formulation.

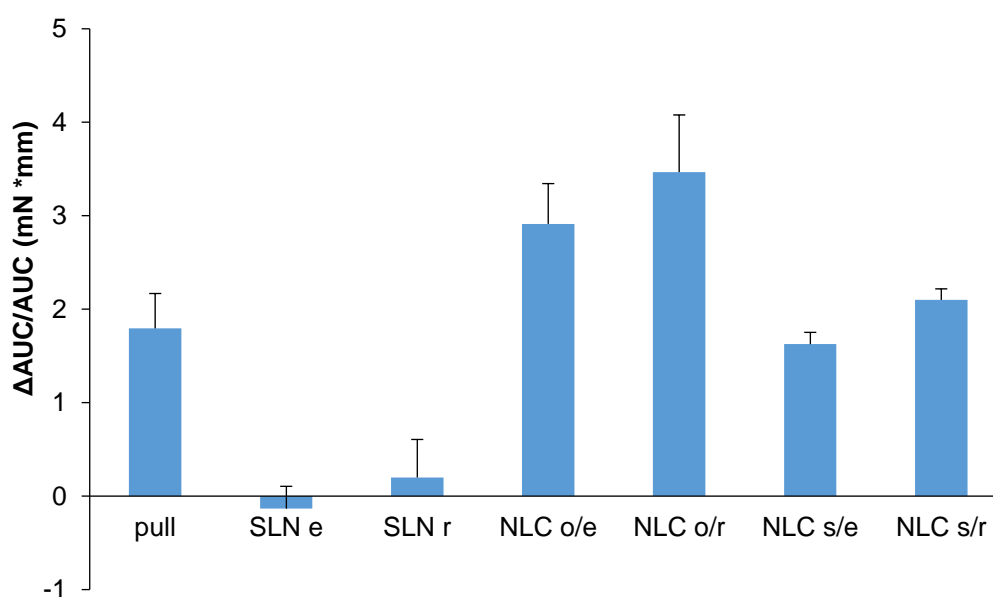


Figure 2: bioadhesion values as normalized work of adhesion ($\Delta AUC/AUC$) evaluated for all the nanosystems developed and for pull solution at 5% w/w (mean values \pm sd; n=6).

2.4.3 In vitro biocompatibility properties

In Figure 3, cytocompatibility (% viability) of all the nanosystems developed, loaded with eucalyptus or rosemary oil are compared. All the nanosystems (independently of the essential oil loaded) were characterized by concentration-dependent cytocompatibility. For a given formulation, the higher nanoparticle concentration (corresponding to the lowest dilution, 1/20) was characterized by % viability ranging from 30 to 50 %, not significantly different than that of 1/40 dilution. On the contrary, 1/100 dilution determined a % viability ranging from 50 to 95%, significantly higher than those of the other two dilutions (one way ANOVA, multiple range test $p < 0.05$). The presence of pullulan (pull) determined an increase in cytocompatibility. NLC systems based on olive oil and containing 5% w/w pullulan were characterized at 1/100 dilution by cytocompatibility not significantly different than that of GM and significantly higher than those of NLC containing sesame oil (one way ANOVA, multiple range test $p < 0.05$).

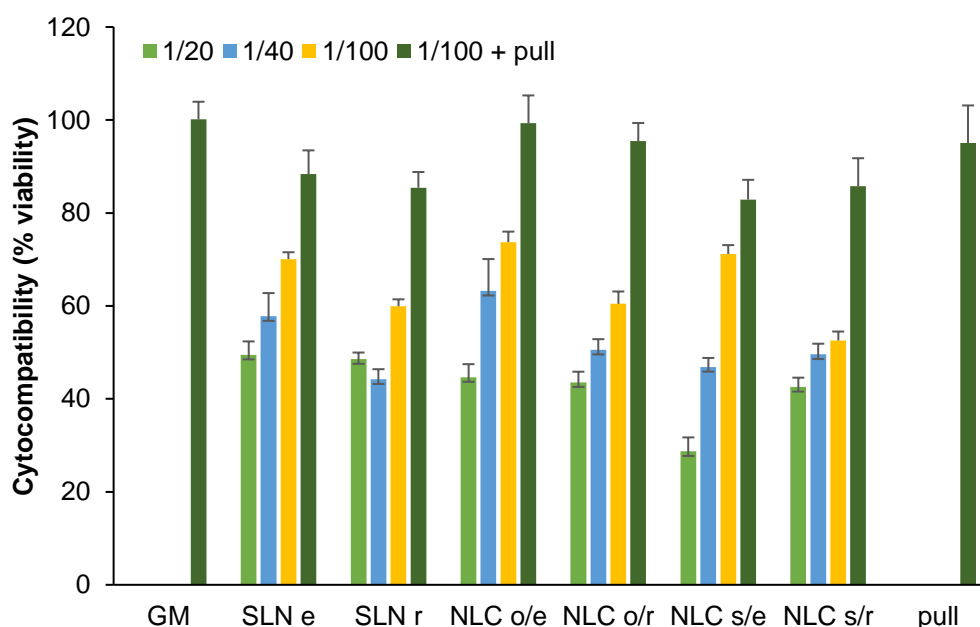


Figure 3: cytocompatibility (viability %) for all the nanosystems developed loaded with eucalyptus or rosemary oils. Three dilutions were tested (1/20, 1/40 and 1/100). Nanoparticles in 5% pullulan solution were also tested at 1/100 dilution. Growth medium (GM) was used as comparison (positive control) (mean values \pm sd; $n=8$).

2.4.4 Proliferation properties

Proliferation (% viability) results of all the nanosystems developed, loaded with eucalyptus or rosemary oil, are reported in Figure 4. Nanoparticles suspension and nanoparticle suspension containing 5% w/w were diluted at 1/100 and their proliferation properties compared. The nanosystems were characterized by proliferation properties not significantly different than those of the control (GM).

In comparison with GM, 5% w/w pullulan solution (dilution 1/100) was able to significantly enhance cell proliferation. All nanosystems containing 5% w/w pullulan solution, were characterized by a relevant improvement of proliferation properties; with the exception of NLC s/e, based on sesame oil and loaded with eucalyptus oil, all nanoparticles determined an enhancement of cell growth significantly higher than that of standard growth conditions (control, GM) (one way ANOVA, multiple range test $p < 0.05$). NLC o/e, based on olive oil and loaded with eucalyptus oil, was characterized by the best performance in terms of proliferation enhancement properties.

The presence of olive oil seems to favor cell proliferation: this result could be due to the high content of oleic acid, a fatty acid previously described for its good proliferation properties:²⁵ in fact the content of oleic acid is almost two folds greater than that of sesame oil.

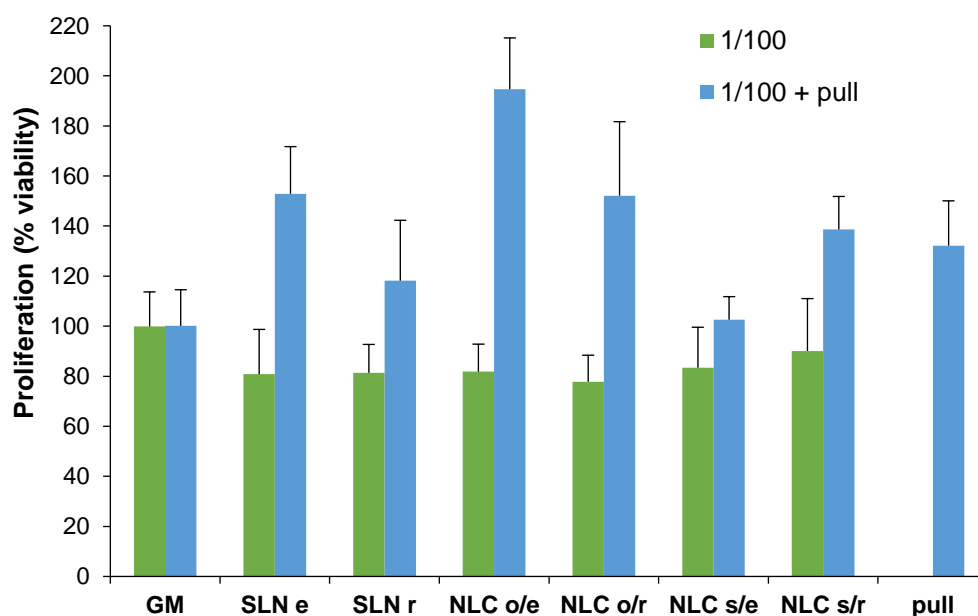


Figure 4: proliferation (% viability) for all the nanosystems developed loaded with eucalyptus or rosemary oils. Nanoparticles at 1/100 dilution and nanoparticles at 1/100 dilution in 5% pullulan solution were tested. Growth medium (GM) was used as comparison (positive control) (mean values \pm sd; n=8).

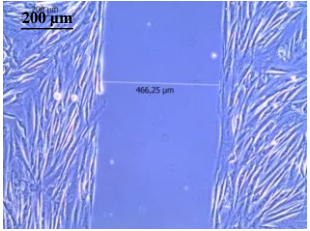
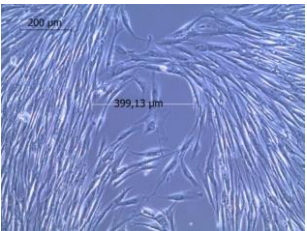
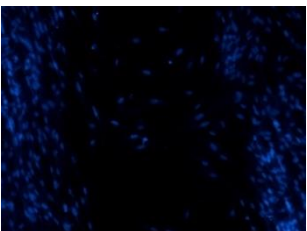
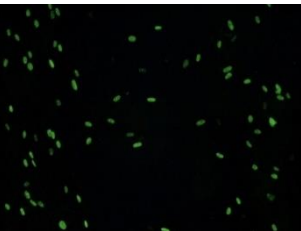
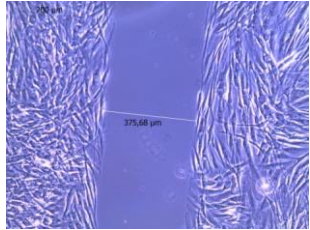
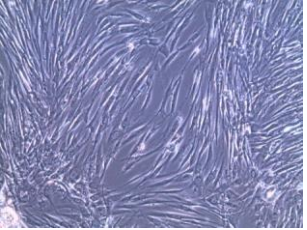
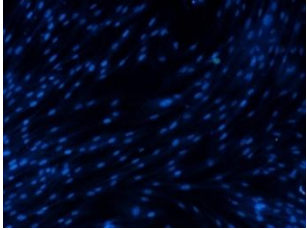
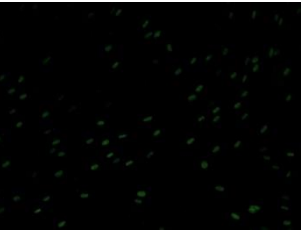
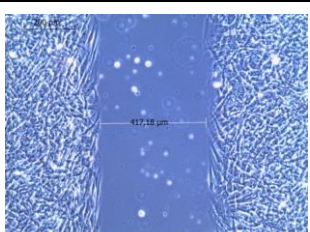
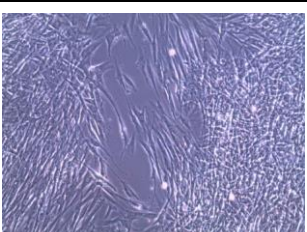
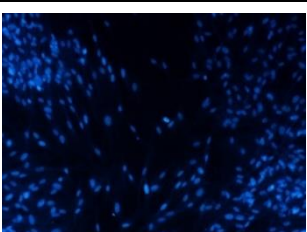
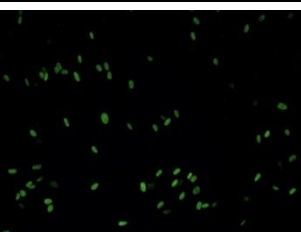
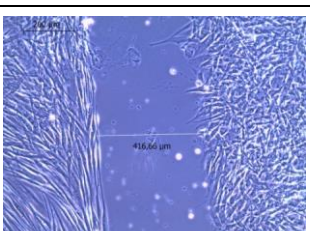
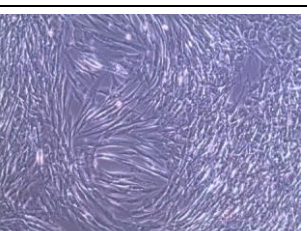
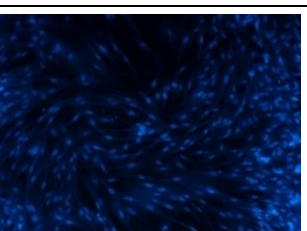
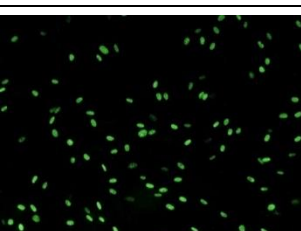
2.4.5 Cell migration/proliferation properties in an *in vitro* wound healing test

Figure 5 reports the microphotographs of cell substrates taken at time 0 (immediately after insert removal) and after 48 h growing, by using an optical microscope or a fluorescence microscope (cell nuclei stained with Hoechst 33258 in blue and proliferating cells stained with anti-BrdU antibody in green).

All the samples were able to promote cell migration/proliferation in the gaps at least as the growth medium (GM). In particular, cell substrates put in contact with NLC o/e, based on olive oil and loaded with eucalyptus oil, containing 5% w/w pullulan, showed a complete gap closure within 48 h after insert removal and a cell concentration higher than that of standard growth condition (control, GM). This

nanosystem, therefore, demonstrated to be more effective in promoting wound healing *in vitro*.

The contact with NLC o/e determined a higher concentration of green stained cells in the gap, that were proliferating cells, with respect to the other nanosystems. It is conceivable that oleic acid determined a synergic effect with eucalyptus oil to enhance cell proliferation. Given these results, NLC o/e was chosen as the most promising nanosystem and subjected to further characterization.

	Time 0	48 h	48 h nuclei	48 h BrdU
GM				
SLN e				
SLN r				
NLC o/e				

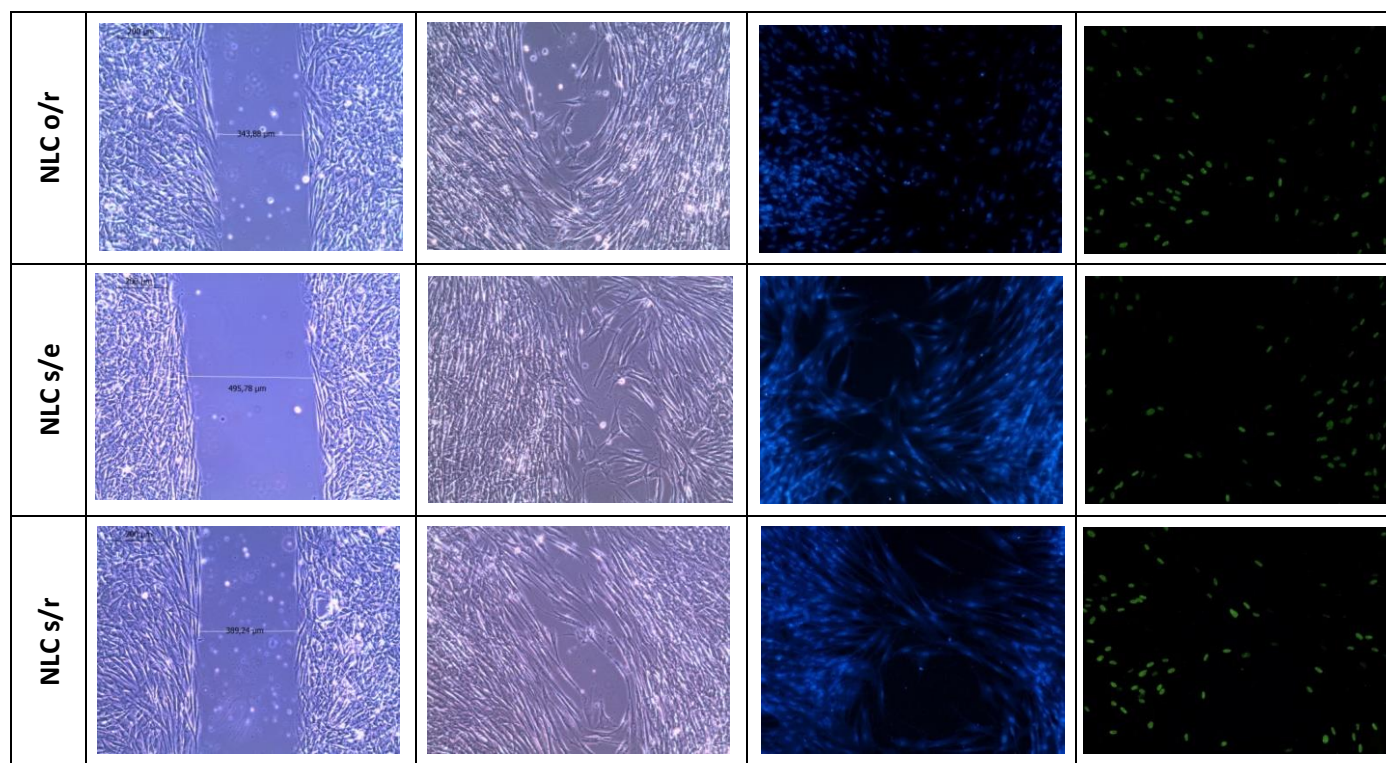


Figure 5: microphotographs of cell substrates taken at time 0 (immediately after insert removal) and growing 48 h by using optical microscope or fluorescence microscope (cell nuclei stained with Hoechst 33258 in blue and proliferating cells stained with anti-BrdU antibody in green).

2.4.6 In vitro characterization of NLCo/e

Figure 6 reports the TEM microphotograph of NLC o/e. Nanoparticles were round shaped and showed a relatively small size-dispersion around 50-60 nm, smaller than that expected on the basis of PCS measurements, which were probably affected by the presence of aggregates, responsible for a high polydispersion index (close to 0.5).²⁶ NLC o/e was characterized by a highly negative zeta potential equal to -22.07 ± 0.29 mV (mean value \pm s.d., n=3). These results should conceivably be due to the presence onto nanoparticle surface of lecithin, which was proved to confer a negative zeta potential to nanosystems.²⁷ The presence of lecithin allowed particle stabilization and controlled particle aggregation as evidenced by 3-month stability results (see paragraph 3.1). Eucalyptus essential oil loaded in NLC o/e was close to 100% (101.74 ± 9.06 %), indicating that the preparation procedure did not impair oil stability and loading, although it is a volatile extract.

Pure cocoa butter melting starts at 31°C and is completed at 34°C. After cutaneous application, given that skin temperature is 32°C, melting of the lipid core was conceivably the mechanism enabling the release of eucalyptus essential oil.

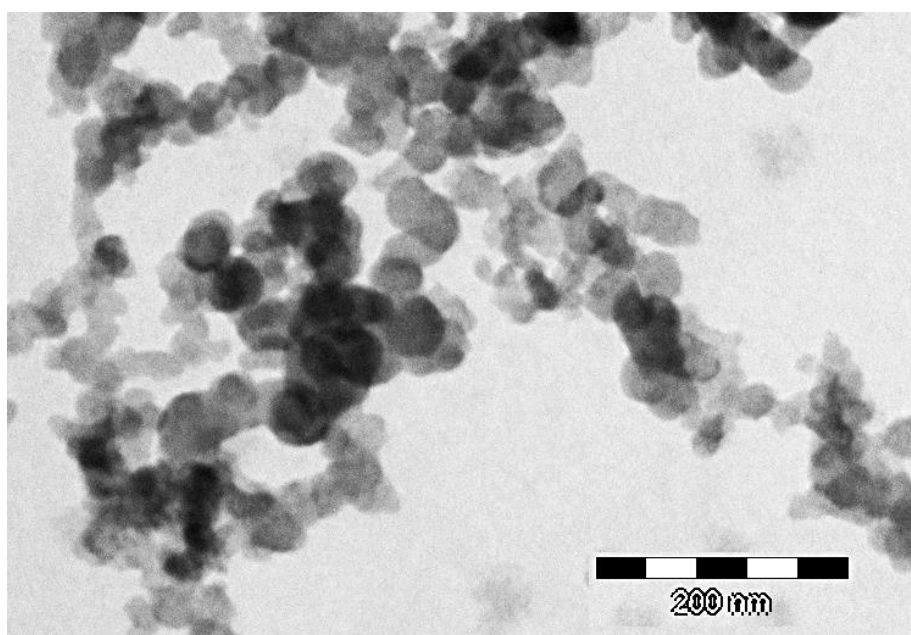


Figure 6: TEM microphotograph of NLCo/e.

The MIC values measured against *Staphylococcus aureus* and *Streptococcus pyogenes* for NLC o/e and for eucalyptus essential oil, at the same essential oil concentration, are reported in Table 2.

Eucalyptus oil was characterized by the same MIC value (3 mg/ml) against *Staphylococcus aureus*, either as a free oil or after loading into NLC, indicating that encapsulation did not impair its antimicrobial activity. On the contrary, it showed an enhanced antimicrobial activity against *Streptococcus pyogenes* when encapsulated in NLC, because MIC values decreased from 1.5 mg/ml, for free oil, to 0.75 mg/ml, for NLC o/e.

Table 2: MIC values against *S. aureus* and *S. Pyogenes* for eucalyptus essential oil and NLC o/e.

	Strain	MIC (mg/ml)
Eucalyptus oil	<i>S. aureus</i> ATCC 6538	3
	<i>S. pyogenes</i> ATCC 19615	1.5
NLC o/e	<i>S. aureus</i> ATCC 6538	3
	<i>S. pyogenes</i> ATCC 19615	0.75

2.4.7 In vivo wound healing efficacy of NLC o/e

Figure 7 reports the profiles of wound area (cm²) as function of time. All the wounds treated with NLCo/e, as either nanoparticle suspension or nanoparticle suspension containing 5% w/w pullulan, and with saline solution (control) showed similar lesion area vs time profiles. After 4 days of treatment, NLCo/e suspension showed a significantly lower lesion area (not significantly greater than time 0) with respect to NLCo/e containing pullulan and saline solution, which were characterized by a significantly greater dimension that time 0 (one way ANOVA, multiple range test

$p < 0.05$). At the 7th and 10th day of treatment both the lesions treated with NLC o/e, as either nanoparticle suspension or as nanoparticle suspension containing pullulan, presented dimensions not significantly different from each other and significantly lower than the lesion treated with of saline solution (one way ANOVA, multiple range test $p < 0.05$). After 15-day treatment NLC o/e suspension presented the highest lesion reduction (one way ANOVA, multiple range test $p < 0.05$) indicating the capability of these nanoparticles to speed up tissue repairing. Given the high variability of results, such a difference could not be observed after 18-day of treatment.

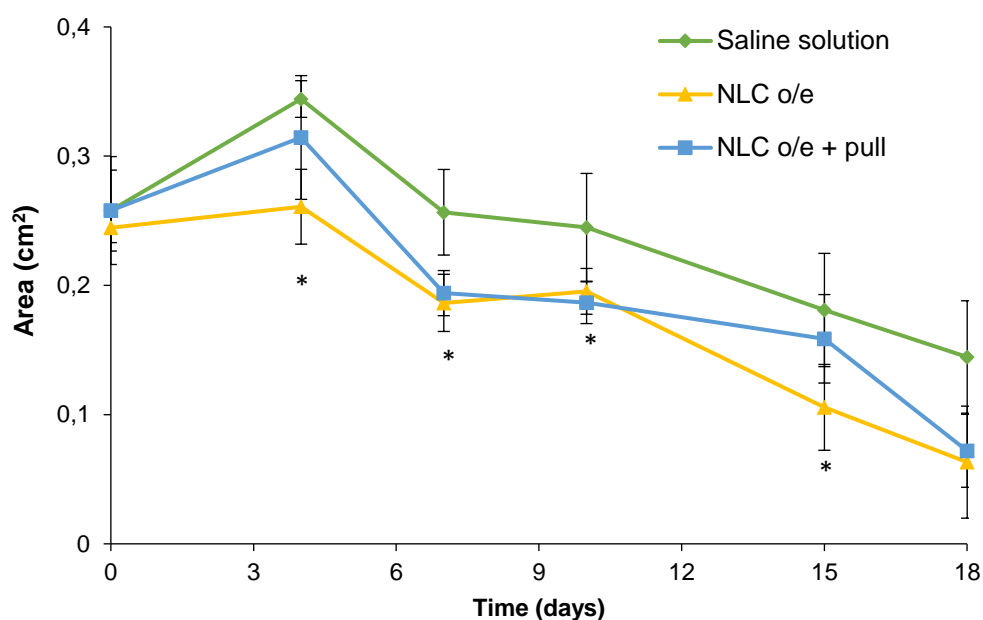


Figure 7: profiles of wound area (cm²) as function of the time evaluated for wounds treated with both the nanosystems (NLC o/e without and with pullulan at 5% w/w solution) and saline solutions (control) (mean values \pm sd; n=3).

Figure 8 reports microphotographs of skin sections of the wounded area, stained with haematoxylin and eosin, taken after 18 days of treatment with saline solution (a), NLC o/e suspension (b) NLC o/e suspension containing pullulan (c). Microphotograph of intact skin (d) is reported for comparison.

In correspondence with the wound treated with saline solution (control) (Fig. 8 a), a large part of epidermis was replaced by an eosinophil necrotic tissue (asterisk) and in the peripheral regions of the lesion, epidermis (bracket) was visible. In the underlying dermal connective, an abundant granulation tissue (arrow) was present; moreover, collagen fibers were dispersed and not yet organized in large bundles, typical of the reticular layer of the dermis. There was no evidence of skin appendages (hair follicles and glands), while there were numerous vacuoles of different size (black star), delimited by a wall consisting of a monolayer of flattened cells (endothelium), probably corresponding to dilated vessels.

In correspondence with the wound treated with NLCo/e suspension (Fig. 8 b), epidermis (bracket) appeared continuous and well organized in multiple cell layers with a fair degree of keratinization. In the underlying connective tissue, skin appendages were vacant, but dermal papillae (white star) began to reform. A mild inflammatory infiltrate was visible (arrow), as well as a number of blood vessels (black star). Some scattered collagen fibers were present at the border with epidermis, while in the reticular layer of the dermis, the typical large bundles of collagen (white arrow) were already formed.

In correspondence with the wound treated with NLC o/e suspension containing 5% w/w pullulan (Fig. 8 c), skin appeared completely re-epithelized, epidermis (bracket) was well organized in multiple cell layers, with a fair degree of keratinization, similar to the structures observed in the section obtained from wound treated with NLCo/e (Fig. 8 b). Dermal papillae (white star) were in developing phase, furthermore granulation tissue (arrows) and dilated vessels (black star) were present in a limited area, while collagen fibers were organized in large bundles, typical of the reticular layer of the dermis (white arrow).

Normal skin (Fig. 8 d) was characterized by epidermis (bracket), well-organized in multiple cell layers, with a fair degree of keratinization and showed numerous dermal papillae (white star). Dermal layer was characterized by large bundles of collagen fibers (white arrow) and showed a lot of dermal appendages (white triangle), such as sebaceous glands and hair bulbs.

In summary, NLC e/o suspension containing pullulan promoted an excellent healing, with a good re-epithelization and stratum corneum formation. Although in the underlying connective tissue skin appendages were vacant, collagen fibers were organized in large bundles typical of the reticular layer of the dermis. Moreover, dermal papillae began to reform. There was only a mild inflammatory infiltrate, visible in a small portion in the center of the wound.

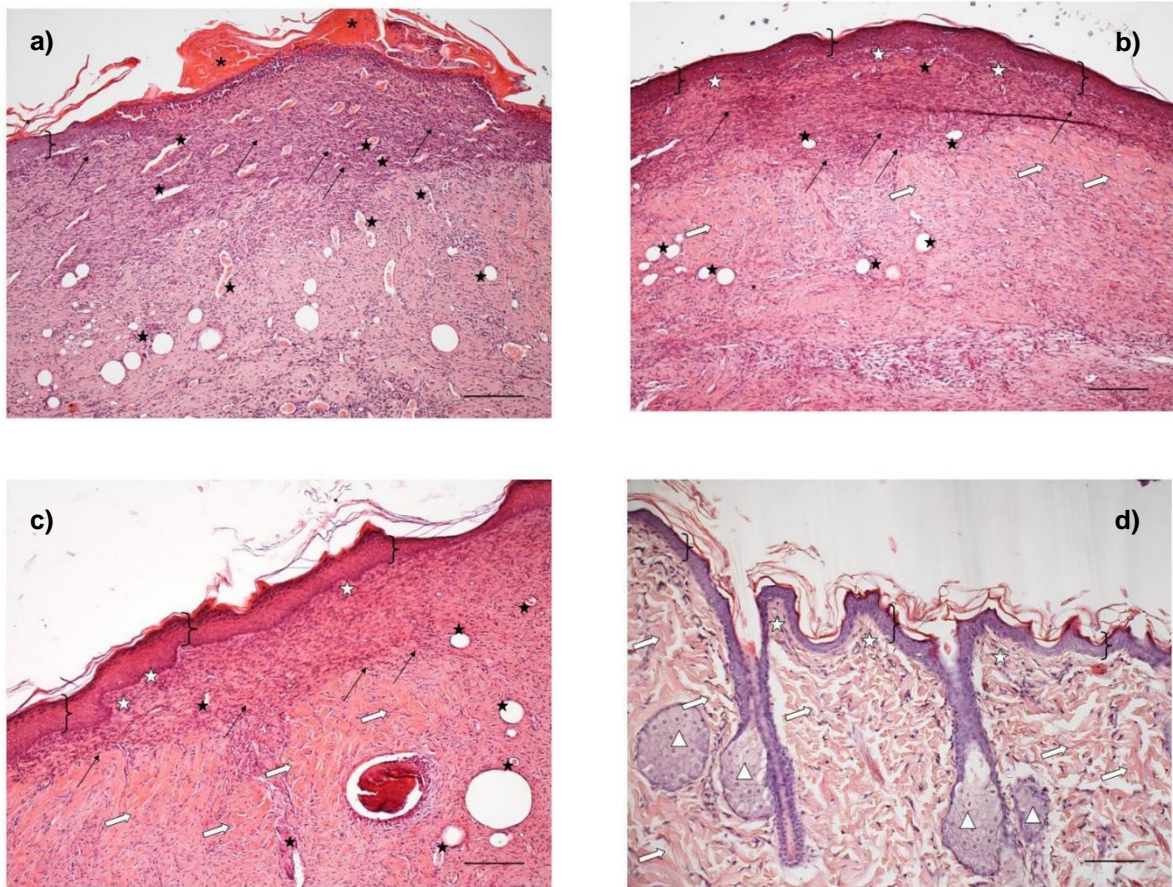


Figure 8: microphotographs of skin sections stained with haematoxylin and eosin from the wounded area after 18 days of treatment with saline solution, as negative control (a), NLC/e without (b) and with pullulan (c) in comparison with intact skin (d) (scale bar: 200 μ m). Asterisk: necrotic tissue; arrow: granulation tissue; black star: vacuoles/blood vessels; white star: dermal papillae; white arrow: bundles of collagen; white triangle: dermal appendages.

2.5 CONCLUSIONS

NLC based on cocoa butter and olive oil, as solid and liquid lipids, respectively, and loaded with eucalyptus oil (NLC o/e) were prepared by high shear homogenization and ultrasound method. Lecithin was used as surfactant to stabilize nanoparticles and to avoid their aggregation. NLC o/e was characterized by a particle size of 200-300 nm and demonstrated to be physically stable up to 3 months (2-8°C). It showed good bioadhesive properties, probably determined by NLC flexibility, that could promote interaction with the biological substrate and the consequent bioadhesive joint formation; this is an important feature to allow an intimate contact between formulation and lesion, to assure treatment efficacy. NLC o/e showed good biocompatibility and proliferation properties towards normal human fibroblasts in an in vitro wound healing model. These properties could be due to the presence of olive oil, a fatty acid with a high content of oleic acid, already known for its good proliferation enhancement potential.

Encapsulation of eucalyptus oil in NLC, did not impair its antimicrobial properties against two gram-positive bacterial strains commonly present in the skin (*Staphylococcus aureus* and *Streptococcus pyogenes*).

The results of in vivo rat burn model represented a proof of concept of efficacy and safety of NLC o/e developed.

Acknowledgement: Dr. F Saporito wishes to thank ABOCA Società Agricola S.p.A. for her PhD grant. The authors wish to thank Dr. F Riva for bromodeoxyuridine (BrdU) test and Dr. M. Boiocchi (Centro Grandi Strumenti, University of Pavia) for TEM images.

2.6 REFERENCES

1. Gould L., Abadir P, Brem H, Carter M, Conner-Kerr T, Davidson J, DiPietro L, Falanga V, Fife C, Gardner S, Grice E, Harmon J, Hazzard WR, High KP, Houghton P, Jacobson N, Kirsner RS, Kovacs EJ, Margolis D, McFarland Horne F, Reed MJ, Sullivan SH, Thom S, Tomic-Canic M, Walston J, Whitney JA, Williams J, Zieman S, Schmader K. Chronic wound repair and healing in older adults: current status and future research. *J Am Geriatr Soc.* 2015; 63(3): 427–438.
2. Boateng J, Catanzano O. Advanced Therapeutic Dressing for Effective Wound Healing-review, *J Pharm Sci.* 2015; 104: 3653-3680.
3. Stejskalova A, Almquist BD. Using biomaterials to rewire the process of wound repair. *Biomater Sci.* 2017; 5: 1421-1434.
4. Gardner SE, Hillis SL, Heilmann K, Segre JA, Grice EA. The neuropathic diabetic foot ulcer microbiome is associated with clinical factors. *Diabetes.* 2013; 62: 923–930.
5. Bowler PG, Duerden BI, Armstrong DG. Wound microbiology and associated approaches to wound management. *Clin Microbiol Rev.* 2001; 14(2):244–269.
6. Jahromi MAM, Zangabad PS, Basri SMM, Zangabad KS, Ghamarypour A, Aref AR, Karimi M, Hamblin MR. Nanomedicine and advanced technologies for burns: Preventing infection and facilitating wound healing. *Adv Drug Deliv Rev.* 2017 doi: 10.1016/j.addr.2017.08.001.
7. Fuzi M. Editorial: The Global Challenge Posed by the Multiresistant International Clones of Bacterial Pathogens. *Front Microbiol.* 2017; 8: 817.
8. Davis SC, Perez R. Cosmeceuticals and natural products: wound healing. *Clin Dermatol.* 2009; 27(5):502–506.
9. Mayaud L, Carricajo A, Zhiri A. Aubert G. Comparison of bacteriostatic and bactericidal activity of 13 essential oils against strains with varying sensitivity to antibiotics. *Lett Appl Microbiol.* 2008; 47: 167–173.

10. Ait-Ouazzou A, Loran S, Bakkali M, Laglaoui A, Rota C, Herrera A, Pagana R, Conchello P. Chemical composition and antimicrobial activity of essential oils of *Thymus algeriensis*, *Eucalyptus globulus* and *Rosmarinus officinalis* from Morocco. *Sci Food Agric*. 2011; 91: 2643–2651.
11. Takahashi T, Kokubo R and Sakaino M. Antimicrobial activities of eucalyptus leaf extracts and flavonoids from *Eucalyptus maculata*. *Lett Appl Microbiol*. 2004; 39:60–64.
12. Moss M, Cook J, Wesnes K, Duckett P. Aromas of rosemary and lavender essential oils differently affect cognition and mood in healthy adults. *Int J Neurosci*. 2003; 113: 15–38.
13. Apostolides NA, El Beyrouthy M, Dhifi W, Samir N, Cazier F, Najem W, Labaki M, AbouKaïs A. Chemical Composition of Aerial Parts of *Rosmarinus officinalis* L. Essential Oil Growing Wild in Lebanon, *Journal of Essential Oil Bearing Plants*, (2013).16(2): 274–282].
14. Sienkiewicz M, Lysakowska M, Pastuszka M, Bienias W, Kowalczyk E. The Potential of Use Basil and Rosemary Essential Oils as Effective Antibacterial Agents. *Molecules* 2013; 18: 9334-9351.
15. Drulis-Kawa Z, Dorotkiewicz-Jach A. Liposomes as delivery systems for antibiotics. *Int J Pharm*. 2010; 387: 187–198.
16. Gokce EH, Korkmaz E, Dellera E, Sandri G, Bonferoni MC, Ozer O. Resveratrol Loaded Solid Lipid Nanoparticles versus Nanostructured Lipid Carriers: Evaluation of Antioxidant Potential for Dermal Applications. *Int J Nanomed*. 2012; 7:1841 – 1850.
17. Gokce EH, Korkmaz E, Tuncay-Tanrıverdi S, Dellera E, Sandri G, Bonferoni MC, Ozer O. A Comparative Evaluation of Coenzyme Q10 Loaded Liposomes and Solid Lipid Nanoparticles as Dermal Antioxidant Carriers. *Int J Nanomed*. 2012; 7: 5109–5117.
18. Sandri G, Bonferoni MC, D'Autilia F, Rossi S, Ferrari F, Grisoli P, Sorrenti M, Catenacci L, Del Fante C, Perotti C, Caramella C. Wound dressings based on silver sulfadiazine SLN for tissue repairing, *Eur J Pharm Biopharm*. 2013; 84: 84-90.

19. Szucs M, Sandri G, Bonferoni MC, Caramella C, Vaghi P, Szabó-Révész P, Eros I. Mucoadhesive behaviour of emulsion containing polymeric emulsifier. *Eur J Pharm Sci.* 2008; 34: 226–235.
20. Sandri G, Rossi S, Bonferoni MC, Ferrari F, Zambito Y, Di Colo G, Caramella C. Buccal penetration enhancement properties of N-trimethyl chitosan: influence of quaternization degree on absorption of a high molecular weight molecule. *Int J Pharm.* 2005; 297: 146-155.
21. Sandri G, Bonferoni MC, Ferrari F, Rossi S, Aguzzi C, Mori M, Grisoli P, Cerezo P, Tenci M, Viseras C, Caramella C. Montmorillonite-chitosan-silver sulfadiazine nanocomposites for topical treatment of chronic skin lesions: in vitro biocompatibility, antibacterial efficacy and gap closure cell motility properties. *Carbohyd Polym.* 2014; 102: 970–977.
22. Saporito F, Sandri G, Rossi S, Bonferoni MC, Riva F, Caramella C, Ferrari F. Freeze dried chitosan acetate dressings with glycosaminoglycans and tranexamic acid. *Carbohyd Polym* 2018; 184:408-417.
23. Yang Y, Corona A, Schubert B, Reeder R, Henson M. The effect of oil type on the aggregation stability of nanostructured lipid carriers. *J Colloid Interface Sci.* 2014; 418: 261-272.
24. Barauskas J, Christerson L, Wadsater M, Lindstrom F, Lindqvist A-K, Tiberg F. Bioadhesive lipid compositions: self-assembly structures, functionality and medical applications. *Mol Pharmaceutics.* 2014; 11: 895-903.
25. Dellera E, Bonferoni MC, Sandri G, Rossi S, Ferrari F, Del Fante C, Perotti C, Grisoli P, Caramella C. Development of chitosan oleate ionic micelles loaded with silver sulfadiazine to be associated with platelet lysate for application in wound healing. *Eur J Pharm Biopharm.* 2014; 88: 643-650.
26. Sandri G, Bonferoni MC, Gökçe EH, Ferrari F, Rossi S, Patrini M, Caramella C. Chitosan-associated SLN: in vitro and ex vivo characterization of cyclosporine A loaded ophthalmic systems. *J Microencapsul.* 2010; 27: 735-746.

This work was objected of 1 conference presentation:

Saporito, F., Sandri, G., Bonferoni, M.C., Rossi, S., Riva, F., Icaro Cornalia A.,
Boselli, C., Caramella, C., Ferrari, F

Lipid nanoparticles loaded dressings for wound healing, 2nd European Conference on
Pharmaceutics, Krakow, Poland, April 3rd-4th, 2017

Introduction-part II

1 THE HEART

The heart is the central organ of the circulatory apparatus, located in the middle mediastinum of the rib cage. It is encapsulated in the pericardium, which protects the heart from other organs, and can be divided in two different layers: the external layer, fibrous pericardium, and the inner layer, serous pericardium. Furthermore, the serous pericardium is divided into parietal and visceral layers. The heart consists of two chambers, divided by a septum: two upper atria and two lower ventricles.

The deoxygenated blood reaches the right ventricle of the heart by means of the superior and inferior venae cava, while the left atrium receives oxygenated blood from the four pulmonary veins [Drake et al., 2005]. The external wall of the human heart is constituted by three layers, going from the external to the inner part we can find: the epicardium, a muscular myocardium, and an endothelial endocardium [Kennedy, 2012]. The cardiac muscle can contract independently by means of an internal conduction system. The electrical impulses originate from the sino-atrial node, named pacemaker, and placed in the right atrium, and result in contraction of the atria. Afterward, the signal passes to the atrioventricular node and it is transmitted to the ventricles, resulting in the myocardial contraction [Drake et al., 2005].

The heart is made up of an extracellular matrix (ECM) consisting of different components such as proteins, glycosaminoglycans, growth factors, cytokines [Hynes, 2009]. The most abundant protein present in the myocardium and having a structural function is collagen type I (85%) and type III (11%) [Bosman and Stamenkovic, 2003]. In the myocardium is possible to find four different cell types: cardiomyocytes (CMCs), cardiac fibroblasts (CFs), smooth muscle cells (SMCs), and endothelial cells (ECs) [Gerecht-Nir et al., 2006]. CMCs are not completely able to regenerate after birth, indeed, less than 50% of all CMCs are substituted during a normal human life [Bergmann et al., 2009]

2. MYOCARDIAL INFARCTION

Myocardial infarction (MI) occurs after the occlusion of a coronary artery that causes an ischemic damage able to induce cellular necrosis. In the most of cases, this condition is concomitant with the formation of an atherosclerotic plaque [Hastings C.L. et al., 2014] (Fig 1). The ischemic death of cardiomyocytes within the infarcted area determines a strong increase in loading conditions with a consequent remodeling of the infarcted border zone. Indeed, different compensatory mechanisms occur immediately after MI, centrally and peripherally, such as hypertrophy, activation of the renin-angiotensin system, vasoconstriction, developing structural changes of the myocardium including dilatation, hypertrophy and formation of a collagen scar. This series of events, named ventricular remodeling, start immediately after damage and may continue for weeks or months [Martin et al., 2000].

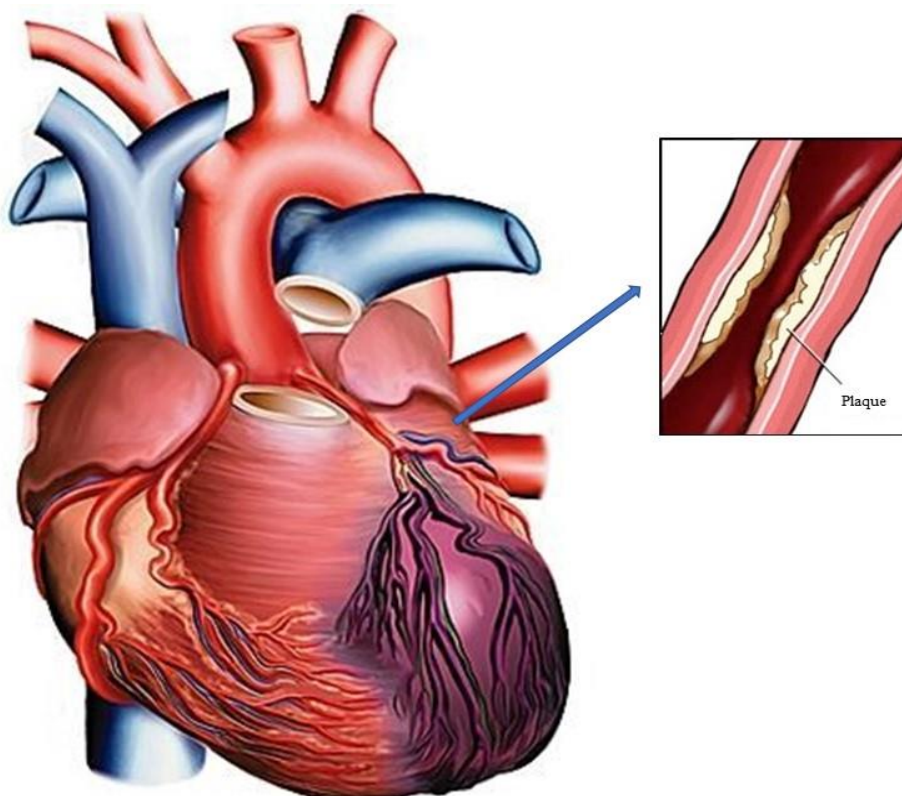


Figure 1: Infarcted heart

2.1 Pathophysiology

MI can be classified, depending on the thickness of the infarcted area, as:

- transmural MI, when the whole wall is damaged;
- intramural MI, when only subendocardial layers of the wall are infarcted.

In the first case, a total vessel occlusion occurs, caused by a thrombosis or a coronary spasm, while in the intramural MI the occlusion is partial.

The events happening after MI can be classified, as macroscopic or microscopic, as follow:

1) Macroscopically:

- after 18-24 h the infarcted area appears pale and dry;
- between the 2nd and the 4th day, a thin yellow halo surrounds the damage area, as production of neutrophil infiltration. Furthermore, the wall of myocardium becomes thinner due to the removal of necrotic muscle tissue;
- between the 8th and 10th day, a red line starts to appear around the infarcted border and then it covers all the damaged area, due to the granulation tissue formation;
- after 4 weeks, the infarcted area become grey, for the formation of the collagen scar.

2) Microscopically

- After 12-15 h, cardiomyocytes necrosis is observed;
- after 48 h, the fibrous muscle structure disappears with a consequent formation of necrotic tissue and the attraction of circulating inflammatory cells, such as neutrophils and monocytes/macrophages.
- starting from the 7th day after MI, neutrophils are replaced by lymphocytes, the granulation tissue is formed;
- starting from the 6-7 weeks to several months after the event, the deposition of type I and III fibrillar collagen produced by fibroblasts replaces the dead tissue with a non-contractile collagen scar.

For many years, the scar formed at the site of infarction, has been considered inert, while today it has been recognized as living tissue composed of population of myofibroblats [Cleutjens et al., 1999]. These cells appear at the infarcted site and

remain there for years, producing continuously a collagen network also after that the integrity of the infarcted heart is established [Sun and Weber 2000].

2.2 Tissue repair after MI

Wound healing is a biological process having as final goal the tissue regeneration. An optimal recovery of the heart after MI depends on the rapid but strictly controlled recruitment of mononucleate cells, in particular monocytes, which are able to degrade cellular debris and necrotic cells, to control the granulation tissue formation and neoangiogenesis, by means of the secretion of cytokines, proteases and growth factors [Ertl and Frantz, 2005].

The remodeling after MI has been divided into two phases: the early phase and the late phase.

During the early phase (within 72 h), only the infarcted zone is involved in the remodeling, while a remodeling expansion area is observed during the late phase (over 72 h) [Martin et al., 2000] (Fig. 2).

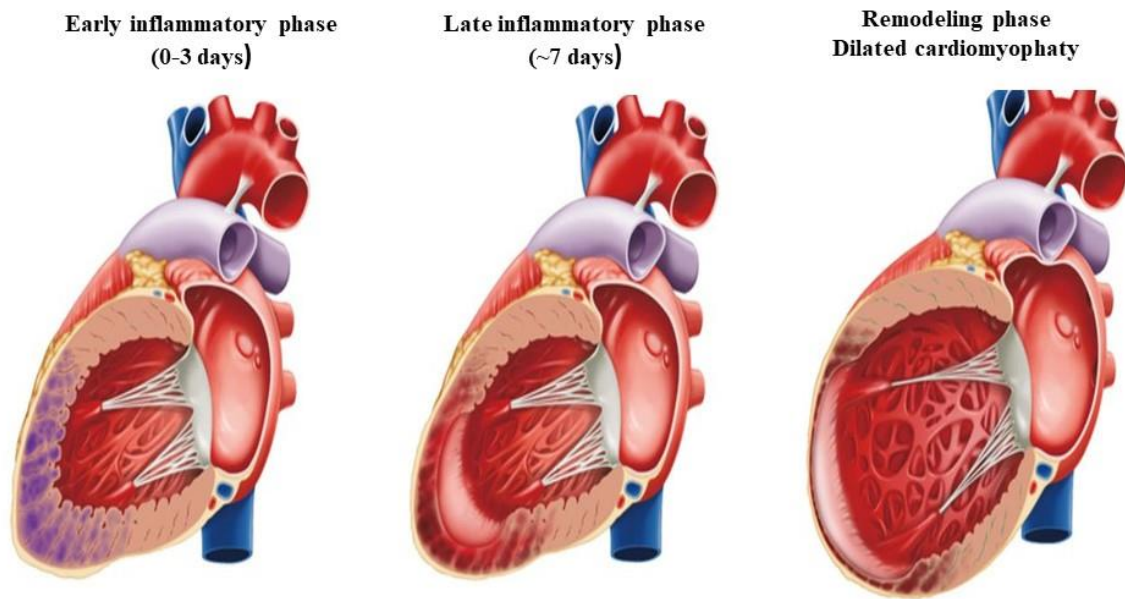


Figure 2: wound healing after myocardial infarction [Martin et al., 2000].

- Early remodeling

Immediately after the necrotic loss of cardiomyocytes, a highly orchestrated process of tissue repair takes place in the infarcted zone. The early remodeling phase begins with the activation of serine proteases and metalloproteinases (MMPs) released from neutrophils, which degrade the existing extracellular matrix [Cleutjens et al., 1995]. The proteolytic activity of MMPs promotes the migration of the inflammatory cells into the infarcted area, where they contribute to the proteolytic digestion and phagocytosis of infarcted tissue. After 1-week post MI, the expression of MMPs inhibitors reduces the proteolytic activity [Sun et al., 2000]. The ECM degradation results in a wall thickness reduction and ventricular dilatation, with the consequent increment of diastolic and systolic wall stress. As consequence of the increased wall stress, mechanoreceptors give the stimuli for hypertrophy and for the expansion of the infarcted area with the deformation of the border zone of myocardium.

Modifications in circulatory hemodynamics activate the sympathetic adrenergic system, stimulating catecholamine synthesis, and activating the renin-angiotensin-aldosterone system.

- Late remodeling

The late phase after MI includes the heart hypertrophy and ventricular alteration caused by the solid collagen scar formation. Collagen deposition onto the infarcted area, starting from the 2nd day after MI, strongly increases upon 4 weeks post MI, until the necrosis of myocytes occurs [Sutton and Sharpe, 2000].

Collagen breakdown begins within 3 hours of infarction and is activated by proteinases and the release of MMPs from neutrophils [Cleutjens et al., 1995]. Proteinases degrade damage tissue and attract factors and cytokines stimulating collagen deposition on the scar by fibroblasts giving fibrosis: the greater the fibrotic area the greater the entity of the cardiomyopathy developed in the final step. Therefore, a balance between degraded tissue and collagen matrix formation is needed [Sutton and Sharpe, 2000]. Indeed, the creation of a collagenous, non-contractile scar tissue, thinning and enlargement of the myocardial wall, contribute to a decrease in ventricular contractile function with the final development of a congestive heart failure (CHF), condition in which the heart is unable to pump enough blood to satisfy the metabolic requests of the body [Templin et al., 2011]

3. MYOCARDIAL TISSUE ENGINEERING

As largely discussed, when a MI occurs, the dead tissue is replaced by a non-contractile collagen scar [Pfeffer and Braunwald, 1990]. As result, the contractile function of the heart is reduced, the electrical impulses are slowly and irregularly conducted. These conditions allow the beginning of a cascade of compensatory mechanisms, initially beneficial and, over time, leading to a left ventricular remodeling together with a hypertrophic condition, with a final development of a congestive heart failure (HF) [Gaudron, et al., 1993].

Heart failures (HF) are the leading global cause of death worldwide. Current state of the treatments for end stage HF primarily include many pharmacological therapies, which can slow down the infarcted area dilation but not restore the contractile function of the tissue [Segers and Lee, 2010]. The optimal solution to avoid problems related to HF includes heart transplantation, allowing the best patient outcomes [Boyle, 2009]. However, the limited availability of donors and the immunoreactions, make this way hard to follow [Lindenfeld et al., 2004]. Nowadays, new devices such as left ventricular assist devices (LVADs), which decrease the load on the heart, are available. These devices can be implanted while the patient is waiting for the organ transplant, but they are highly expensive [Buckeberg, 2002].

Therefore, to overcome these problems, a more recent and achievable strategy includes myocardial tissue engineering (MTE).

MTE is an inter-disciplinary field of research aimed to the cardiac tissue repairing after heart failures, by mimicking the nature of the heart. It applies principles of engineering, material chemistry and cell biology to obtain different cell based and cell free strategies as therapeutic systems able to sustain cardiac functionalities. The strategies employed in tissue engineering can provide a mechanical support in the form of biomaterials and biomolecules with similar properties to that of the ECM of the heart.

The properties that a bioengineered construct should possess are: biocompatibility, non-antigenicity, bioadhesion, appropriate physical properties, ability for complete integration with host. At this purpose, a myocardial construct should stay long enough to improve the integration of cells or biomolecules with native tissue, without interferences with the physiologic events, and should go under degradation once the tissue is completely repaired. It has been shown, that endothelial and cardiomyocytes adhesion is improved by specific modifications of biomaterials surface chemistry, for example adding growth factors for cell attachment or chemotactic recruitment [Mukherjee et al., 2010].

Different in vivo and in vitro strategies have been developed in tissue engineering; among these there are: cell transplantation, cell seeded scaffolds implantation,

acellular cardiac constructs implantation, injectable scaffold with or without cells (Fig. 3)

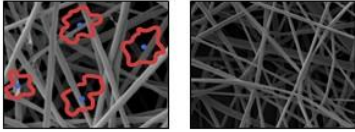
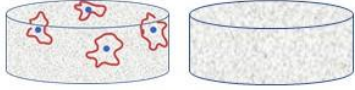


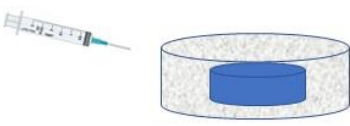
Cell therapy		
1) <u>Somatic muscle cells</u> - foetal or neonatal CMs - foetal or neonatal skeletal myoblasts	2) <u>Myocardium-generating cells</u> - embrione stem cells - bone marrow-derived mesenchimal stem cells - adipose stem cells	3) <u>Angiogenesis-stimulating cells</u> - fibroblast progenitor cells - endothelial progenitor cells
Cellular or acellular preformed scaffolds		
Electrospun fibers 	Polymeric scaffolds 	Decellularized heart 
Injectable scaffolds		
<i>In situ</i> 		<i>In vitro</i> 

Figure 3: in vitro and in vivo strategies developed for cardiac repair.

3.1 Cell therapy

Cellular strategies are based on the injection and delivery of different types of cells directly into the infarcted heart of the patient [Laflamme et al., 2007]. Different routes of administration are used for cell delivery: intravenous [Barbash et al., 2003], intracoronary [Janssens et al., 2006], transmyocardial [Perin and Lopez, 2006], catheter based transendocardial [Sherman et al., 2006].

Preclinical and clinical trials have investigated a large number of cell types for cardiac regeneration, such as mesenchymal stem cells (MSCs), endothelial progenitor cells

(EPCs), bone marrow cells (BMCs), resident cardiac stem cells, skeletal myoblast cells (SMCs), embryonic stem cells (ESCs), and induced pluripotent stem cells (iPS). Many studies conducted on the use of foetal and neonatal cardiomyocytes from murine models, demonstrated the similar electrophysiological, structural and contractile properties of these cells, together with a mild proliferative capacity. A lot of works, reported that cardiac myocytes from neonatal or embryonic models can be injected also into infarcted hearts obtaining promising results. Muller-Ehmsen et al. [Muller-Ehmsen et al., 2002]. isolated and injected neonatal rat cardiomyocytes into the left ventricular wall of a rat model of chronic myocardial infarction, demonstrating that these cells could survive and improve cardiac functions for up 6 months. Furthermore, Soonpa et al. demonstrated that foetal cardiomyocytes could be able to be aligned with the surviving donor cells of a healthy myocardium of mice [Soonpaa et al., 1994].

The effectiveness of cardiomyocytes transplantation in the prevention of cardiac dilation and remodeling after infarction and the improvement of the ventricular function, has been explained by different mechanisms: direct contribution of the transplanted cells to contractility, reduction of the infarcted area expansion, angiogenesis induced by growth factors secreted from the foetal cells [Etzion et al., 2001].

3.1.1 Cell types used in myocardial tissue engineering

The choice of the cells for implantation in myocardial tissue engineering plays an important role for cardiac muscle regeneration. The numerous studies focused on the investigation of the different cell types to improve myocardial function and regeneration, started from 1978 when Bader and Oberpriller demonstrated the possibility of amphibian heart to regenerate after autologous implantation of ventricular tissue samples into injured new heart [Bader and Oberpriller, 1978]. Since then, a lot of cell models have been investigated and they can be classified into three groups: 1) somatic muscle cells (fetal or neonatal cardiomyocytes and skeletal myoblasts), 2) myocardium-generating cells (embryonic stem cells, bone-marrow

derived mesenchymal stem cells and adipose stem cells), 3) angiogenesis-stimulating cells (fibroblast and endothelial progenitor cells).

Foetal or neonatal cardiomyocytes can proliferate and, as different works have been demonstrated, once they are transplanted into a healthy or injured myocardium, they can integrate with the native tissue and they can be aligned with recipient cells and formed cell-to-cell contacts [Soonpaa et al., 1994].

Muller-Ehmsen et al., isolated and injected male donor neonatal rat cardiomyocytes into the left ventricular wall of adult female rats., demonstrating that these cells could survive and improve cardiac function for a long period (6 months).

One or more of the following mechanisms can be implicated in improved heart functions following cardiomyocyte transplantation: a) direct contribution to contractility, b) controlled of the infarcted area expansion thanks to the contractile properties of the cardiomyocytes; c) angiogenesis induced by growth factors released by injected cells.

Fibroblasts, also named myofibroblasts because they contain alpha-smooth muscle actin microfilaments, are contractile cells, that are responsible for collagen deposition on the scar at the site of injury and so for fibrous tissue formation. The regulation of collagen turnover occurs due to angiotensin II production.

The major limitation of cell therapy is immune rejection caused by the implanted cells.

3.2 Polymers used in cardiac tissue repair

The choice of the biomaterial for the development of cardiac tissue constructs plays a key role in tissue engineering. The ideal biomaterial should be biocompatible and biodegradable, and able to provide a physical support for cell growth. Natural and synthetic biomaterials are used to produce engineered cardiac constructs.

Natural biopolymers represent the favorite substrates for tissue engineering since they mimic the heart microenvironment, providing a natural matrix for cellular attachment, proliferation, and differentiation, furthermore, they usually avoid the occurrence of typical response of foreign materials implanted into the body.

Among the natural materials, the ECM components, such as collagen and its derivatives gelatin, fibrinogen, glycosaminoglycans, represent the most used [Dinsmore and Dib, 2008]. They are named “biomimetics” and promote the interaction between matrix and cells. Collagen, the most abundant protein in animals, is a good surface-active biomaterial, characterized by a higher biocompatibility, biodegradability, and weak antigenicity as compared with other natural polymers. Different epicardial heart patches [Zimmermann et al., 2004], gel and 3D tissue engineering constructs were developed [Xiang et al., 2006].

Gelatin is obtained from collagen after a controlled hydrolysis. The sources of collagen are animal bones, connective tissue or skin. Depending on the hydrolyzation process, two types of gelatin can be obtained: gelatin type A, resulting after an acidic pretreatment, and gelatin type B, derived after an alkaline hydrolysis. When collagen is hydrolyzed, its helices can be destroyed in hot water and after cooling some chains reassociate into triple helix structures. The formation of this triple helix in gelatin is thermoreversible and depending on transition temperature and enthalpy. Molecular weight, amino acid composition, amount of plasticizers influence the temperature at which gelatin triple helices dissociate upon heating (T_d) [Gomez-Guillen et al., 2011]. Above the denaturation temperature, gelatin is soluble in water, while upon cooling a hydrogel is formed as consequence of physical crosslinks formation due to the intramolecular microcrystalline junction zones created after the coil-to-helix transition [Roussanova et al., 2014].

Different strategies have been used to obtain cold water-soluble gelatin, as hydrolysis, which leads to biochemical enzymatic degradation resulting in a low molecular weight product. In the last years, gelatin nanofibers have been studied for biomedical applications as new therapeutic approach [Goh et al., 2013; Sridhar et al., 2015].

Even if natural biopolymers are the favorite materials to obtain engineered constructs, synthetic polymers are an optimal choice for scaffolds because they are easily modifiable in order to control the final properties of the cardiac substrate such as the structure, and the pore size. The control of polymer composition can lead to specific mechanical strength and degradation properties [Gunatillake and Adhikari, 2003].

Among the synthetic polymers, poly (lactic-co-glycolic acid) (PLGA) has been extensively studied because it can provide a controllable degradation profile by changing the concentration of the constituents in the polymer composition. Thanks to this property, a lot of PLGA scaffolds have been developed by using different methods [Kenar et al., 2010].

Although the synthetic polymers represent a good choice because they allow to obtain a control of the internal architecture and degradation profiles, there are some disadvantages of their use in cardiac tissue repair. In fact, they are often poorly biocompatible, if compared to the natural polymers, because sometime the degradation process can release acidic degradation components that at high concentrations can lead to inflammation [Thomson et al., 1995].

3.3 Strategies for tissue engineering cardiac constructs

The choice of the ideal biomaterial is also related to the type of cardiac tissue engineered construct to develop. Current treatment for myocardial infarction can be classified as *in vitro* and *in vivo* approaches. The *in vitro* approaches include preformed acellular or cellular scaffolds in culture dishes or bioreactors, able to mimic the extracellular matrix of the injured site, or scaffoldless cell sheets [Leor et al., 2005]. The *in vivo* strategies include injectable hydrogel, with or without cells.

3.3.1 Preformed scaffolds

Preformed scaffolds represent a good strategy for tissue repair since they are able to recreate a tridimensional environment that provides a physical support on which the cells can adhere and proliferate. Preformed scaffold can be developed by using different techniques such as by lyophilizing the biomaterial solution [Shapiro and Cohen, 1997], by using salt extraction to create highly porous scaffold with interconnected pores [Caspi et al., 2017], by electrospinning of polymer solutions [Zhong et al., 2006]. Scaffolds produced by electrospinning are usually acellular

because the forces needed for fiber formation can damage the cells. Indeed, the cells must be seeded after scaffold production.

Another method of creating preformed scaffolds include EMC decellularization. The decellularized ECM present all the chemical components, many growth factors and signals that affect cell response, the geometry of the native myocardium that are usually difficult to reproduce with the tissue engineering technologies.

Preformed scaffolds are characterized by good biodegradability, non-immunogenicity, high porosity properties necessary for cell growth. Limitations of preformed scaffolds include the difficulty in seeding the cells in an uniform mode, indeed the cell density is initially high only at the surface of the construct. Another limitation includes the invasive technique necessary for the implant.

3.3.2 Scaffoldless cell sheets

Scaffoldless approach is another way to produce a cardiac tissue engineered constructs. This technique is based on the possibility to seed the cells onto surfaces allowing them to create a structure themselves with any addition of biomaterials. The best advantage of this technique is that no immunogenic and rejection reactions occur because no extraneous material is injected or implanted into the body [Anderson et al., 2008].

The first cell sheet was created in 1999 by the Okano group, using a temperature-responsive culture surface for the cardiac cells [Kushi et al., 1999]. Briefly, a slightly hydrophobic PNIPAAm (poly(*N*-isopropylacrylamide, a temperature-responsive polymer) surface is created onto culture surface at 37°C, which leads the polymer binding and the attachment and proliferation of the cells. Once the cells reach the confluence, the temperature is decreased below 32°C (polymer's critical solution temperature), the polymer becomes hydrophilic, swells and create a hydration layer between cell sheet and the culture surface. The cells can detach creating a 3D structure.

3.3.3 Injectable hydrogels

Hydrogels are three-dimensional cross-linked networks able to include a large amount of water or biological fluids between the polymer chains [Peppas et al., 2000]. They can be injected as liquid directly into the wall of the heart where they can form a gel, entrapping the bioactive molecules or cells injected together with the biomaterial. This can overcome the problems of scarce cell retention observed in the scaffoldless technique. The major advantage of in situ gelling systems is the minimal invasive technique needed for their administration. Intramyocardial injection occurs usually into the left ventricle, using an epicardial method or a catheter technique. This last approach avoids local toxicity and leads to a better retention.

There are several methods to obtain the gelation of solutions from liquids: temperature, pH, ionic crosslinking, photo crosslinking. Among the ionic crosslinking-dependent polymers there is alginate, a polysaccharide isolated from brown algae; it undergoes reversible gelation in aqueous solution in presence of divalent cations, such as Ca^{2+} , that, in substitution of sodium ions, create ionic inter-chain bridges between the polymer chains. A lot of studies have been conducted for studying the injection of alginate implants on infarcted and normal heart of rats.

Temperature-sensitive hydrogels are liquid at room temperature and becomes hydrogel at body temperature. In fact, when the temperature increases, a dehydration of polymer chains occurs leading to the formation of hydrophobic domains. Most studies thermo-sensitive materials include poloxamers, poly(ethylene oxide) (PEO), poly(propylene oxide) (PPO) [Van Tomme et al., 2008].

Different parameters have to be considered in order to design the optimal hydrogel, such as the physical material, biological properties, biocompatibility, biodegradability, and the bioresorbability [Yu and Ding, 2008]. The consideration of these parameters is essential for obtaining the optimal engineered tissue construct, for cardiac implantation, that should be elastic to sustain heart contractions., well-vascularized, allowing the encapsulated cells to receive nutrients and oxygen [Singelyn et al., 2009; Ravichandran et al., 2012].

4 ELECTROSPINNING TECHNIQUE

Electrospinning is a versatile, promising and simple technique to produce nanofibers scaffolds applying a high voltage to polymer solutions of both natural and synthetic polymers [Ahn et al., 2006; Reneker and Yarin, 2008]. Basically, an electrospinning set-up consists of three major components: a high voltage power supply, a spinneret, and an electrically conductive collector, covered by an aluminum foil (Fig.4).

The term electrospinning has been used around 1994 and derived from “electrostatic spinning”, but the technique originated more than 60 years ago. This method has received much attention in the last decades because it is a versatile and simple technique, of course, but also thanks to the possibility to produce fibers in the order of submicron, difficult range to achieve by using standard technologies. [Schreuder-Gibson et al., 2002; Theron et al., 2005]. Furthermore, electrospun nanofibers present many advantages in particular a high surface to volume ratio and an adjustable porosity.



Figure 4: electrospinning apparatus.

4.1 Effecting parameters on electrospinning process

Different parameters effect the electrospinning process and can be classified as: solution parameters (viscosity, conductivity, polymer molecular weight, and surface tension) process parameters (applied electric filed, type of collector, distance between needle and collector, feeding rate, and flow rate), and ambient parameters (temperature and humidity). Modifying each of these parameters, it is possible to manipulate fibers morphology and diameter [Chong et al., 2007].

4.1.1 Solution parameters

4.1.1.1 Concentration

Depending on the solution concentration, beads, at low concentration, or uniform fibers, when the concentration increases, are obtained. Increasing the concentration, an increment in fibers diameter occurs due to the higher viscosity resistance [Haghi and Akbari, 2007]. An optimal concentration should be to find playing also with solution surface and viscosity parameters [Deitzelet al., 2001].

4.1.1.2 Molecular weight

Molecular weight affects rheological and electrical properties of the polymer solution [Haghi and Akbari, 2007]. Also in this case, a low molecular weight of the solution brings to beads rather than fibers and high molecular weight solution lead to fibers with a larger diameter.

Molecular weight of the polymer is an index of entanglements capability of polymer chains and consequently of the solution viscosity. Indeed, when polymer concentration is low, a polymer can usually maintain entanglements of their chains to allow enough viscosity to obtain uniform fibers [Tan et al., 2005].

4.1.1.3 Viscosity

Solutions viscosity influence the fiber size and morphology: solution characterized by low viscosity do not produce fibers, while solution with very high viscosity cannot

be ejected from the spinneret. Thus, the optimal viscosity must be found in maximum range between 0.1 and 21.5 Pa.s, as reported in a lot of works [Doshi and Reneker, 1995; Deitzel et al., 2002].

4.1.1.4 Surface tension

Surface tension plays an important role in the electrospinning process. In general, the highest the surface tension, the lowest the spinnability because of the instability of the jet and the formation of beads [Hohman et al., 2001].

4.1.1.5 Conductivity

Solution conductivity depends on the polymer type, the solvent used, and the presence of conductivity salts. It influences fiber diameters: increasing the electrical conductivity of the solution, a significant decrease in the diameter of the electrospun nanofibers occurs. On the contrary, decreasing the electrical conductivity of the solution an insufficient elongation of the jet occurs and no uniform fibers are produced.

4.1.2 Processing parameters

4.1.2.1 Applied voltage

The electrospinning process starts when the voltage surpasses a threshold value and the electrical forces can overcome the surface tension. There is a little debate about the influence of the applied voltage on fiber diameters: some works showed that the electrical field doesn't affect fiber diameter [Reneker and Chun, 1996], other researchers have demonstrated that when a higher voltage is applied, fibers with a higher diameters can be obtained because there is a greater polymer ejection [Zhang et al., 2005], and other authors have reported that an increase in the applied voltage causes a reduction of fiber diameter, due to a greater stretching of the solution [Haghi and Akbari, 2007].

4.1.2.2 Feed rate/flow rate

Depending on the distance between the needle and the collector, a lower feed rate is usually required as the solvent will have enough time for evaporation [Yuan et al., 2004]. It has been observed that the fiber diameter increases with an increase in the polymer flow rate.

4.1.2.3 Distance between needle and collector

The distance between needle and collector has to be optimal because the fibers need sufficient time to dry before reaching the collector, in order to obtain uniform fibers without beads [Ki et al., 2005].

REFERENCES

- Ahn, Y. C., Park, S. K., Kim, G.T., Hwang, Y. J., Lee, C. G., Shin, H. S. (2006). Development of high efficiency nanofilters made of nanofibers. *Current Applied Physics*, 6, 1030–1035.
- Anderson, J. M., Rodriguez, A., Chang, D. T. (2008). Foreign body reaction to biomaterials. *Seminars in immunology*, 20, 86-100.
- Bader, D., Oberpriller, J. O. (1978) Repair and reorganization of minced cardiac muscle in the adult newt (*Notophthalmus viridescens*). *Journal of Morphology*, 155, 349–357.
- Barbash, I. M., Chouraqui, P., Baron, J., Feinberg, M. S., Etzion, S., Tessone, A., Miller, L., Guetta, E., Zipori, D., Kedes, L. H., Kloner, R. A., Leor, J. (2003). Systemic Delivery of Bone Marrow–Derived Mesenchymal Stem Cells to the Infarcted Myocardium. *Circulation*, 108, 863–868.
- Bergmann, O., Bhardwaj, R. D., Bernard, S., Zdunek, S., Barnabé-Heider, F., Walsh, S., Zupicich, J. (2009). Evidence for cardiomyocyte renewal in humans. *Science*, 324, 98–102.
- Bosman, F.T., Stamenkovic, I. (2003). Functional structure and composition of the extracellular matrix. *Journal of Pathology*, 200, 423–428.
- Boyle, A. (2009). Current status of cardiac transplantation and mechanical circulatory support. *Current Heart Failure Reports*, 6, 28–33.
- Buckberg, G. D. (2002). Basic science review: The helix and the heart. *The Journal of Thoracic and Cardiovascular Surgery*, 124, 863-883.
- Caspi, O., Lesman, A., Basevitch, Y., Gepstein, A., Arbel, G., Habib, I. H. M. (2017). Tissue engineered of vascularized cardiac muscle from human embryonic stem cells. *Circulation Research*, 100, 263-272.
- Chong, E. J., Phan, T. T., Lim, I. J., Zhang, Y. Z., Bay, B. H., Ramakrishna, S. (2007). Evaluation of electrospun PCL/gelatin nanofibrous scaffold for wound healing and layered dermal reconstitution. *Acta Biomaterialia*, 3, 321–30.

- Cleutjens, J. P., Blankesteyn, W. M., Daemen, M. J., Smits, J. F. (1999) The infarcted myocardium: simply dead tissue, or a lively target for therapeutic interventions. *Cardiovascular Research*, 44, 232–241.
- Cleutjens, J. P., Kandala, J. C., Guarda, E., Guntaka, R. V., Weber, K. T. (1995). Regulation of collagen degradation in the rat myocardium after infarction. *Journal of Molecular and Cellular Cardiology*; 27, 1281–1292.
- Deitzel, J. M., Kleinmeyer, J., Harris, D., Tan, N. C. B. (2001). The effect of processing variables on the morphology of electrospun nanofibers and textiles. *Polymer*, 42, 261–72.
- Deitzel, J. M., Kosik, W., McKnight, S. H., Ten, N. C. B., Desimone, J. M., Crette, S. (2002). Electrospinning of polymer nanofibers with specific surface chemistry. *Polymer*, 43, 1025–9.
- Dinsmore, J. H., Dib, J. (2008). Stem Cells and Cardiac Repair: A Critical Analysis
- Doshi, J., Reneker, D. H. (1995) Electrospinning process and applications of electrospun fibers. *Journal Electrostatics*, 35, 151–6.
- Drake, R. L, Vogl, W, Mitchell A. W. M. (2005). Gray's Anatomy for Students. Churchill Livingstone
- Ertl, G., Frantz, S. (2005). [Healing after myocardial infarction. *Cardiovascular Research*, 66, 22– 32.
- Etzion, S., Kedes, L.H., Kloner, R. A., Leor, J. (2001). Myocardial regeneration. *American Journal of Cardiovascular Drugs*, 1, 233–244.
- Gaudron, P., Eilles, C., Kugler, I., Ertl, G. (1993). Progressive left ventricular dysfunction and remodeling after myocardial infarction. Potential mechanisms and early predictors. *Circulation*, 87, 755–763.
- Gerecht-Nir, S., Radisic, M., Park, H., Cannizzaro, C., Boublik, J., Langer, R., Vunjak-Novakovic, G. (2006). Biophysical regulation during cardiac development and application to tissue engineering. *The International Journal of Developmental Biology*, 50, 233.
- Goh, Y.-F., Shakir, I., Hussain, R. (2013). Electrospun fibers for tissue engineering, drug delivery, and wound dressing. *Journal of Materials Science*, 48, 3027-3054

- Gomez-Guillen, M. C., Gimenez, B., Lopez-Caballero, M. E., Montero, M. P. (2011). Functional and bioactive properties of collagen and gelatin from alternative sources: a review. *Food Hydrocolloids*, 25, 1813-1827.
- Gunatillake, P.A., Adhikari R. (2003). Biodegradable synthetic polymers for tissue engineering. *European Cells and materials*, 5, 1-16.
- Haghi, A. K., Akbari, M. (2007). Trends in electrospinning of natural nanofibers. *Physic Status Solidi*, 204, 1830–4.
- Hohman, M. M., Shin, M., Rutledge, G., Brenner, M. P. (2001). Electrospinning and electrically forced jets. *II. Applications. Physics Fluids*, 13, 2221–36.
- Hynes, R.O. (2009). The extracellular matrix: not just pretty fibrils. *Science*, 326, 1216–1219.
- Janssens, S., Dubois, C., Bogaert, J., Theunissen, K., Deroose, C., Desmet, W., Kalantzi, M., Herbots, L., Sinnaeve, P., Dens, J., Maertens, J., Rademakers, F., Dymarkowski, S., Gheysens, O., Van Cleemput, J., Bormans, G., Nuyts, A., Belmans, L., Mortelmans, L., Boogaerts, M., Van de Werf, F. (2006). Autologous bone marrow-derived stem-cell transfer in patients with ST-segment elevation myocardial infarction: double-blind, randomised controlled trial. *The Lancet*, 367, 113–121.
- Journal Cardiovascular Translational Research*, 1, 41-54.
- Kenar, H., Kose, G. T., Hasirici, V. (2010). Design of a 3D aligned myocardial tissue construct from biodegradable polyesters. *Journal of materials science. Materilas in medicine*, 21, 989-997.
- Kennedy, J. (2012). Clinical anatomy series: cardiac anatomy. *Scottish Universities Medical Journal*, 1, 76–8.
- Ki, C. S., Baek, D. H., Gang, K. D., Lee, K. H., Um, I. C., Park, Y. H.(2005). Characterization of gelatin nanofiber prepared from gelatin-formic acid solution. *Polymer*, 46, 5094–102.
- Kushi, D. A, Yamato, M., Konno, C., Kikuchi, A., Sakurai, Y., Okano, T. (1999). Decrease in culture temperature releases molayer endothelial cells sheets together with deposited fibronectin matrix from temperature-responsive culture surface *Journal of Biomedical material research*, 45, 355-362.

- Laflamme, M. A., Zbinden, S., Epstein, S. E., Murry, C. E. (2007). Cell-based therapy for myocardial ischemia and infarction: Pathophysiological mechanisms. *Annual Review of Pathology*, 2, 307–339.
- Leor, J, Amsalema, Y, Cohen, S. (2005). Cells, scaffolds, and molecules for myocardial tissue engineering. *Pharmacology and Therapeutics*, 105,151–63.
- Lindenfeld, J., Miller, G. G., Shakar, S. F., Zolty, R., Lowes, B. D., Wolfel, E. E. (2004). Drug therapy in the heart transplant recipient: Part I: Cardiac rejection and immunosuppressive drugs. *Circulation*, 110, 3734–3740.
- Martin, G., Sutton, S. J., Sharpe, N. (2000). Left Ventricular Remodeling After Myocardial Infarction Pathophysiology and Therapy. *Circulation*, 101, 2981-2988.
- Mukherjee, S., Venugopal, J. R., Ravichandran, R., Ramakrishna, S., Raghunath, M. (2010).Multimodal biomaterial strategies for regeneration of infarcted myocardium. *Journal of Materials Chemistry*, 20, 8819-8831.
- Muller-Ehmsen, J., Whittaker, P., Kloner, R. A., Dow, J. S., Sakoda, T., Long, T. I., Laird, P. W., Kedes, L. (2002). Survival and Development of Neonatal Rat Cardiomyocytes Transplanted into Adult Myocardium. *Journal of Molecular and Cellular Cardiology*, 34, 107-116.
- Peppas, N.A., Bures, P., Leobandung, W., Ichikawa, H. (2000). Hydrogels in pharmaceutical formulations. *European Journal of Pharmaceutics and Biopharmaceutics*, 50, 27–46.
- Perin, E. C., Lopez, J. (2006). Methods of stem cell delivery in cardiac diseases. *Nature reviews Cardiology*, 3, S110-S113.
- Pfeffer, M. A., Braunwald, E. (1990). Ventricular remodeling after myocardial infarction. Experimental observations and clinical implications. *Circulation*, 81, 1161–1172.
- Ravichandran, R., Venugopal, J. R., Sundarrajan, S., Mukherjee, S., Sridhar, R., Ramakrishna, S. (2012). Minimally invasive injectable short nanofibers of poly(glycerol sebacate) for cardiac tissue engineering. *Nanotechnology*, 23, 5102.
- Reneker, D. H., Chun, L. (1996). Nanometre diameters of polymer, produced by electrospinning. *Nanotechnology*. 7, 216–23.

- Reneker, D. H., Yarin, A. L. (2008). Electrospinning jets and polymer nanofibers. *Polymer*, 49, 2387–425.
- Roche. E. T., Hastings, C. L., Lewin, S. A., Shvartsman, D. E., Brudno, Y., Vasilyev, N. V., J.O'Brien, F., Walsh, C. J., Duffy, G. P., Mooney, D. J. (2014). Comparison of biomaterial delivery vehicles for improving acute retention of stem cells in the infarcted heart. *Biomaterials*, 35, 6850-6858.
- Roussenova, M., Enrione, J., Diaz-Calderon, P., Taylor, A. J., Ubbink, J., Alam, M. (2014). Effect of polyols on the molecular organization and thermodynamic properties of low water content gelatin oligomers. *Polymer*, 55, 6827-6836.
- Schreuder-Gibson, H. L., Gibson, P., Senecal, K., Sennett, M., Walker, J., Yeomans, W. (2002) Protective textile materials based on electrospun nanofibers. *Journal Advanced Material*, 34, 44–55.
- Segers, V. F. M., Lee, R. T. (2010). Protein therapeutics for cardiac regeneration after myocardial infarction. *Journal of Cardiovascular Translational Research*, 3, 469–477.
- Shapiro, L., Cohen, S. (1997). Novel alginate sponges for cell culture and transplantation. *Biomaterials*, 18, 583-590.
- Sherman, W., Martens, T. P., Viles-Gonzalez, J. F., Siminiak, T. (2006). . Catheter-based delivery of the cells t the heart. *Nature reviews Cardiology*, 3, S57–S64].
- Singelyn, J. M., DeQuach, J. A., Seif-Naraghi, S. B., Littlefield, R. B., Schup-Magoffin, P. J., Christman, K. L. (2009). Naturally derived myocardial matrix as an injectable scaffold for cardiac tissue engineering. *Biomaterials*,30, 5409.
- Soonpaa, M. H., Koh, G. Y., Klug, M. G., Field, L. J. (1994). Formation of nascent intercalated disks between grafted fetal cardiomyocytes and host myocardium. *Science*, 264, 98–101.
- Sridhar, R., Lakshminarayanan, R., Madhaiyan, K., Amutha Barathi, V., Lim, K. H. C., Ramakrishna, S. (2015). Electrospayed nanoparticles and electrospun nanofibers based on natural materials: applications in tissue regeneration, drug delivery and pharmaceuticals. *Chemical Society Reviews*, 44, 790-814.
- Sun, Y., Weber, K. T. (2000) Infarct scar: a dynamic tissue. *Cardiovascular Research*, 46- 250–256.

- Sun, Y., Zhang, J. Q., Zhang, J., Lamparter, S. (2000). Cardiac remodeling by fibrous tissue after infarction in rats. *Journal of Laboratory & Clinical Medicine*, 135, 316–323.
- Sutton, M.G.S.J., Sharpe, N. (2000). Left Ventricular Remodeling After Myocardial Infarction: Pathophysiology and Therapy, *Circulation*, 101, 2981-2988.
- Tan, E. P. S., Ng, S. Y., Lim, C. T. (2005) Tensile testing of a single ultrafine polymeric fiber. *Biomaterials*, 26, 1453–6.
- Templin, C., Lüscher, T. F., Landmesser, U. (2011). Cell-based cardiovascular repair and regeneration in acute myocardial infarction and chronic ischemic cardiomyopathy current status and future developments. *International Journal Developmental Biology*, 55, 407–417.
- Theron, S. A., Yarin, A. L., Zussman, E., Kroll, E. (2005). Multiple jets in electrospinning: experiment and modeling. *Polymer*; 46, 2889–99.
- Thomson, R., Wake, M., Yaszemski, M., Mikos, A. (1995). Biodegradable polymer scaffolds to regenerate organs. *Advances in polymer science*, 122, 245-274.
- Van Tomme, S. R., Storm, G., Hennink, W. E. (2008). In situ gelling hydrogels for pharmaceutical and biomedical applications. *International Journal of Pharmaceutics* 355, 1–18.
- Xiang, Z., Liao, R., Kelly, M. S., Spector, M. (2006). Collagen–GAG Scaffolds Grafted onto Myocardial Infarcts in a Rat Model: A Delivery Vehicle for Mesenchymal Stem Cells. *Tissue Engineering*, 12, 2467–2478.
- Yu, L., Ding, J., (2008). Injectable hydrogels as unique biomedical materials. *Chemical Society Reviews*, 37, 1473.
- Yuan, X. Y., Zhang, Y. Y., Dong, C. H., Sheng, J. (2004). Morphology of ultrafine polysulfone fibers prepared by electrospinning. *Polymer International*, 53, 1704–10.
- Zhang, C., Yuan, X., Wu, L., Han, Y., Sheng, J. (2005). Study on morphology of electrospun poly (vinylalcohol) mats. *European Polymers Journal*, 41, 423–32.
- Zhong, S., Teo, W. E., Zhu, X., Beuerman, R. W., Ramakrishna, S., Yue, L. (2006). An aligned nanofibrous collagen scaffold by electrospinning and its effects on in vitro fibroblasts culture. *Journal of Biomedical Materials Research. Part A*, 79, 456-463.

Zimmermann, W. H., Melnychenko, I., Eschenhagen, T. (2004). Engineered heart tissue for regeneration of diseased hearts. *Biomaterials* 25, 1639–1647.

Chapter 3

Injectable in situ gelling scaffolds loaded platelet growth factors to improve cardiomyocyte survival after myocardial infarction

Saporito, F., Sandri, G., Rossi S., Bonferoni, M. C., Perotti, C., Ferrari, F., Black, L.

Submitted: ACS Biomaterial Science and Engineering

Corresponding author: Giuseppina Sandri

3.1 ABSTRACT

Myocardial infarction is one of the main causes that leads to heart failures. The aim of the present work was the development of in situ gelling systems, based on poloxamer 407 (P407) or sodium alginate (Alg), loaded with platelet lysate (PL) to enhance cardiomyocyte survival after myocardial infarction, as injectables into myocardial walls. Chondroitin sulfate (CS), a negatively charged glycosaminoglycan able to interact with different positively charged bioactive molecules, such as growth factors, was associated with both the systems.

Formulations were characterized by gelation properties (viscosity, consistency by means of penetrometry and injectability). Furthermore, the ability of the developed systems to improve CMs survival after infarction was assessed by means of *in vitro* assays toward cardiomyocytes (CMs) and cardiac fibroblasts (CFs) isolated from fetal rats.

Both the systems were characterized by gelation properties in physiological environment and by a suitable consistency to be injected into myocardial walls.

In vitro evaluation of biocompatibility toward cardiac cells (cardiomyocytes and cardiac fibroblasts) showed PL loaded alginate/chondroitin sulfate system allowed the highest number of viable cells with equal distribution of the populations of cardiomyocytes and fibroblasts.

Moreover, PL was able to allow the highest survival of cardiomyocytes after the oxidative damage (representing ischemic conditions due to MI) and Alg + CS PL and, much more, PL alone showed a considerable survival of cardiomyocytes and in the case of PL these represented the majority of cell population.

In conclusion, in situ gelling alginate chondroitin sulfate system, loaded with platelet lysate, was able to improve the survival of cardiomyocytes after oxidative damage resulting in a promising system to improve cardiac cell viability after MI.

3.2 INTRODUCTION

Heart failure, a condition derived from different heart diseases including myocardial infarction (MI), is the main cause of morbidity and mortality worldwide ¹⁻²

MI occurs after an ischemic event usually caused by the occlusion of a coronary artery related to the formation of an atherosclerotic plaque. This condition leads to the partial loss of contractile function of the heart followed by the formation of non-contractile fibrotic scar. As consequence, different compensatory mechanisms occur causing infarcted wall thinning, left ventricular chamber dilation, and eventually, heart hypertrophy. All these changes lead to heart failure development ³. Current therapies to treat MI aim to slow down heart failure progression but not to restore the contractile function of the myocardium ⁴. Indeed, the most promising therapeutic option to restore heart function loss is transplantation, a strategy limited by the insufficiency of donors as well as by serious complications caused by the necessary lifelong immune suppression ⁵.

Different strategies have been proposed to treat the damages caused by MI, including a cellular approach, based on the injection of different cell types directly into the infarcted heart, preformed cellular or acellular scaffolds, able to recreate the tridimensional structure of heart ECM (extracellular matrix). Among scaffolds, injectable in situ gelling systems could have many advantages and moldability (the ability to adapt to the shape of damaged tissue), and minimal invasive method of administration in comparison with other in vitro engineered constructs, giving smaller scar size, less complication during surgery, and less pain for the patients are the more attracting ⁶.

In situ gelling systems could be acellular or cellular scaffolds able to release bioactive molecules increasing cell survival after MI. They should be characterized by liquid or low viscous state before gelation (allowing easy administration and a homogeneous dispersion of eventually loaded biomolecules), controlled sol gel transition and system degradation (to avoid toxicity and severe reactions), physical stability upon myocardial contractile activity, polymeric network with a suitable

structure to allow cell infiltration, cell-cell contact and free exchange of oxygen and nutrients and capability to support new tissue formation ⁷.

In situ gelation could be driven by different mechanisms such as temperature, pH and ionic crosslinking,

Poloxamer and alginate are polymers well known for their in situ gelling properties. Poloxamers, triblock copolymers of poly(ethylene oxide) (PEO) and poly(propylene oxide) (PPO) (PEO–PPO–PEO), are a class of synthetic materials with thermally responsive properties. These amphiphilic copolymers form micelles above CMC (critical micelle concentration) in an aqueous solution when a critical temperature is reached (critical micelle temperature-CMT). Gelation is due to micellar packing and entanglement ⁸.

Alginate is a polysaccharide based on alternating units of β -D-mannuronate (M-block) and α -L-guluronate (G-block): sol gel transition is due to the presence of divalent cations such as calcium, strontium, and barium, which cross-link guluronic-blocks resulting in the typical egg-box structure ⁹.

Given these premises, the aim of the work was the development of in situ gelling systems to improve cell viability after MI. Two different hydrogel systems were developed: a thermosensitive gel, based on poloxamer 407 (P407), and ion-dependent hydrogel, based on sodium alginate. Both polymers were associated with chondroitin sulfate (CS), a glycosaminoglycan based on N-acetylgalactosamine-glucuronic acid disaccharide units and able to interact with bioactive positively charged molecules, and with growth factors ¹⁰. The formulations were loaded with platelet lysate (PL), a hemoderivative obtained from platelet lysis, rich in growth factors (GF). GF from platelets should support cardiomyocyte survival and neoangiogenesis, critical step in repairing process after MI ¹¹.

Formulations were characterized by gelation properties (viscosity, consistency by means of penetrometry and injectability). Furthermore, the ability of the developed systems to improve CMs survival after infarction was assessed by means of *in vitro* assays toward cardiomyocytes (CMs) and cardiac fibroblasts (CFs) isolated from fetal rats.

In particular, oxidative stress, that usually occurs after MI, was simulated in the absence or presence of the developed systems and cardiac (fibroblasts and cardiomyocytes) cell survival was assessed.

3.3 EXPERIMENTAL PART

3.3.1 Materials

The following polymers were used: alginic acid sodium salt (Alg), medium viscosity from brown algae average molecular mass 80000-120000 Da, 61% of mannuronic (M) residues and 39% of guluronic (G) residues; M/G ratio of 1.56 (Sigma-Aldrich, Italy); poloxamer 407 (P407), poly(ethylene glycol)-block-poly(propylene glycol)-block-poly(ethylene glycol, average molecular mass 10000-14600 Da; oxyethylene content, 71.5-74.9%, Kolliphor® P 407, Sigma-Aldrich, Italy); chondroitin sulfate (CS) (100 EP, low MW, 14000 Da, mixture of A (chondroitin 4 sulfate) and C (chondroitin 6 sulfate), (Bioiberica, Barentz, Italy).

Platelet lysate (PL) was obtained from the Apheresis Service of Immunohaematology and Transfusion Service Center for transplant immunology, by employing a sterile connection technique. Aliquots of hyperconcentrate platelets (high platelet concentration in small plasma volume and minimal leukocyte contamination) were obtained from apheresis, carried out on regular blood donors. The platelet pool was frozen at -80°C for 5 h and subsequently thawed in a sterile water bath at 37°C . An automated platelet count and tests for aerobic, anaerobic and fungi contamination were performed after saline dilution.

3.3.2 Methods

3.3.2.1 Preparation of polymeric solutions

Two different polymeric systems were prepared.

Alg+CS system was based on Alg 2% (w/w), CS 2% (w/w) and mannitol 5,07% (w/w) in bidistilled water. The components were hydrated under stirring at room temperature. P407+CS system was based on P407 at 22 % (w/w), CS 2% (w/w) and mannitol 5,07% (w/w) in bidistilled water. The components were hydrated under stirring at 4°C by using an ice bath. All the systems were prepared with two folds concentration per each component and loaded 1:1 weight ratio by mixing with FBS

(fetal bovine serum, Lonza, Italy) (to simulate PL loading and to evaluate the interference of proteins toward gelation process) or with PL.

3.3.2.2 Determination of the gelation properties

3.3.2.2.1 Rheological measurements

Viscosity measurements were performed by using a rotational rheometer (Rheostress 600, Haake, Enco, Italy), equipped with a cone-plate combination (C35/1: diameter= 35 mm; cone angle= 1°) measuring system. All measurements were carried out by using a constant shear rate (at 5 s⁻¹) in a range of temperature between 4-40°C maintained for 3 minutes before measurements.

3.3.2.2.2 Penetrometry

Penetrometry measurements were carried out by means of a dynamometer (TA.XT plus, Stable Microsystems, ENCO, Italy) equipped with a 1 kg load cell. At this purpose, 2.3 g of the polymeric mixture were poured in a Petri dish having 2.7 cm diameter. In the case of Alg+CS system (in presence and without FBS), each sample was covered by means of a dialysis membrane (cut-off 12-14 kDa, Emanuele Mires, Italy). Each sample was dipped in 50 ml of a CaCl₂ solution (5% w/w) under magnetic stirring at room temperature to allow ion dependent gelation. As for P407+CS system (in presence and without FBS), each sample was stored at different controlled temperatures (4°C – storage temperature; 25°C – room temperature and 37°C – physiological temperature).

At prefixed intervals of time (0, 12 and 24 h), penetrometry measurements were carried out by using a spherical probe (1/4” sph. Stainless p/0.25S) or cylindrical probe (20 mm Cyl/perpex p/20) for Alg and P407 based samples, respectively. The probes were lowered at 0.1 mm/s speed up to 0.2 mm. The work of penetration was calculated as the area under the force vs distance curve.

3.3.2.2.3 Injectability properties

Injectability properties of the systems were carried out by using a dynamometer (TA.XT plus, Stable Microsystems, ENCO, Italy) equipped with a particular system that allows to fix the plunger of the syringe to the mobile arm of the instrument. At the base of the instrument a metallic support, perpendicular to the syringe, was set. In the middle of the metallic support, a hole that allows the passage of the syringe was present. The syringe plunger was pushed down at 0.1 mm/s speed rate up to 10 mm of plunger displacement. Extrusion force of the polymeric mixtures from 27 gauge needle (0.40x13 mm) with a 1 ml syringe, was measured as a function of the plunger displacement.

3.3.2.3 In vitro tests

3.3.2.3.1 Fetal cardiomyocytes and cardiac fibroblasts isolation

Cardiac cells (cardiomyocytes, CMs, and cardiac fibroblasts, CFs) were obtained from rat heart fetuses. All animal procedures were performed in accordance with the Institutional Animal Care and Use Committee at Tufts university and the NIH guide for the Care and Use of Laboratory Animals.

Hearts were harvested from euthanized fetuses at 17-18th days of pregnancy (adult Sprague Dawley rats, SD, Charles River Laboratories) and collected in ice-cold sterile PBS supplemented with 20 mM glucose and 1 ml/l of penicillin-streptomycin solution (100 IU/ml-100 µg/ml, Sigma-Aldrich, USA).

Heart tissues were transferred in a conical tube and 7 ml of collagenase solution (15000 IU/litter, collagenase type II, Worthington Biochemical Corporation, USA) were added and the tissue digested for 7 min by stirring with orbital shaker. Hearts were then triturated and the supernatant was collected. The undigested tissues were subjected to subsequent digestion cycles up to the complete digestion. The supernatants were filtered (70 µm pore size membrane, ThermoFisher, MA). Cells were centrifuged at 500 rpm for 10 min, resuspended in DMEM (Dulbecco's Modified Eagle's Medium, ThermoFisher, MA) added with 10% w/w horse serum

(ThermoFisher, MA), 2% w/w FBS (fetal bovine serum, ThermoFisher, MA) and 1% w/w pen/strep/ampho (100 IU/ml-100 µg/ml-0.25 µg/ml, Sigma-Aldrich, USA).

3.3.2.3.2 Biocompatibility properties of the formulations

2.1×10^4 cells/cm² cardiac cells were seeded in a 24 well/plate. 500 µl of each system loaded with PL (mixtures 1:1 volume ratio – polymer final concentrations as described in the paragraph “Preparation of polymeric solutions”) were placed into a transwell insert (porosity of 0.8 µm, Transwell®, Corning Costar, USA) and the proliferation properties of cardiac cells were evaluated after 48 h and 7 days of contact, at 37° C in a 5% CO₂ atmosphere with 95% relative humidity (RH), by using a live dead assay (described in paragraph “Live dead assay”). Furthermore, a specific staining of CMs or CFs (described in paragraph “Fluorescence microscopy analysis of the cell substrates”) was performed to identify and count both cell populations.

3.3.2.3.3 Evaluation of the optimal conditions to simulate the oxidative damage

To determine the right H₂O₂ concentration and exposure time of culture, to induce approximate 50% of cell viability, cells were seeded at a density of 2.1×10^4 cells/cm² in a 24 well/plate and grown to confluence. Then, cells were washed with a PBS solution (Dulbecco’s Phosphate Buffered Saline, ThermoFisher, MA) and put in contact with 400 µl of H₂O₂ at two different concentrations, 0.05 and 0.25 mM, for three different time intervals, 30-45-90 min. Cells were kept at 37° C in a 5% CO₂ atmosphere with 95% relative humidity (RH). The cell viability was assessed by means of a live dead assay (described in paragraph “Live dead assay”). Furthermore, a specific staining of CMs or CFs (described in paragraph “Fluorescence microscopy analysis of the cell substrates”) was performed to identify and count both cell populations.

3.3.2.3.4 Evaluation of cardiac cell survival after oxidative damage and treatment with formulations

$2.1 \times 10^4/\text{cm}^2$ cardiac cells were seeded in a 24 well/plate. 500 μl of each system loaded with PL were placed into a transwell insert (porosity of 0.8 μm , Transwell®, Corning, Costar, USA) into wells of 24 transwell plates. After 3 days of culture, at confluence, cardiac cells were put in contact with 0.25 mM H_2O_2 for 30 min at 37° C in a 5% CO_2 atmosphere with 95% relative humidity (RH).

After 30 minutes, cells were washed by using PBS solutions and 500 μl of the formulations loaded with PL were placed into a transwell insert. The viability of cardiac cells was evaluated after 48 h and 7 days of contact at 37° C in a 5% CO_2 atmosphere with 95% relative humidity (RH), by using a live dead assay (described in paragraph “Live dead assay”). Furthermore, a specific staining of CMs or CFs (described in paragraph “Fluorescence microscopy analysis of the cell substrates”) was performed to identify and count both cell populations.

3.3.2.3.5 Live dead assay

Live dead assay is a cell viability test to assess and quantify intracellular esterase activity and plasma membrane integrity, by using two fluorescent probes: acetoxymethyl calcein (calcein AM) (ex/em ~494 ~515 nm) (ThermoFisher, MA) and ethidium homodimer (EthD-1) (ex/em ~528/~617 nm) (ThermoFisher, MA).

Briefly, live cells are identified by the presence of the intracellular esterase activity, determined by the enzymatic conversion of calcein AM, non-fluorescent and cell-permeant, to fluorescent calcein (in green), not permeable in the viable cells. Dead cells are identified by means of the binding of nucleic acids to EthD-1 (red fluorescence), able to reach cell nuclei through damaged membranes.

Fluorescent probes were solubilized in 10 ml PBS at the following concentrations:

2 μM calcein AM and 4 μM EthD-1.

Cell culture medium was removed from the wells and the cells washed with PBS; then, 135 μl of the fluorescent solution previously prepared were distributed in each well and kept in contact with the cells for 30 min.

A fluorescence microscope (KEYENCE BZ-X710) was used to capture the images, then processed by using specific software (Image J and Cell Profiler 2.2.0).

3.3.2.3.6 Fluorescence microscopy analysis of the cell substrates

Cell substrates were fixed by using 4% (w/v) paraformaldehyde solution in PBS (Sigma Aldrich, USA) for 10 min at 4° C. The substrates were then washed three times with PBS and cell membranes permeated with Triton X 0.5 % (w/v) (Sigma Aldrich, USA) at 20° C. After three-time rinsing, the substrates were put in contact with 1% (w/v) BSA (Bovine serum albumin, Sigma, USA) block solution added with 5% (v/v) donkey serum (Sigma, Aldrich, USA) for 1 h at room temperature.

Cardiomyocytes were stained by using 88 µl primary antibody anti- α -actinin (sarcomeric) produced in mouse (30.3 mg/ml diluted at 1:1600, Sigma-Aldrich, USA) (contact time 1 h), and after washing with PBS primary antibodies were conjugated with 88 µl fluorescence secondary antibody CF™ 555 (TRITC, λ_{ex} =555 nm, λ_{em} =565 nm) (2 mg/ml concentration diluted at 1:400, Sigma-Aldrich, USA) (contact time 1 h).

Cardiac fibroblasts were stained by using 50 µl primary antibody anti-actin α -smooth muscle antibody (mouse monoclonal) produced in mouse (2.3 mg/ml diluted at 1:460, Sigma-Aldrich, Italy), and after washing with PBS primary antibodies were conjugated with 50 µl the secondary antibody CF™ 555 (TRITC, λ_{ex} =555 nm, λ_{em} =565 nm).

All the substrates were subjected to proliferating cell staining by means of 88 µl Ki-67 primary antibody (1 mg/ml concentration diluted at 1:200, Sigma-Aldrich, USA), and, after washing with PBS, primary antibodies were conjugated with the fluorescence secondary antibody Atto 488 goat anti-rabbit IgG (Atto 488, λ_{abs} =501 nm, λ_{em} =523 nm) (1 mg/ml concentration diluted at 1:200, Sigma-Aldrich, USA).

All the cardiac cells nuclei were stained with DAPI (1:10000 diluted, Sigma-Aldrich, USA).

A fluorescence microscope (KEYENCE BZ-X710) was used to capture the images, then processed by using specific software (Image J and Cell Profiler 2.2.0).

3.3.2.3.7 Statistical analysis

Statistical differences were evaluated by means of a non-parametric test: Mann Whitney (Wilcoxon) W test, (Stat Graphics 5.0, Statistical Graphics Corporation, MD, USA). Differences were considered significant at $p < 0.05$.

3.4 RESULTS AND DISCUSSION

3.4.1 Gelation properties of the systems

Figure 1 reports viscosity profiles as a function of temperature, measured at fixed shear rate (5 s^{-1}), evaluated for the formulations based on P407 in presence and without FBS.

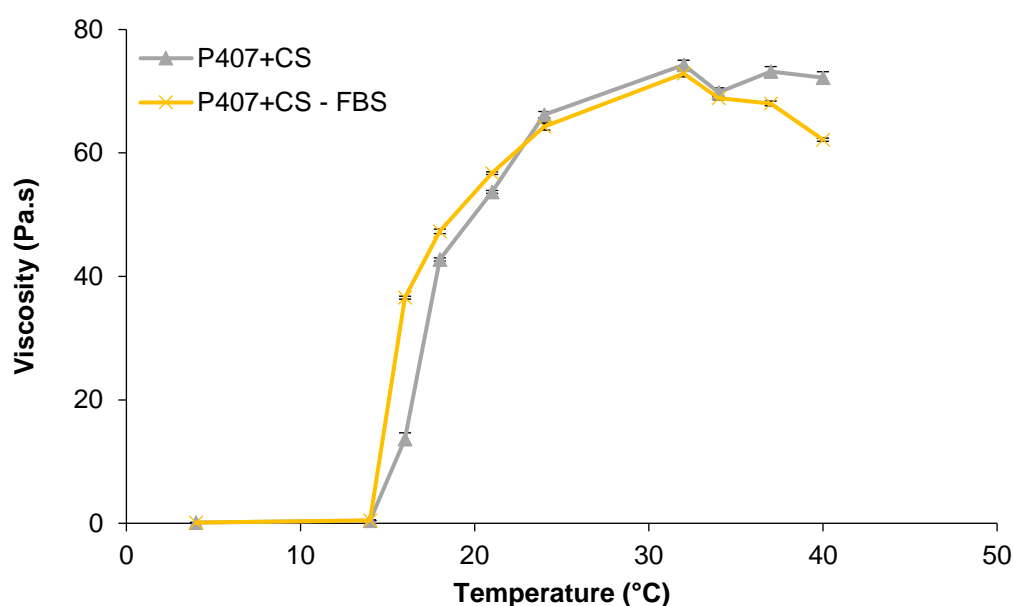


Figure 1: viscosity profiles as a function of temperature, measured at fixed shear rate (5 s^{-1}), evaluated for the formulations based on P407 in presence and without FBS (mean values \pm sd; n=3).

P407 started the gelation process at temperature higher than 14°C , viscosity increased almost linearly up to 32°C and above 32°C viscosity remained constant. The presence of FBS did not change the gelation process and the consistency of the resulting gel. This means that plasma proteins did not impair gelation behavior. It is conceivable that proteins and CS did not alter micelle structure that is responsible for poloxamer transition from sol to gel state.

Figure 2 and 3 report the work of penetration (mN*mm) for P407+CS and Alg+CS systems, respectively, in presence and without FBS. P407 systems were evaluated at different controlled temperatures (4°C – storage temperature; 25°C – room temperature and 37°C – physiological temperature) while Alg + CS systems before and after dipping samples in 50 ml of a CaCl₂ solution (5% w/w) for 12 and 24 h. P407 systems were characterized by very low consistency at 4°C. 25 and 37°C allowed system gelation with an increase of work of penetration of 30-40 folds. The presence of both CS and FBS conferred a higher stiffness to the resulting gel. The gelation process seems complete also at 25°C and this could guarantee a fast gelation after application.

Alg CS + formulation showed a significant increase of consistency after 12 h in contact with Ca²⁺ suggesting that neither CS nor FBS proteins interfere with gelation process and that Ca²⁺ could freely interact with guluronic residues forming egg-box structure responsible to gelation. The alginate gelation process could not be followed by rheological behavior because the gelled system was too rigid and was broken by the measuring system.

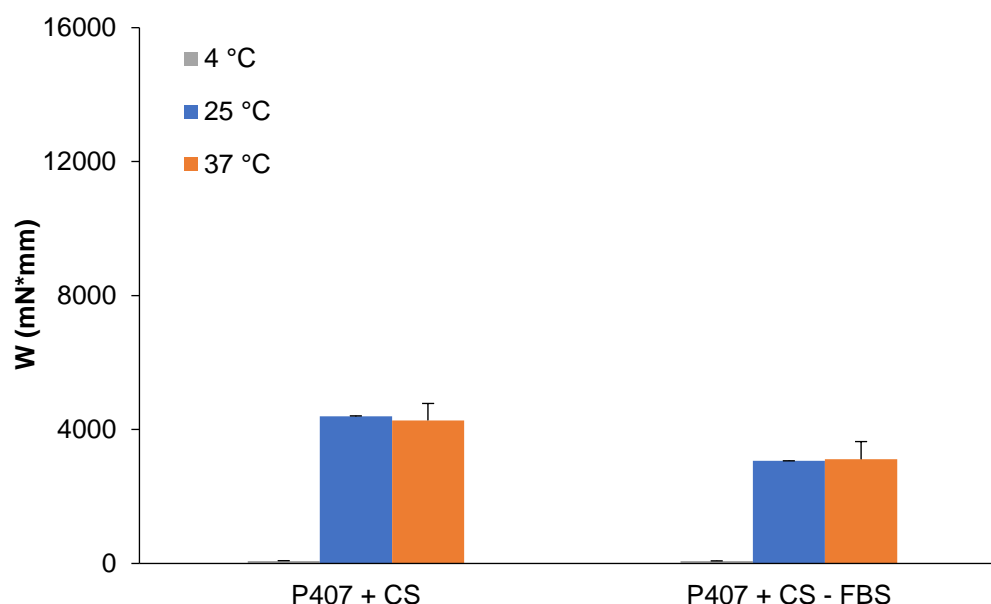


Figure 2: Work of penetration (mN*mm) of P407 systems evaluated at different controlled temperatures (4°C – storage temperature; 25°C – room temperature and 37°C – physiological temperature) (mean values \pm sd; n=6).

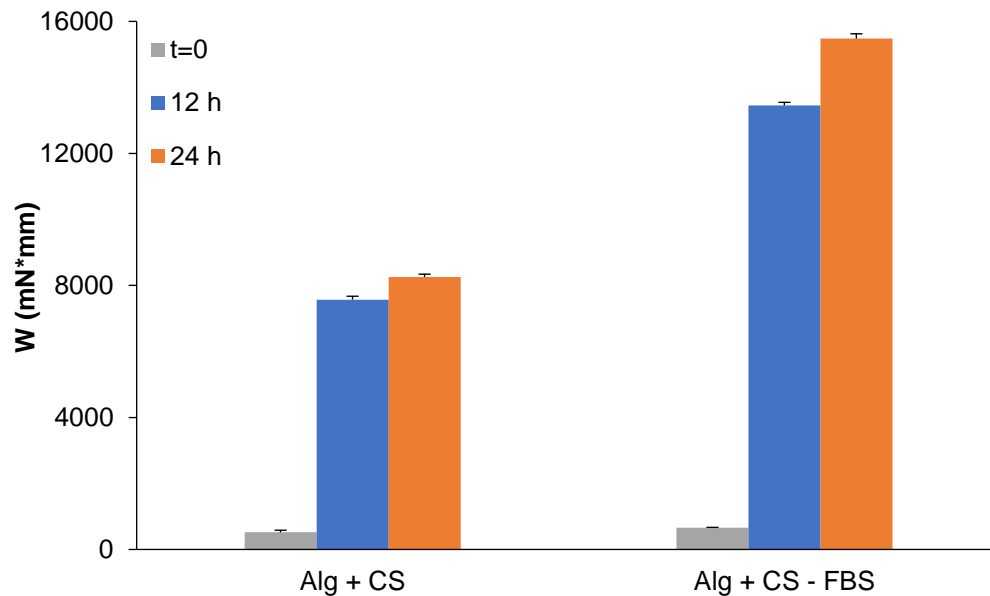


Figure 3: Work of penetration (mN*mm) of Alg + CS with or without serum before and after dipping samples in 50 ml of a CaCl₂ solution (5% w/w) for 12 and 24 h (mean values \pm sd; n=6).

3.4.2 Injectability properties

P407 + CS was characterized by a force of extrusion of 22.1 ± 0.5 N (mean values \pm sd; n=3). The association of FBS slightly decreased force of extrusion giving a force of extrusion of 19.5 ± 0.4 N (mean values \pm sd; n=3). Analogously, Alg + CS systems was characterized by an extrusion force of 25.4 ± 0.1 (mean values \pm sd; n=3) and also in this case the association of FBS decreased the force of extrusion 22.2 ± 0.1 (mean values \pm sd; 3). According to clinical practice, needles with small gauges as in this case (27-gauge needle) are routinely used to reduce damages at site of injection. Considering that the pressure generated for any particular syringe at a predetermined speed depends on the force exerted by the physician and by surface area of the syringe section ($\text{pressure}_{\text{generated}} = \text{force}_{\text{thumb}} / \text{area}_{\text{syringe diameter}}$), the average maximum force of injection is of about 80 N (males: 95.4 N, females: 64.1 N)¹². All the developed systems were characterized by good injectability.

3.4.3 In vitro tests

3.4.3.1 Biocompatibility properties of the formulations

Figure 4 reports the average number per cm^2 of dead cells, of CMs and of CFs after the contact with the following samples: GM, as control (standard growth conditions), PL, P407 + CS PL and Alg +CS PL in situ gelling systems, for 48 h and 7 days.

The total cell number was low after 48 h of culture: the standard growth conditions (growth medium, GM) was characterized by a high number of dead cells not significantly different from those in contact with PL and Alg + CS PL. GM and PL determined also similar growth of CMs and CFs while Alg + CS PL allowed a limited CMs and CFs growth not significantly different from P407 + CS PL.

After 7 days of culture the number of cells/ cm^2 was higher than those after 48 h of growth. GM caused the lowest cell viability considering the highest number of dead cells while all the other samples were characterized by low cell mortality not significantly different in all cases.

PL determined the highest number of viable cells almost equally distributed in CMs and CFs. Alg + CS PL determined a good cell growth although cell population was 4 folds lower than that of PL. Also in this case cells grown consisted of equal populations of CMs and CFs.

P407 + CS PL did not enhance cell growth and cell population was mainly composed by fibroblasts.

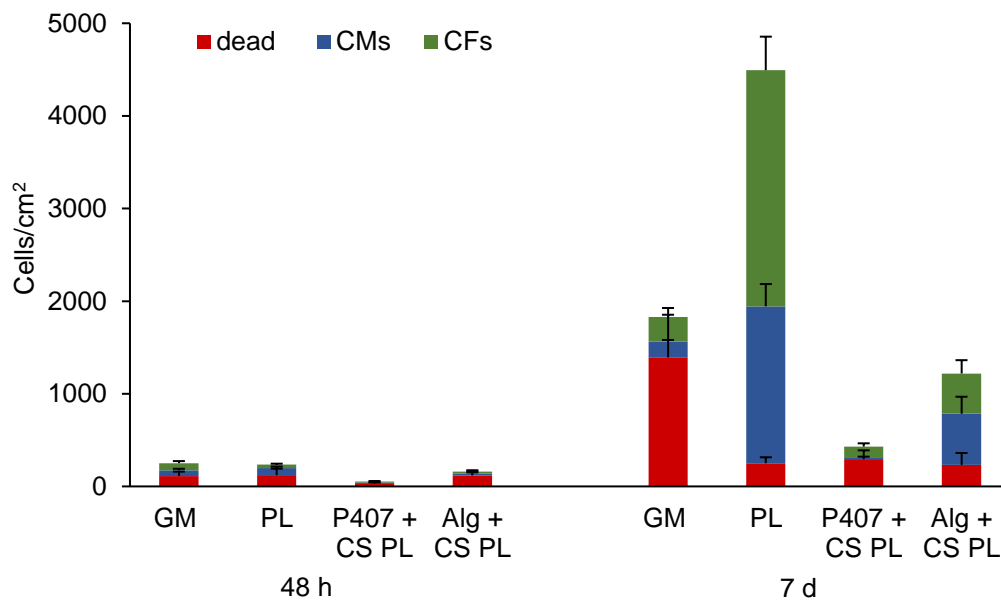


Figure 4: biocompatibility of cardiac cells in contact with P407 + CS PL and Alg + CS PL systems for 48 h and 7 days. The results are reported as number of dead, CMs and CFs per cm^2 . Growth medium (GM) and PL were considered as control (mean values \pm sd; $n=9$).

Figures 5 and 6 report microphotographs of cell substrates after 48 h and 7 days of growth in presence of P407 + CS PL and Alg + CS PL systems and GM and PL as references. The nuclei are in blue (DAPI staining), the proliferating cells in green (proliferation marker in green – KI67) and CMs or CFs were in red (α actinin antibody for CMs - Fig. 5 and smooth muscle actin antibody for CFs – Fig. 6).

After 48 h of growth, the fluorescence microscopy analysis confirmed the scarce cell growth for both CMs (Fig. 5) and CFs (Fig. 6) although the presence of PL, especially alone, in all the samples enhanced cell proliferation, as evidenced from green-blue co-localization in nuclei. In fact, green signal was determined by Ki-67 that detects nuclear antigen present in proliferating cells (G_1 , S, G_2 phases and mitosis) and absent in quiescent cells (G_0 phase).

After 7 days of growth, CMs were present in all the samples and the in situ gelling system Alg + CS in presence of PL allowed the best cell growth (Fig. 5) and cardiomyocytes were characterized by aligned actin fibers to form bundles that

connected cell clusters. On the contrary CFs remained less aggregated with smooth muscle actin fiber less organized.

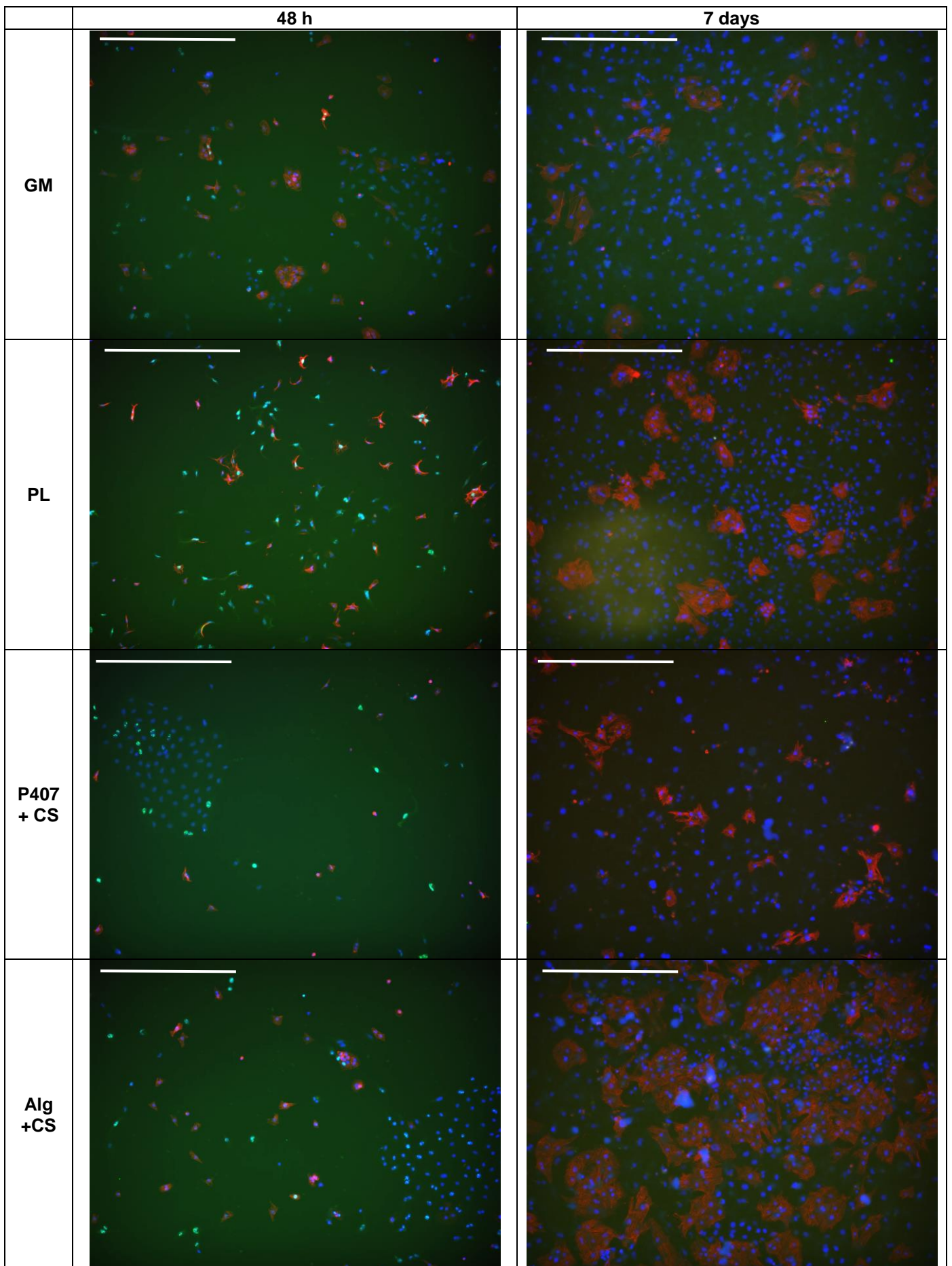


Figure 5: microphotographs of CMs after 48 h and 7 days of growth in presence of formulation and platelet lysate (nuclei in blue - DAPI; muscle fiber in red – α actinin antibody; proliferation marker in green – KI67). Scale bar: 500 μ m.

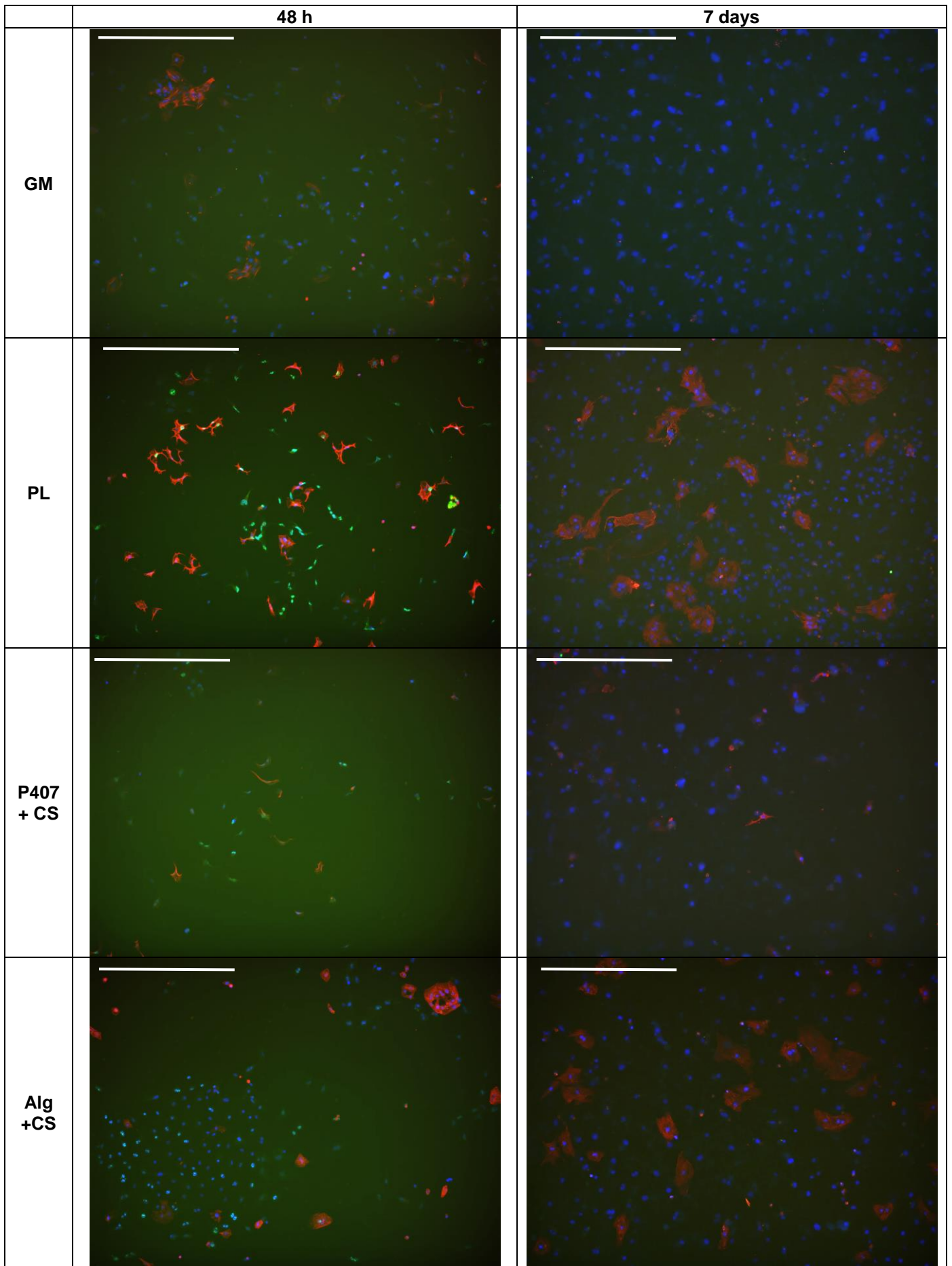


Figure 6: microphotographs of CFs after 48 h and 7 days of growth in presence of formulation and platelet lysate (nuclei in blue - DAPI; fibroblast muscle fiber in red – smooth muscle actin, SMA, antibody; proliferation marker in green – KI67). Scale bar: 500 μ m.

3.4.3.2 Oxidative damage

To determine the efficacy of the in situ thermosensitive and ion-dependent systems for promoting cell survival after myocardial infarction, cardiac cells were exposed to H_2O_2 to mimic oxidative stress concomitant to hypoxia due to ischemic event.

Figure 7 reports number/cm² of dead cells, of CMs and of CFs after treatment with 0.05 and 0.25 mM H_2O_2 for 30-45-or 90 minutes.

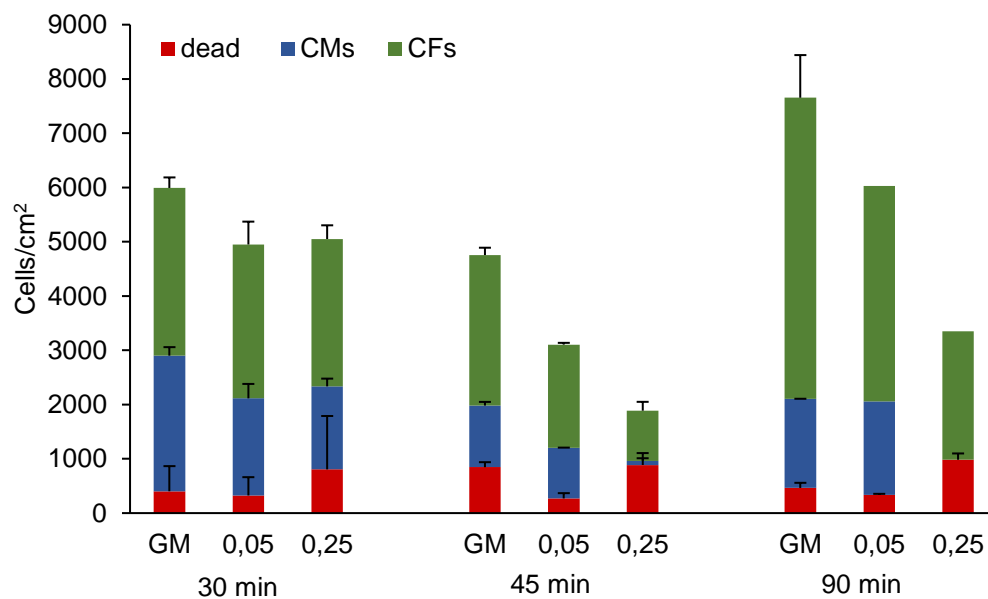


Figure 7: number/cm² of dead cells, of CMs and of CFs after treatment with 0.05 and 0.25 mM H_2O_2 for 30-45-or 90 minutes (mean values \pm sd; n=9).

Considering all the exposure times and particularly 45 and 90 min of contact time, the total cell number significantly decreased increasing H₂O₂ concentrations. However, the number of CMs and CFs was not so dramatically influenced by exposure times considering low H₂O₂ concentration (0.05 mM) while H₂O₂ at higher concentration (0.25 mM) caused an almost complete death of CM and a significant reduction of CFs considering 45 and 90 min of exposure time. Such results could be explained by the resistance of fetal cardiac cells to oxidation, a characteristic behavior due to their glycolytic metabolism. Therefore, 30 min of the exposure time and 0.25 mM of oxidative conditions were considered as able to simulate ischemic damage.

3.4.3.3 Cardiac cell survival after oxidative damage and treatment with formulations

Figure 8 reports number/cm² of dead cells, of CMs and of CFs after the contact with 0.25 mM H₂O₂ for 30 minutes (after 3 days of growth to reach confluence) and the treatment with GM, as control (standard growth conditions), PL, P407 + CS PL and Alg +CS PL systems for 48 h and 7 days.

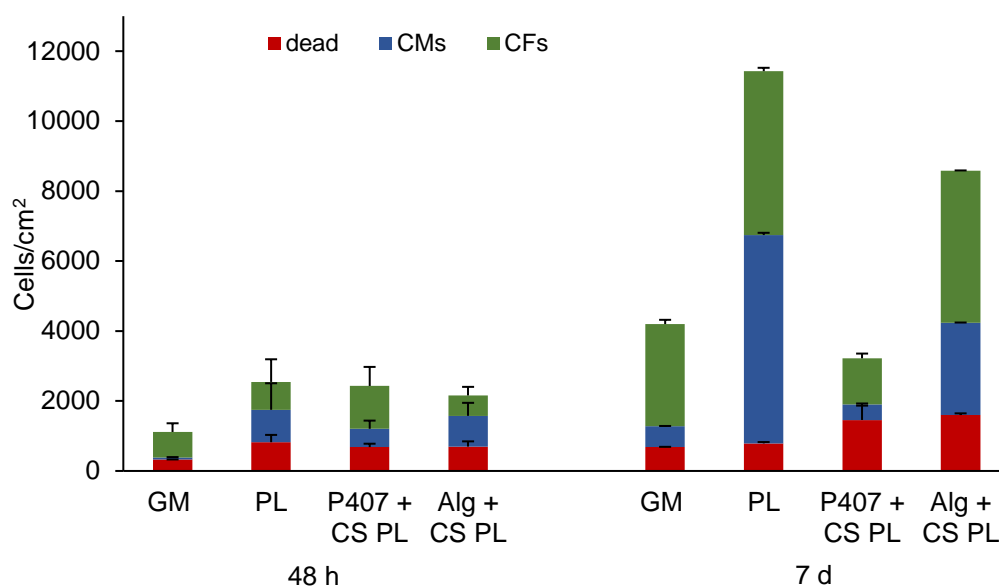


Figure 8: number of cells/cm² after contact with 0.25 mM H₂O₂ for 30 minutes and treatment with the developed in situ gelling systems P407 + Cs and Alg + CS both loaded with PL. GM (growth medium) and PL were considered as negative and positively control respectively. (mean values \pm sd; n=9).

After 48 h of contact with the samples, GM was characterized by the lower amount of dead cells, significantly less than in the presence of PL. However, GM did not allow the growth of CMs while the presence of PL alone or loaded in both in situ gelling systems determined a significant proliferation enhancement of CMs. On the contrary, the growth of CFs in standard conditions (GM) was not significantly different with respect to the in situ gelling systems.

After 7 days of growth, the number of dead cells in standard growth conditions was slightly but significantly higher than that after 48 h growth. PL determined cell death superimposable than that of GM while both in situ gelling systems determined a slightly but significantly higher cell dead, not significantly different from each other. The presence of PL alone or loaded in Alg + CS formulation allowed a significantly higher cell proliferation: the number of CFs was not significantly different in PL, Alg + CS PL with respect to standard growth conditions, while CFs number was the lowest for P407 + CS PL.

Moreover, CMs number was the lowest but similar considering GM and P407 + CS PL while PL alone determined the greater CMs proliferation followed by Alg + CS PL.

After 7 days of contact GM and PL determined the lower number of dead cells while the in situ gelling systems caused a slightly higher amount of dead cells. Considering cardiomyocytes, GM and P407 + CS PL system determined the survival of similar amounts of cells while Alg + CS PL and, much more, PL showed a considerable survival of cardiomyocytes and in the case of PL these represented the majority of cell population.

Figures 9 and 10 report microphotographs of cell substrates, subjected to oxidative damage with 0.25 mM H₂O₂ for 30 minutes, after 48 h and 7 days of growth in presence of P407 + CS PL and Alg + CS PL systems and GM and PL as references. The nuclei are in blue (DAPI staining), the proliferating cells in green (proliferation marker in green – KI67) and CMs or CFs cells were in red (α actinin antibody for CMs - Fig. 9, and smooth muscle actin antibody for CFs – Fig. 10).

As for CMs, CLSM analysis confirmed the viability results and PL and Alg + CS PL showed the higher density of cardiomyocytes (Fig. 9). In particular, after 48 h or 7 days of growth, cardiomyocytes showed a restrained cell growth with few cells interconnected and actin fibers scarcely organized. The presence of PL, alone or loaded in P407 + CS system, allowed CMs survival, although CMs were characterized by almost spheroidal cell clusters. On the contrary, Alg + CS PL determined a greater cardiomyocyte survival and a CMs proliferation to restore cell interconnections and actin fiber bundles.

As for CFs, after 48 h of growth the cell substrates treated with PL were characterized by a remarkable CFs growth: the smooth muscle actin staining revealed that fibroblasts possessed their normal shape. Moreover, fibroblasts reached confluency when PL was loaded in in situ gelling systems. After 7 days of growth, CFs population remained constant in substrates grown in standard growth conditions (GM) or in contact with PL and PL loaded in P407 CS, while in the case of Alg + CS PL CFs population seem less dense.

Cardiac fibroblasts are key cellular component of left ventricle remodeling after MI due to their number, location and capability to generate scar. Scar is a cellular, vascularized, and highly metabolically active tissue with contractile function¹³. In fact, following MI injury, the oxidative stress and the presence of reactive oxygen species stimulate an inflammatory response in fibroblasts, that are activated and transdifferentiated to myofibroblasts, which express α smooth muscle actin and microfilaments that guide contractile behavior¹⁴.

Recently it was proposed a novel idea that a well-healed infarct will actually contain more myofibroblasts than the infarct undergoing adverse remodeling¹⁵. These myofibroblasts are responsible for the production and deposition of collagen, leading to the establishment of a dense ECM that acts as support and minimizes infarcted area expansion¹⁵. Moreover, cardiac fibroblasts produce different types of ECM proteins, including fibronectin, laminins, and matricellular proteins. These ECM proteins are key mediators of intercommunication between the cardiac fibroblasts and other cell types, including cardiomyocytes and endothelial cells¹⁴⁻¹⁵.

Alginate and chondroitin sulfate based in situ gelling system (Alg + CS) loaded with PL allowed a cell proliferation lower than that observed for PL alone (Fig. 8). However, cardiomyocyte population was organized better than those growth in standard conditions or after the treatment with PL alone or loaded in P407 + CS in situ gelling system. Moreover, the simultaneous growth of activated fibroblasts (myofibroblasts) and cardiomyocytes was an important aspect. Following myocardial infarction fibroblast activation to myofibroblasts causes abundant synthesis and deposition of collagen (the major component of the scar. However due to the negligible regenerative capability of heart a collagen based scar is necessary to support myocardium integrity and replace the extensive loss of cardiomyocytes. The occurrence of contemporary cardiomyocyte and cardiac fibroblast survival due to Alg + CS PL should balance ECM accumulation caused by myofibroblasts, and this should avoid increased heart wall stiffness and compliance impairment. Furthermore, in situ gelation capability should guarantee a prolonged residence time with respect to PL alone.

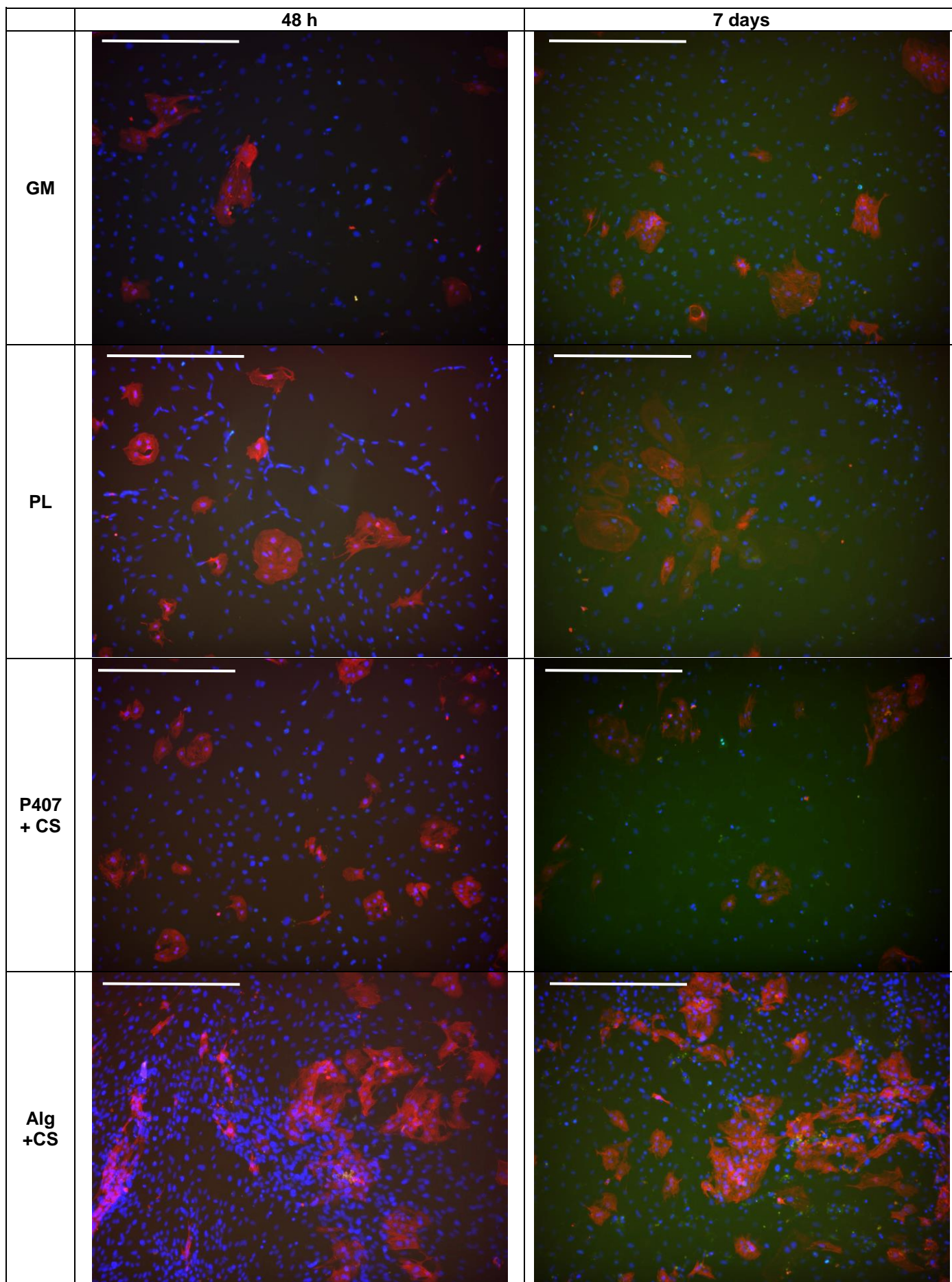


Figure 9: microphotographs of damaged CMs proliferation after 48 h and 7 days of growth in presence of formulation and platelet lysate (nuclei in blue - DAPI; muscle fiber in red – α actinin antibody; proliferation marker in green – KI67). Scale bar: 500 μ m.

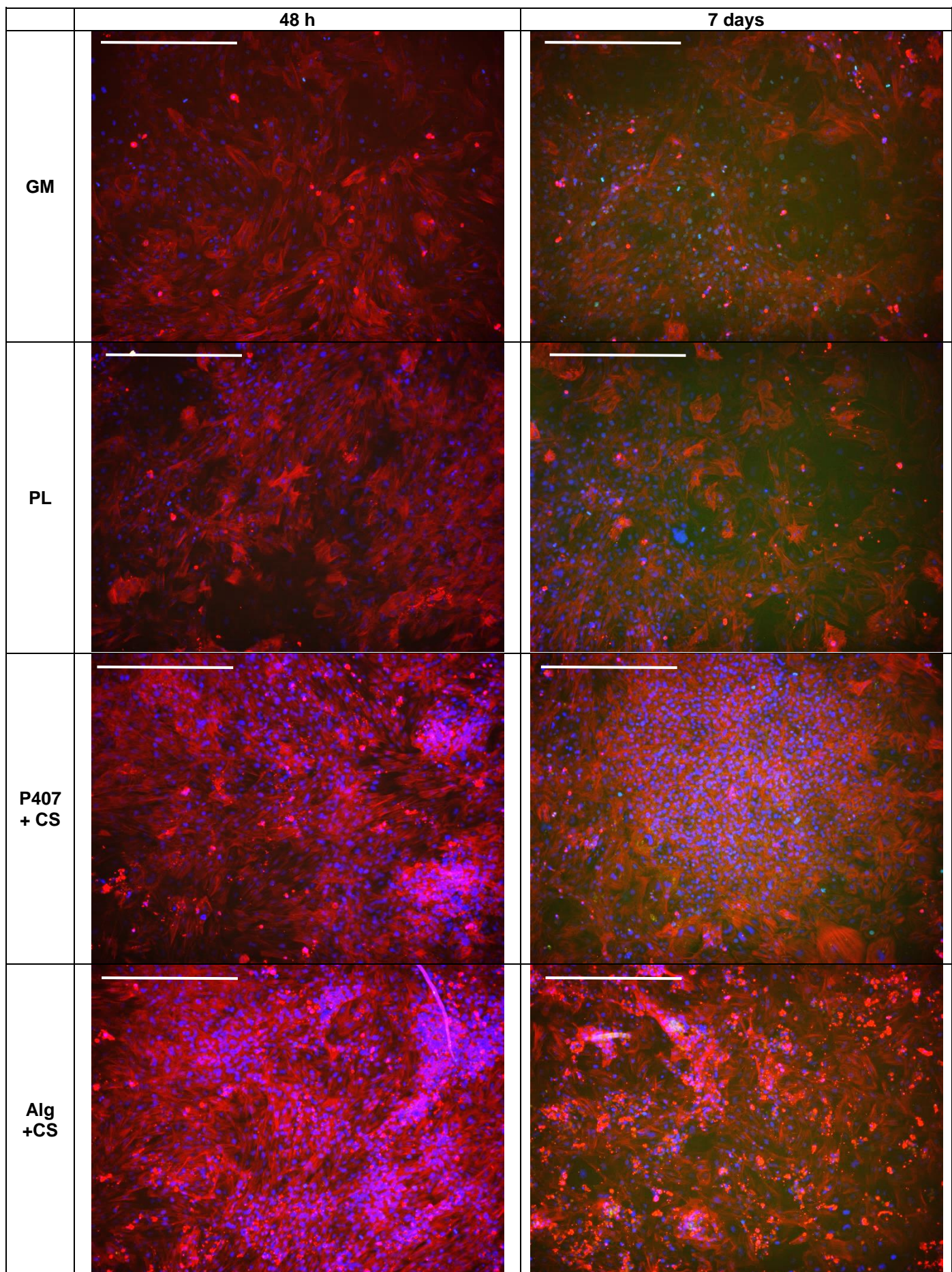


Figure 10: microphotographs of damaged CFs after 48 h and 7 days of growth in presence of formulation and platelet lysate (nuclei in blue - DAPI; fibroblast muscle fiber in red – smooth muscle actin, SMA antibody; proliferation marker in green – KI67). Scale bar: 500 μ m.

3.5 CONCLUSIONS

Thermosensitive in situ gelling systems based on poloxamer 407 and ion-dependent systems based on sodium alginate, in association with chondroitin sulfate, were prepared and characterized.

P407 + CS formulation was characterized by good thermogelling properties at 32°C, with a gelation process completed at 37°C. Alg + CS formulation presented a Ca²⁺ dependent gelation with a gelation time in physiological environment within 12 h.

The addition of serum proteins of FBS (to simulate platelet lysate proteins) did not affect both the system gelation properties and injectability was compatible to administration by using a 27 G needle.

In vitro evaluation of biocompatibility toward cardiac cells (cardiomyocytes and cardiac fibroblasts) isolated from fetus rat heart showed that PL and PL loaded alginate/chondroitin sulfate systems caused the highest number of viable cells with equal distribution of the populations of cardiomyocytes and fibroblasts, although PL allowed a cell growth 4 folds greater than in situ gelling alginate based system.

Moreover, PL was able to allow the highest survival of cardiomyocytes after the oxidative damage (representing ischemic conditions due to MI) and Alg + CS PL and, much more, PL alone showed a considerable survival of cardiomyocytes and in the case of PL these represented the majority of cell population.

The occurrence of contemporary cardiomyocyte and cardiac fibroblast survival due to Alg + CS PL should balance ECM accumulation caused by myofibroblasts, and this should avoid increased heart wall stiffness and compliance impairment. Furthermore, in situ gelation capability should guarantee a prolonged residence time with respect to PL alone.

In conclusion in situ gelling alginate system was able to improve the survival of cardiomyocytes after oxidative damage resulting a promising system to improve cardiac cell viability after MI.

3.6 REFERENCES

- (1) McMurray, J.; Stewart, S. Heart failure. Epidemiology, aetiology, and prognosis of heart failure. *Heart*. **2000**, 83 (3), 596-602. DOI:10.1136/heart.83.5.596.
- (2) Mozaffarian, D.; Benjamin, E. J., Go, A. S.; Arnett, D. K.; Blaha, M. J.; Cushman, M. Heart disease and stroke statistics-2014 update: a report from the American Heart Association. *Circulation*, **2014**, 13, 29–322. DOI: 10.1161/01.cir.0000441139.02102.80.
- (3) Tateishi, K; Takehara, N; Matsubara, H.; Hidemasa, O. Stemming heart failure with cardiac-or reprogrammed-stem cells. *J. Cell. Mol. Med.* **2008**, 12 (6a), 2217–2232. DOI: 10.1111/j.1582-4934.2008.00487.x.
- (4) Ye, K. Y.; Black, L. D. Strategies for tissue engineered cardiac constructs to affect functional repair following myocardial infarction. *J. Cardiovasc. Transl. Res.* **2011**, 4, 575. DOI: 10.1007/s12265-011-9303-1.
- (5) Zimmermann, W. H.; Cesnjevar, R. Cardiac tissue engineering: implications for pediatric heart surgery. *Pediatr. Cardiol.* **2009**, 30 (5) 716–723. DOI: 10.1007/s00246-009-9405-6.
- (6) Christman, K. L.; Lee, R. J. Biomaterials for the treatment of myocardial infarction. *J. Am. Coll. Cardiol.* **2006**, 48 (5), 907–13. DOI: 10.1016/j.jacc.2006.06.005.
- (7) Singelyn, J. M.; Christman, K. L. Injectable materials for the treatment of myocardial infarction and heart failure: the promise of decellularized matrices. *J. Cardiovasc. Transl. Res.* **2010**, 3 (5), 478–86. DOI 10.1007/s12265-010-9202-x.
- (8) Klouda, L. Thermoresponsive hydrogels in biomedical applications A seven-year update. *Eur. J. Pharm. Biopharm.* **2015**, 97 (1) 338-349. DOI: 10.1016/j.ejpb.2015.05.017
- (9) Cho, S. H.; Lim, S. M.; Han, D. K.; Yuk, S. H.; Im, G. I.; Lee, J. H. Time-dependent alginate/polyvinyl alcohol hydrogels as injectable cell carriers. *J.*

- Biomater. Sci. Polym. Ed. **2009**, 20 (7-8), 863–76. DOI: 10.1163/156856209X444312.
- (10) Yamada, S., Sugahara, K. Potential therapeutic application of chondroitin sulfate/dermatan sulfate. *Curr. Drug Disc. Tec.* **2008**, 5, 289-301.
- (11) Ertl, G.; Frantz, S. Healing after myocardial infarction. *Cardiovasc. Res.* **2000**, 66 (1), 22– 32. DOI: 10.1016/j.cardiores.2005.01.011.
- (12) Vo, A.; Doumit, M., Rockwell, G. The Biomechanics and Optimization of the Needle-Syringe System for Injecting Triamcinolone Acetonide into Keloids. *J. Med. Eng.* **2016**, 2016. DOI: 10.1155/2016/5162394.
- (13) Ma, Y.; Halade, G. V.; Lindsey, M. L. Extracellular matrix and fibroblast communication following myocardial infarction. *J. Cardiovasc. Transl.* **2012**, 5 (6) 848–857 DOI:10.1007/s12265-012-9398-z
- (14) Ma, Y.; Iyer, R. P.; Jung, M.; Czubyrt, M. P.; Lindsey, M. L. Cardiac fibroblast activation post-myocardial infarction: current knowledge gaps. *Trends Pharmacol. Sci.*, **2017**, 38, (5), 448-458. DOI: 10.1016/j.tips.2017.03.001
- (15) Daskalopoulos, E.P.; Janssen, B.J.; Blankesteyjn, W.M. Myofibroblasts in the infarct area: concepts and challenges. *Microsc Microanal.* **2012**, 18(1), 35-49. doi: 10.1017/S143192761101227X.

This work was objected of 2 conference presentations:

Saporito, F., Sandri, G., Bonferoni, M.C., Rossi, Ferrari, F., Caramella, C.

Sistemi gelificabili in situ per la veicolazione di emoderivati nel trattamento dell'infarto del miocardio, 55° Simposio AFI, Rimini, 10-11-12 Giugno 2015 (poster presentation).

Saporito, F., Sandri, G., Bonferoni, M.C., Rossi, Del Fante, C., Perotti, C., Caramella, C., Ferrari, F., Black, D. L.

Growth factor-loaded in situ gelling systems for myocardial infarction treatment, 2nd European Conference on Pharmaceutics, Cracovia, Polonia, 3-4 Aprile 2017 (poster presentation).

Chapter 4

Electrospun Gelatin-Chondroitin Sulfate Scaffolds Loaded with Platelet Lysate Promote Immature Cardiomyocyte Proliferation

Francesca Saporito, Giuseppina Sandri, Maria Cristina Bonferoni, Silvia Rossi, Lorenzo Malavasi, Claudia Del Fante, Barbara Vigani, Lauren Black, Franca Ferrari

Submitted: Polymers

Corresponding author: Giuseppina Sandri

4.1 ABSTRACT

The aim of the work was the development of heart implants as electrospun scaffolds based on gelatin (G) and chondroitin sulfate (CS) for the treatment of myocardial infarction.

Platelet lysate (PL), a hemoderivative from platelets rich in growth factors was embedded in the scaffolds.

Scaffolds were characterized for morphology and mechanical properties and for the capability to support in vitro adhesion and proliferation of fibroblasts and endothelial cells. Moreover, adhesion and proliferation of cardiac cells (cardiomyocytes and cardiac fibroblasts from rat fetuses) onto PL scaffolds were evaluated.

Scaffolds presented good elasticity and high stiffness suitable for in vivo adaptation to heart contraction. CS improved adhesion and proliferation of fibroblasts and endothelial cells and this behavior could be related to elastic properties, which could favor cell motility.

The presence of platelet lysate and CS seems crucial to allow adhesion and proliferation of cardiac cells and in particular of cardiomyocytes: G/CS scaffold embedded with PL seems able to select cell population leading cardiomyocytes proliferation rather than cardiac fibroblast one.

In conclusion, G/CS scaffold seems a promising system to assist myocardium reparation process preserving cardiomyocyte viability and preventing fibroblast proliferation, probably reducing consequently uncontrolled collagen deposition by fibroblasts.

4.2 INTRODUCTION

Congenital heart defects (CHD) (due to a failure of morphogenesis) occur in ~1% of all live births (reported prevalence ranking from 6 to 13 per 1000 live births) and are the most common type of birth defect. ^[1] The definitive therapeutic option for the most severe of these defects, such as HLHS (hypoplastic left heart syndrome) or ToF (tetralogy of Fallot), is corrective surgery with multiple operations within the first few years of life. These are generally palliative in nature, aimed at maintaining cardiac function as long as possible to increase the likelihood of transplant. However, although medical and surgical interventions have significantly improved survival over the years, CHD is still leading cause of mortality in infants and young children in industrialized countries since many patients develop heart failure. ^[2]

CHD often require major reconstructive surgery with surgical placement of implants lacking growth potential. ^[3, 4] Current patches consist of synthetic materials as polytetrafluoroethylene (PTFE), not biodegradable, prone to calcification and necessitating replacement in 14 % of patients. In addition, these patches induce an inflammatory foreign-body response, resulting in their encasement in stiff fibrous scar-like tissue without functionality. ^[3, 5]

Allografts, xenografts and autologous tissues such as pericardium and saphenous vein have been used as alternatives, but all are associated with similar complications to varying degrees and none have growth potential. ^[3] As a result, all types of implants increase risk of infections, heart failure, arrhythmia and aneurism. ^[5]

To overcome these limitations, myocardial tissue engineering plays an important role in the development of engineered cardiac tissue to restore contractile heart function. An optimal bioengineered scaffold should possess similar properties to those of heart extracellular matrix (ECM), to promote cell adhesion and to be physiologically reabsorbed as the new tissue regenerates. It should be able to persist during the regenerative process, trying to balance increased scar stiffness. ^[6]

In humans cardiomyocyte proliferation lasts until heart reached adult size and the rate of cardiomyocyte cell cycle activity is highest in infants and declines to very low levels in adults. ^[7, 8]

Although it is not yet fully elucidated which multiple extracellular factors are integrated by signal transduction cascades to control cardiomyocyte proliferation and cardiac regeneration, growth factors produced by epicardium, seem to promote differentiation and proliferation of cardiomyocytes. [7, 8]

The ideal material for heart repair would be naturally derived, structurally sound, and able to support adhesion and proliferation of cardiomyocytes and endothelial cells while limiting the growth of cardiac fibroblasts, which have the potential to promote scar formation upon surgical healing. Collagen type I and III are the major components of cardiac ECM and glycosaminoglycans can serve as both non-structural and structural proteins. [9, 10] Moreover ECM also has biochemical and mechanobiological functions by serving as a reservoir for growth factors. [11] Collagen seems the best candidates to obtain 3D scaffolds for cardiac repair but in the literature it has been reported as an immunogenic material. [12, 14]

Gelatin (G) is prepared starting from natural sources rich in collagen I by denaturation-hydrolysis process and in case of type-B G a partial alkaline hydrolysis of collagen occurs. [15]

G is a non-immunogenic material, which appears to be related to the absence of aromatic ring with respect to collagen, as G is deficient in Tyr and Trp and contains only a very small amount of Phe. [11]

A major challenge is the design of an implant as tridimensional (3D) support to mimic cardiac ECM allowing the cell-cell communication and cardiomyocyte contraction. Indeed, the 3D nanofiber network provides a high surface-to-volume ratio and high porosity to promote cell adhesion, proliferation and migration and sufficient oxygen and nutrient exchange. [16] Electrospinning is an enabling nanotechnology, simple and efficient to obtain nanofibrous scaffolds. [17]

Given these premises, the aim of the present work was the development of implants as electrospun scaffolds based on a combination of G with CS for potential use in CHD repair.

CS is a sulfated glycosaminoglycan, able to interact with various positively charged bioactive molecules and in particular with growth factors (GF). [18, 19] Among different GF involved in the cardiac repair, VEGF (vascular endothelial growth factor), TGF-

b1 (transforming growth factor), FGF (fibroblast growth factor) have a crucial role in promoting angiogenesis, fibrinogenesis and cardiomyocyte proliferation. [8, 19] Moreover in literature there are several evidences of CS effectiveness in enhancing cell proliferation in association with platelet lysate (PL), a hemoderivative from platelets rich in GF. [20-22]

Scaffolds were characterized for morphology and mechanical properties and for the capability to support fibroblasts and endothelial cells adhesion and proliferation in vitro. Moreover, scaffolds were embedded with platelet lysate as source of growth factors and the adhesion and proliferation of cardiac cells (cardiomyocytes and cardiac fibroblasts from fetal rats) were evaluated.

4.3 EXPERIMENTAL PART

4.3.1 Materials

Gelatin (G) from bovine skin 225 g Bloom type B (Sigma Aldrich, Italy) and chondroitin sulfate 100 EP (CS) low MW 14000 Da, mixture of A (chondroitin 4 sulfate) and C (chondroitin 6 sulfate), (Bioiberica, Barentz, Italy) were used as polymers.

Platelet lysate was obtained from the Apheresis Service of Immunohaematology and Transfusion Service Center for transplant immunology, by employing a sterile connection technique. Aliquots of hyperconcentrate platelets (high platelet concentration in small plasma volume and minimal leukocyte contamination) were obtained from apheresis, carried out on regular blood donors. The platelet pool was frozen at -80°C for 5 h and subsequently thawed in a sterile water bath at 37°C . An automated platelet count and tests for aerobic, anaerobic and fungi contamination were performed after saline dilution.

4.3.2 Methods

4.3.2.1 Preparation of polymeric solutions

Two different polymeric solutions were prepared: G and G/CS.

G was based on gelatin at 20% (w/w) in 10% (w/v) acetic acid, while G/CS was based on gelatin at 20% (w/w) and chondroitin sulfate at 2% (w/w) in 10% acetic acid. This latter solution was prepared by mixing 1:1 in weight ratio of G at 40% (w/w) in 20% w/v acetic acid and CS at 4% (w/w) in distilled water. G solutions were stirred at 40°C for 1 h. Citric acid (monohydrated citric acid, EP grade, Carlo Erba, Italy) was added at 5% (w/w) concentration to both G and G/CS solutions.

4.3.2.2 Rheological measurements

G and G/CS were subjected to viscosity measurements by means of a rotational rheometer (Rheostress 600, Haake, Enco, Italy), equipped with a cone-plate combination (C35/1: diameter= 35mm; cone angle= 1°) measuring system. All measurements were carried out at 25-37-40 °C, after a rest time of 3 min, applying a shear rate of 100 s⁻¹.

4.3.2.3 Physical properties of the solutions

4.3.2.3.1 Surface tension

The surface tension of G and G/CS solutions was measured using a tensiometer (DY-300 – Kyowa, Japan) having a measurement range between 0 and 100 mN.m. Measurements were carried out at 32°C, the temperature used during the electrospinning process, by a time-based detection.

4.3.2.3.2 Conductivity

The electrical conductivity of G and G/CS solutions was measured by means of an electrical conductometer (FiveGo™ - Mettler Toledo), after a calibration with a standard solution having a conductivity of 1413 μs/cm at room temperature.

4.3.2.4 Preparation of electrospun scaffolds

Scaffolds were obtained by using an electrospinning apparatus (STKIT-40, Linari Engineering), equipped with a high-voltage power supply (Razel R99-E 40, kV), a 10 ml syringe with 21 G needle (0.8x20 mm), and a conductive static collector, covered by aluminum foil. The following parameters were used: voltage was fixed at 28 kV, the distance between collector and needle was 15 cm, a polymeric solution flux of 0.4 ml/h, and spinning time of 1 h. The scaffolds were crosslinked by heating at 150°C for 2 h.

4.3.2.5 Nanofibers characterizations

4.3.2.5.1 SEM analysis

Scaffold morphology was analyzed by means of scanning electron microscopy (SEM, Tescan, Mira3XMU, ARVEDI Center, University of Pavia). Samples were sputter-coated by means of graphite deposition under vacuum. The scaffolds were analyzed before and after heating crosslinking and after 1 week dipped in distilled water. Nanofiber diameters were obtained by means of image analysis software (Image J) from the SEM images.

4.3.2.5.2 FT-IR analysis

Spectroscopic measurements were carried out by means of Infrared Imaging Microscope (Nicolet iN10 MX, Thermo Scientific, ARVEDI Center, University of Pavia). The infrared spectra were acquired over a wavelength range of 4000-500 cm^{-1} and a resolution of 10-20 μm^2 .

4.3.2.5.3 Mechanical properties

Scaffolds were subjected to tensile measurements by means of a TA.XT plus apparatus (Stable Microsystems, ENCO, Italy), equipped with a 1 kg load cell and A/TG tensile grips. Each scaffold was cut (3 cm length and 1 cm width) and kept vertical by means of two jaws, the lower one fixed and the upper one movable at a constant rate of 0,5 mm/s. Dried or hydrated scaffolds were stretched up to fracture and force as a function of grip distance was recorded. Tensile strength was calculated as the ratio between maximum force recorded (break force) and break area. Elongation % was calculated as the percentage ratio between the distance of the two grips at scaffold breaking and the initial scaffold length.

4.3.2.6 In vitro adhesion and proliferation assay: fibroblasts and endothelial cells

Adhesion and proliferation assays were carried out using two cell lines: fibroblasts (normal human dermal fibroblasts (NHDF) from juvenile foreskin, PromoCell, WVR, Italy) and endothelial cells from human umbilical vein (HUVEC, Lonza, Italy). All cells were used between passages 2 and 5.

Fibroblasts were cultured in presence of Dulbecco's modified Eagle medium (Sigma-Aldrich, Italy) and supplemented with 10% fetal calf serum (FCS, Euroclone, Italy) with 200 IU/ml penicillin and with 0.2 mg/ml streptomycin (Sigma-Aldrich, Italy) and kept at 37° C in a 5% CO₂ atmosphere with 95% relative humidity (RH).

Endothelial cells were cultured in endothelial basal medium (EBM2, Lonza, Italy) supplemented with 2% FCS, 0.4% hFGF-B, 0.1% VEGF, 0.1% R3-IGF-1, 0.1% ascorbic acid, 0.1% hEGF, 0.1% heparin and 0.04% hydrocortisone (Lonza, Italy) and with 1% penicillin/streptomycin (Sigma, I), and kept at 37°C in a 5% CO₂ atmosphere with 95% RH.

Scaffolds were cut to have a final area of 0.36 cm² (0.2 cm diameter) to cover the bottom of a 96 well-plate. Both fibroblasts and endothelial cells were seeded onto each scaffold at 10⁵ cells/cm² seeding density and grown for 7 days. Fibroblast growth on tissue culture plastic and endothelial growth on collagen coated tissue culture plastic ^[20] were considered as standard growth (GM).

At prefixed end points, cell growth was assessed by means of MTT test, SEM analysis or CLSM analysis after nuclear and cytoskeleton staining.

4.3.2.6.1 MTT test

50 µl of MTT solution (Sigma Aldrich, Italy) at 2.5 mg/ml concentration in HBSS (Hank's Buffered Salt Solution) pH 7.4 was put in contact with each cell substrate for 3 h.^[22] Subsequently, MTT solution was removed from each well, and the substrates were washed with 200 µl of PBS. After the removal of PBS, 100 µl of DMSO was put in each well, and the absorbance was assayed at 570 nm by means of

an ELISA plate reader (Imark Absorbance Reader, Biorad, Italy), with a reference wavelength of 690 nm. Cell viability was reported as optical density (OD).

4.3.2.6.2 SEM analysis

Cell substrates grown onto scaffolds were fixed using a 3% (w/v) glutaraldehyde solution in PBS (Sigma-Aldrich, Italy) for 2 h at room temperature. The substrates were then washed three times with PBS and dehydrated by means of ethanol solutions at increasing concentrations (50-75-100% v/v). Scaffolds were sputtered with platinum and analyzed as previously described above.

4.3.2.6.3 CLSM analysis

Cells grown on the scaffolds were fixed using a 3% (w/v) glutaraldehyde solution in PBS (Sigma-Aldrich, Italy) for 2 h at room temperature. The substrates were then washed three times with PBS. Cellular cytoskeleton was stained by incubating with 50 μ l (50 μ g/ml) phalloidin-TRITC (Sigma-Aldrich, Italy) for 40 min, in the dark. Then each substrate was washed twice, and cell nuclei were stained with 100 μ l of Hoechst 33258, diluted 1:10000 (Sigma-Aldrich, Italy), for 10 min in the dark. Scaffolds were placed on a microscope slide and imaged using a Confocal Laser Scanning Microscope (CLSM, Leica TCS SP2, Leica Microsystems, Italy) with λ_{ex} =346 nm and λ_{em} =460 nm for Hoechst 33258 and λ_{ex} =540 nm and λ_{em} =570 nm for phalloidin-TRITC. The acquired images were processed with software associated with the microscope (Leica Microsystem, Italy).

4.3.2.7 In vitro adhesion and proliferation assay: cardiac cells

Cardiac cells were obtained from rat heart fetuses. All animal procedures were performed in accordance with the standard international ethical guidelines (European Communities Council Directive 86/609/EEC) approved by Italian Health Ministry (D.L. 116/92). The study protocol was approved by the Local Institutional Ethics Committee of the University of Pavia for the use of animals.

Adult female Sprague Dawley rats (Sprague Dawley SD) 17-18 days gestation were anesthetized with intramuscular injection of Zoletil® 50/50 mg/ml (250 mg tiletamine in powder (as hydrochloride) and 250 mg zolazepam in powder (as hydrochloride) per ml, (Virbac S.r.l., Italy) at 1 ml/kg dose. After cervical dislocation of mother rat, fetuses were euthanized by conscious decapitation and their hearts were collected in ice-cold sterile PBS supplemented with 20 mM glucose and 1 ml/l of penicillin-streptomycin solution (100 IU/ml and 100 µg/ml respectively, Sigma-Aldrich, Italy).

Heart tissues were transferred to a conical tube and 7 ml of collagenase solution (15000 IU/ml, collagenase from *Clostridium histolyticum*, Sigma, Italy) were added and the tissue was digested for 7 min with stirring on the orbital shaker. Hearts were then triturated 5 times with a 5 ml pipette and the larger chunks were allowed to settle to the bottom of the tube before the supernatant was collected. The undigested tissues were subjected to subsequent digestion cycles until complete digestion of the tissue. The supernatants were filtered (70 µm pore size membrane, WVR, Italy) and the resulting cells were centrifuged at 500 rpm for 10 min, resuspended in DMEM containing 10% w/w horse serum (Sigma-Aldrich, Italy), 2% w/w FBS and 1% w/w pen/strep/ampho (Sigma, Italy) and seeded at a density of 10^5 cells/cm² onto each scaffold (0.36 cm² - 0.2 cm diameter) in a 96 well-plate. Scaffolds were employed as such or embedded with 100 µl of platelet lysate. Cells were grown for 3 days. Cardiac cell growth directly on tissue culture plastic with or without PL coatings were considered as control conditions (GM and PL, respectively).

At prefixed end points, cell growth was assessed by means of MTT test, SEM analysis (both as previously described) or CLSM analysis after staining as described below.

4.3.2.7.1 CLSM analysis

Cells grown on scaffolds were fixed using a 3% (w/v) glutaraldehyde solution in PBS (Sigma-Aldrich, Italy) for 2 h at room temperature. The substrates were then washed three times with PBS. Cardiomyocytes were stained by using 50 µl anti- α -actinin (sarcomeric) antibody produced in mouse (30.3 mg/ml diluted at 1:1600, Sigma-

Aldrich, Italy) (contact time 1 h), and after washing with PBS primary antibodies were conjugated with 50 μ l fluorescence secondary antibody CFTM 555 (TRITC, λ_{ex} =555 nm, λ_{em} =565 nm) (2 mg/ml concentration diluted at 1:400, Sigma-Aldrich, Italy) (contact time 1 h).

Cardiac fibroblasts were stained by using 50 μ l anti-actin α -smooth muscle antibody (mouse monoclonal) produced in mouse (2.3 mg/ml diluted at 1:460, Sigma-Aldrich, Italy), and after washing with PBS primary antibodies were conjugated with 50 μ l the secondary antibody CFTM 555 (TRITC, λ_{ex} =555 nm, λ_{em} =565 nm).

Subsequently, all the substrates were assessed for cell proliferation by staining with 50 μ l Ki-67 primary antibody (Sigma, I), and, after washing with PBS, primary antibodies were conjugated with the fluorescence secondary antibody Atto 488 goat anti-rabbit IgG (Atto 488, λ_{abs} =501 nm, λ_{em} =523 nm) (1 mg/ml concentration diluted at 1:200, Sigma-Aldrich, Italy).

All cardiac cell nuclei were stained with Hoechst 33258 as previously described.

As above, scaffolds were placed on a microscope slide and imaged using a CLSM as previously described.

4.3.2.8 Statistical analysis

Statistical differences were evaluated by means of a non-parametric test: Mann Whitney (Wilcoxon) W test, (Statgraphics Centurion XV, Statistical Graphics Corporation, MD, USA). Differences were considered significant at $p < 0.05$.

4.4 RESULTS AND DISCUSSION

4.4.1 Characterization of polymeric solutions

The viscosity of G and G/CS polymeric solutions was characterized at 25, 32 and 40°C by applying a shear rate of 100 s⁻¹ (Figure 1). G had viscosity of 458±11, 342±4 and 323±25 mPa.s (mean values ± sd; n=3) at 25, 32 and 40°C, respectively, while G/CS had viscosity of 200±5, 117±7 and 82±6 mPa.s (mean values ± sd; n=3) at 25, 32 and 40°C, respectively. G and G/CS solutions both presented decreasing viscosity values with increasing temperature, and G solution had higher viscosity values than G/CS solution, at each temperature (one way Anova, multiple range test p<0.05). The decrease of viscosity due to the addition of CS to G is probably due to a charge-charge interaction between G and CS chains and the resulting interaction product should be probably characterized by a less degree of chain entanglement resulting in a decrease of consistency. Gelatin and chondroitin sulfate interaction was previously reported in a paper by Chang ^[23] describing hydroxyapatite gelatin nanocomposite modified with the addition of chondroitin sulfate. G solution demonstrated electrical conductivity of 2585±15.3 μS/cm and surface tension of 40 ± 1.0 mN/m while G/CS had electrical conductivity of 3450±11.8 μS/cm and surface tension of 41 ± 0.1 mN/m. While surface tension was similar for the two solutions, G/CS possessed an electrical conductivity significantly higher than that of G/CS (one way Anova, multiple range test p<0.05) and this is conceivably due to the higher charge density of the polymeric mixture due to the presence of CS that has a maximum charge density of 1, as number of negatively charged functional groups per repeated unit.

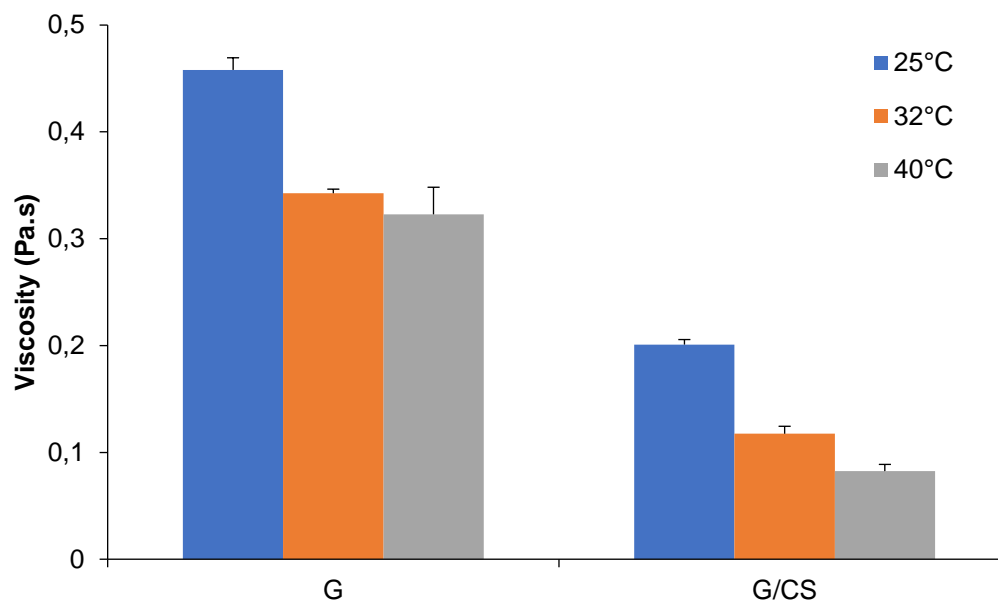


Figure 1: viscosity values (Pa.s) at 100 s⁻¹ of G and G/CS polymeric solutions at 25, 32 and 40°C (mean values±sd; n=3).

4.4.2 Characterization of nanofibrous scaffolds

SEM microphotographs of nanofibrous scaffolds immediately after preparation, after cross-linking and after 6 days in water are shown in Figure 2. G and G/CS nanofibers demonstrated a random orientation with regular structure and smooth surface, without the presence of beads or ribbons. The cross-linking did not change fiber morphology. After 6-days of hydration, the nanofibrous structure was still present although the inter-fiber spaces (porosity) were smaller.

Nanofiber diameters were measured immediately after preparation (not crosslinked, NC), after cross-linking and after 6 days in water (Figure 3). G scaffolds had 151 (± 0.03) nm fibers and the cross-linking caused a slight increase in diameters to 180 (± 0.03) nm without any visible alteration of system morphology. G/CS had smaller fiber diameters of 120 nm (± 0.09) and again the crosslinking did not markedly modify the fiber dimensions (109 ± 0.02) (mean values \pm sd; n=100). G scaffolds and G/CS scaffolds were characterized by fiber dimensions not significantly different: to indicate that the addition of chondroitin sulfate to gelatin did not alter spinning process and fiber formation. On the contrary, 6 days hydration caused a significant increase (one way Anova, multiple range test $p < 0.05$) in nanofiber diameters for both the nanofibrous scaffolds: hydrated G scaffolds had nanofiber diameters of 446 (± 0.10) nm while hydrated G/CS scaffolds had diameters of 306 (± 0.06) nm (mean values \pm sd; n=100). The presence of chondroitin sulfate determined a significantly lower degree of swelling that could be related to the presence of gelatin and chondroitin sulfate interaction. ^[23] The hydration conceivably allowed nanofiber swelling without modification of nanofibrous structure. The correlation between fiber dimensions (diameter) and cell adhesion and proliferation is not completely understood: structural similarity of the fibers to the native ECM and physicochemical characteristics of the polymer forming fibers seem crucial, moreover topographical surface (fibers and pores) seem fundamental on cell migration. ^[24]

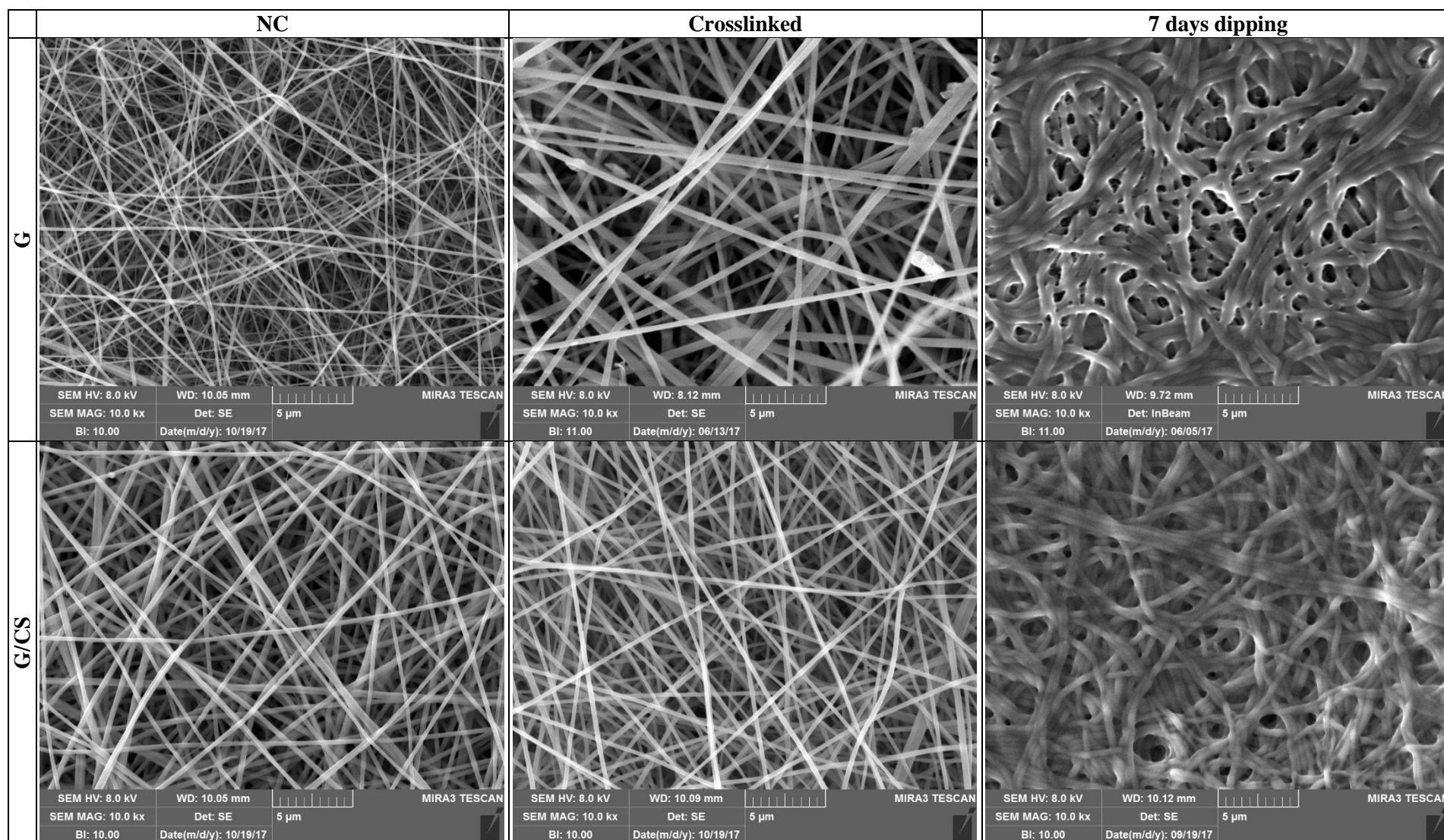


Figure 2: SEM microphotographs of nanofibrous scaffolds immediately after preparation (not crosslinked, NC), after cross-linking and after 6 days dipping in water.

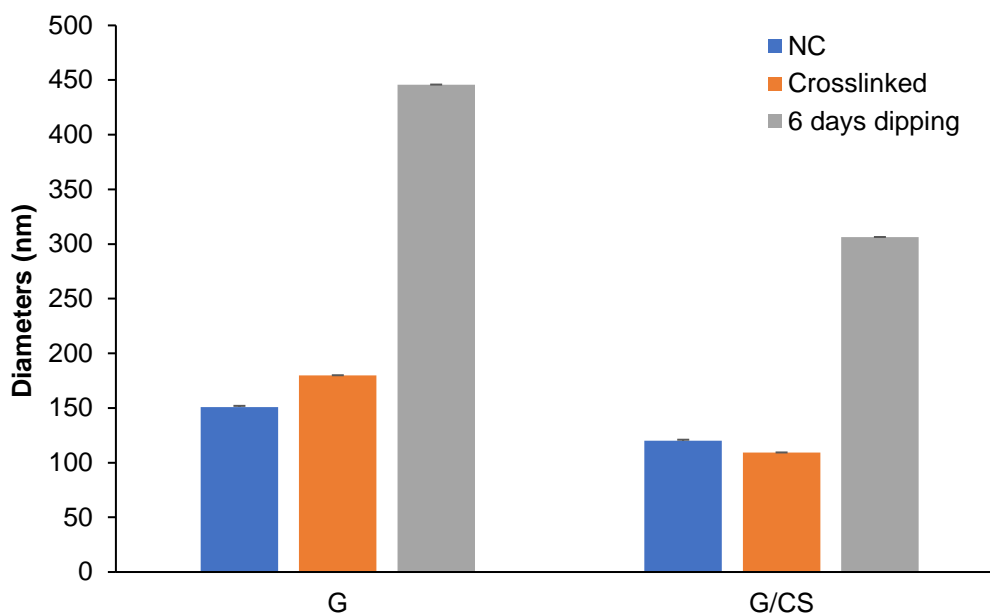


Figure 3: nanofiber diameters measured immediately after preparation (not crosslinked, NC), after cross-linking and after 6 days dipping in water (mean values \pm sd; n=100).

Figure 4 reports FT-IR spectra for G (A) and G/CS (B) scaffolds, comparing the profiles before and after crosslinking. For the G scaffold, the two spectra were superimposed thus indicating the absence of any significant modification due to the crosslinking. For the G/CS scaffold, small variations were found in the region below ca. 1200 cm^{-1} . This region of the FT-IR spectra is of complex origin and considered of limited use for the extraction of structural information.^[25] However, it has been associated with a possible disorder in gelatin molecules and more likely associated with the loss of the triple helix state.

The absence of any variations at higher wavenumbers, in particular in the region defined as amide A about 3400 cm^{-1} and amide B about 3090 cm^{-1} , confirms the absence of any newly formed hydrogen bonds or any variations in the backbone conformation or hydrogen bonding pattern.^[26]

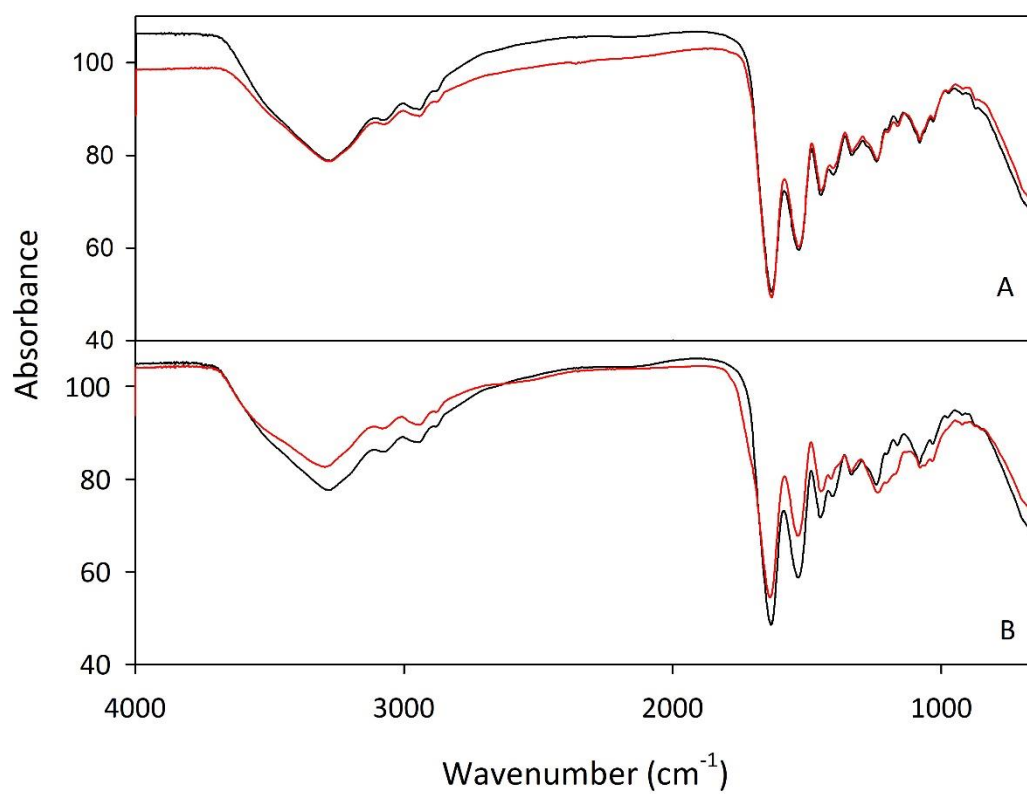


Figure 4: FT-IR spectra for G (A) and G/CS (B) scaffolds before (black line) and after crosslinking.

Figure 5 reports the results of scaffold mechanical properties as tensile strength (N/cm^2) and elongation % measured for dry and hydrated scaffolds.

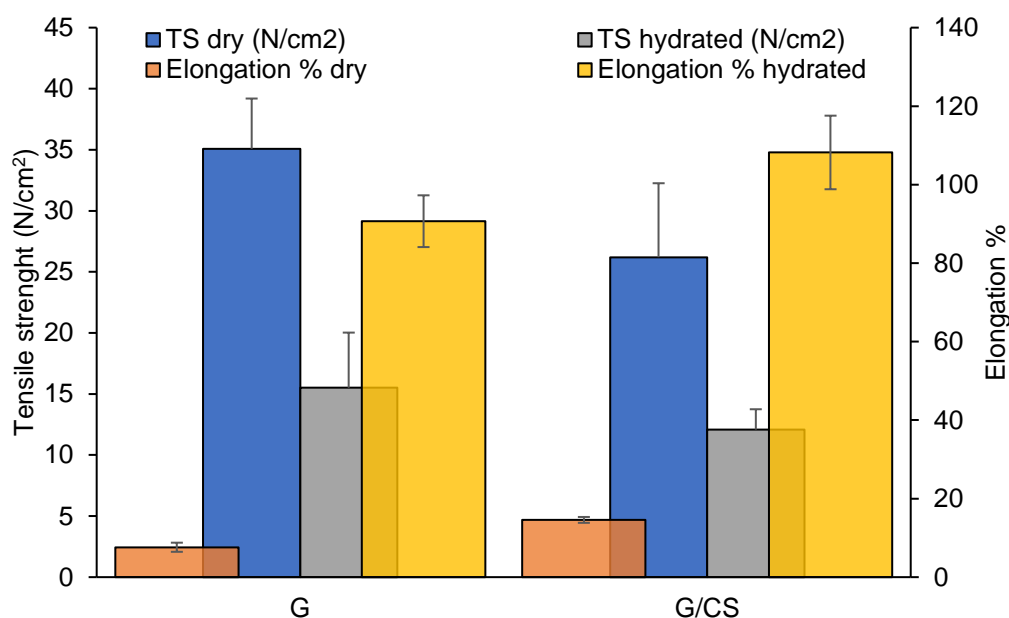


Figure 5: scaffold mechanical properties as tensile strength TS (N/cm^2) and elongation % measured for dry and hydrated scaffolds (mean values \pm sd; n=20).

Overall, tensile strength was higher when the scaffolds were in the dry state while the G scaffold was characterized by a significantly higher force at breaking compared to the G/CS scaffolds. In the hydrated state, G scaffolds maintained a stiffness greater than that of the G/CS scaffolds, although both of the scaffolds presented significantly lower Tensile Strength than in the hydrated state. On the contrary, elongation (directly related to scaffold elasticity) was lower in the hydrated state for both the systems, while G/CS showed a significantly greater elasticity. The presence of CS in the nanofiber structure could change the gelatin tridimensional conformation causing a decrease in chain organization, which could eventually cause a partial loss of stiffness. Since myocardial tissue is characterized by left ventricle stiffness ranging from 0.1 to 0.2 N/cm^2 (10–20 kPa) during diastole and of 2–5 N/cm^2 (200–500 kPa)

during systole ^[27] and additionally, cardiomyocytes preserve their characteristics as in native tissue if the scaffold mimics the stiffness characteristics of native tissue ^[28, 29], G and G/CS scaffolds showed mechanical properties that should be suitable for in vivo adaptation to heart contraction.

4.4.3 In vitro adhesion and proliferation assay: fibroblasts and endothelial cells

Figure 6 reports fibroblast and endothelial cell (HUVEC) viability (optical density, OD) evaluated for cells grown on G and G/CS scaffolds in standard conditions (GM), for 7 days.

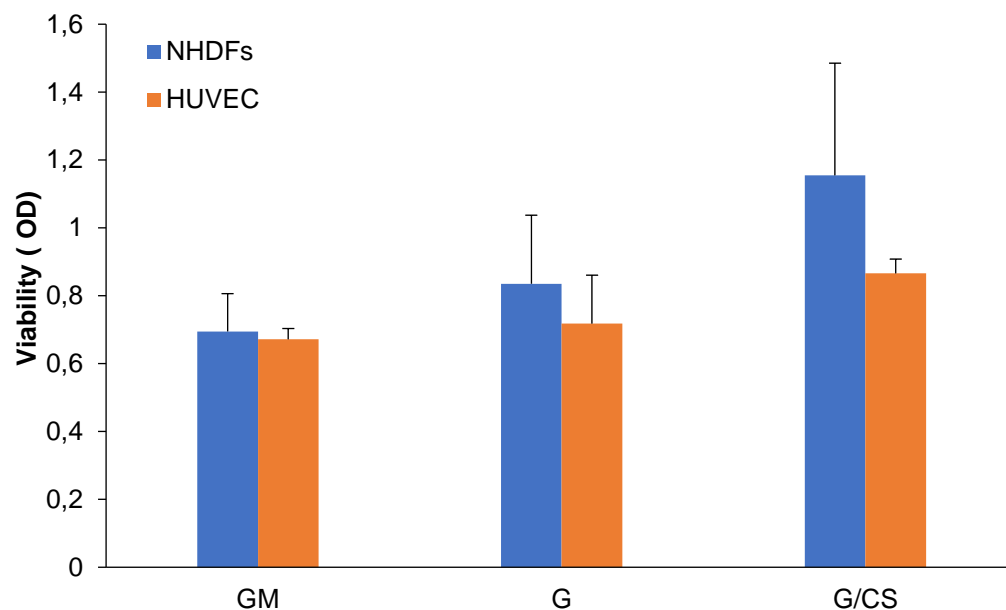


Figure 6: fibroblast and HUVEC viability (optical density, OD) evaluated for cells grown onto G and G/CS scaffolds and in standard conditions (GM), for 7 days; cells grown directly on plastic well bottom was considered as standard growth (GM) (mean values \pm sd; n=8).

G scaffold determined a fibroblast adhesion and growth not significantly different (one way Anova, multiple range test) as compared to standard growth (GM) conditions.

G/CS scaffolds was amenable to fibroblast adhesion and growth to a significantly greater extent as compared to standard growth (GM) conditions, indicating that this scaffold was likely able to enhance cell adhesion and proliferation. Chondroitin sulfate was previously described as an enhancer of cell adhesion and proliferation towards fibroblasts and endothelial cells. ^[19]

Figure 7 reports microphotographs of fibroblasts and HUVECs grown on G and G/CS scaffolds for 7 days. The cell substrates were subjected to CLSM (staining nuclei in blue - Hoechst 33258; cytoskeleton in red, TRICT-phalloidin) and SEM analysis.

CLSM analysis confirmed viability results. Independently of the scaffold type, fibroblasts maintained their fusiform shape, as demonstrated by cytoskeleton labelling (red staining), and normal nuclei (blue staining). Moreover, it is clearly visible that G/CS scaffolds enhanced cell growth and proliferation better than G scaffold and as cells reached confluence.

Endothelial cells (HUVEC) cells also maintained normal nuclei (blue staining) and cytoskeletons (red staining) and they showed their classical polygonal shape. Moreover, G/CS scaffolds again led to cell confluence, likely because of enhanced cell growth and proliferation as compared to the G scaffold.

SEM imaging demonstrated that the cells adhered to the nanofibrous scaffolds and that they appeared fully integrated and in contact with them. G scaffolds allowed fibroblast or endothelial cell growth in isolated clusters localized onto nanofibers or as agglomerated groups adhered to the nanofiber scaffold surface and both cell types demonstrated a relatively smooth surface with some granules. On the contrary, both fibroblasts and endothelial cells formed a uniform sheet on G/CS scaffolds also demonstrating a relatively homogeneous surface with some granules. Moreover, in the case of the G/CS scaffolds, the nanofibers were well integrated in the biological substrate. Endothelial cell proliferation is a crucial mediator of cardiac repair. ^[30]

In fact, heart muscle, and in particular cardiomyocytes, have a high metabolic rate, which is reflected by the high capillary density in the heart. It should come as no surprise that vascularization is one of the greatest challenges in cardiac tissue engineering ^[31], and thus a scaffold that promotes endothelial cell growth and attachment is critical.

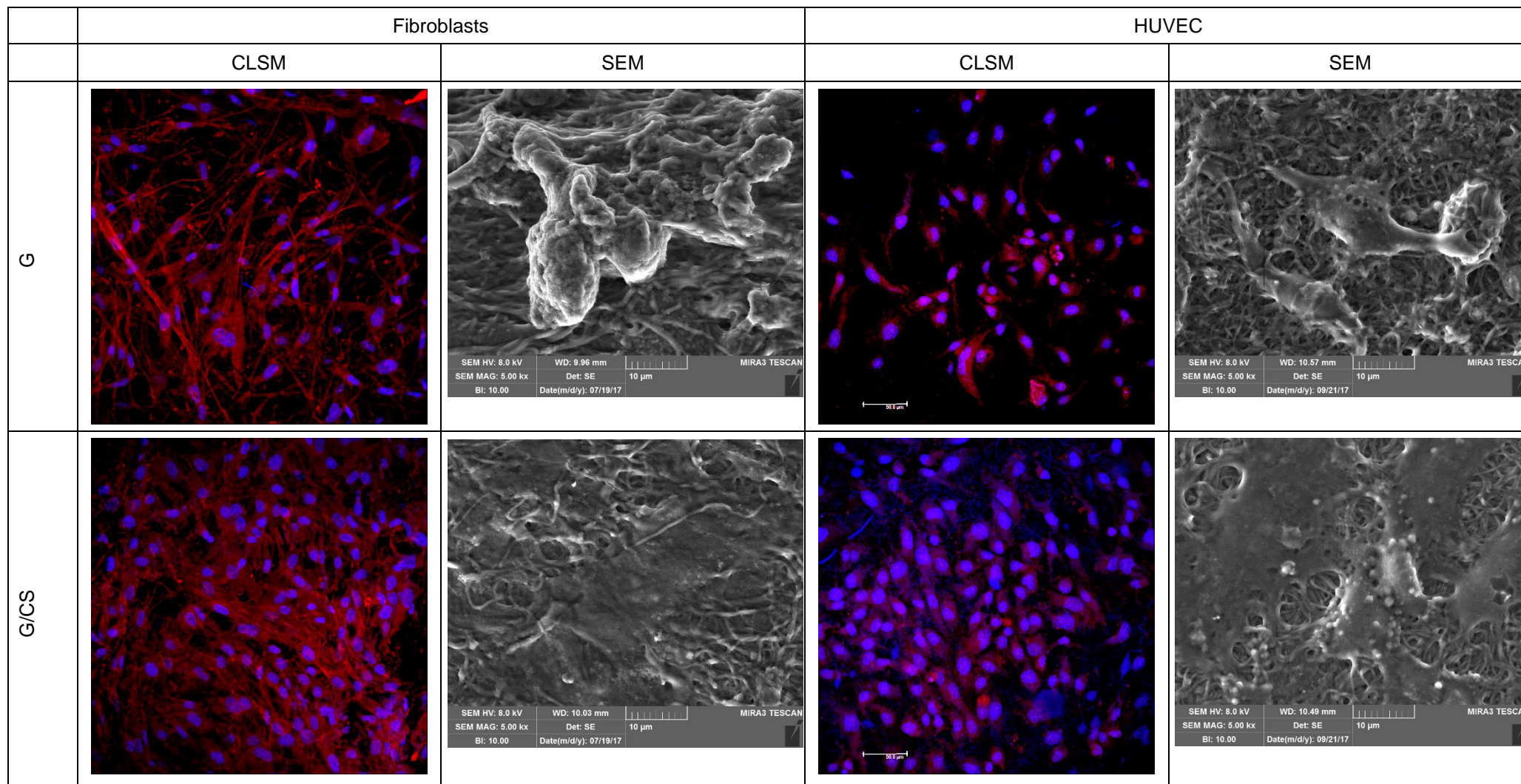


Figure 7: Microphotographs of fibroblasts and HUVEC grown onto G and G/CS scaffolds for 7 days: CLSM (nuclei in blue - Hoechst 33258; cytoskeleton in red, TRICT-phalloidin) and SEM analysis.

4.4.4 In vitro adhesion and proliferation assay: cardiac cells

Figure 8 shows the viability (optical density, OD) of cardiac cells (a mixed population of cardiomyocytes and cardiac fibroblasts isolated from the heart) evaluated for cells grown on the G and G/CS scaffolds and in standard conditions (GM), for 3 days with or without the addition of platelet lysate (PL or w/o PL, respectively). Cardiac cells grown directly on tissue culture plastic with or without PL were considered control conditions (PL and GM, respectively).

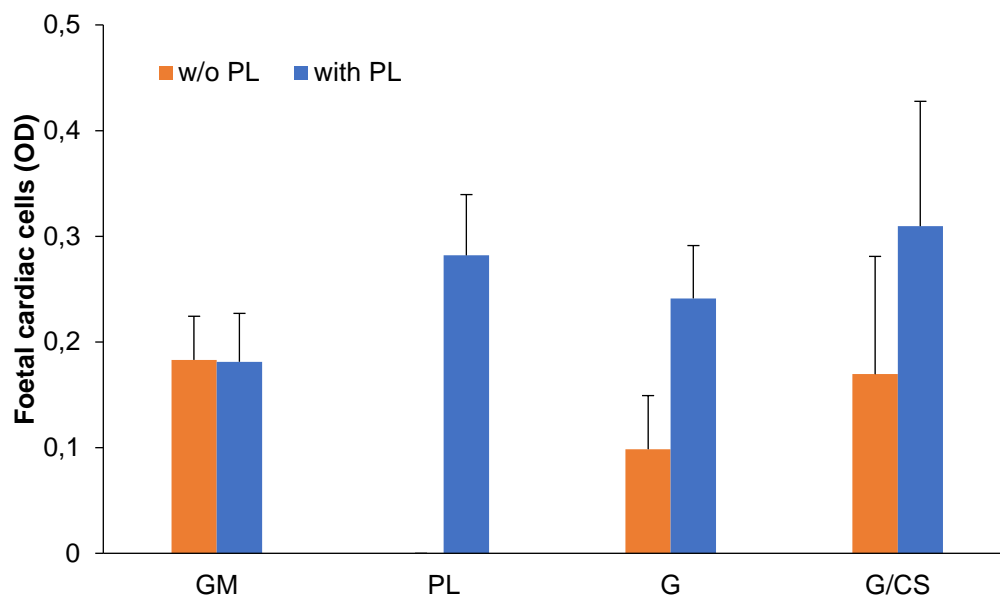
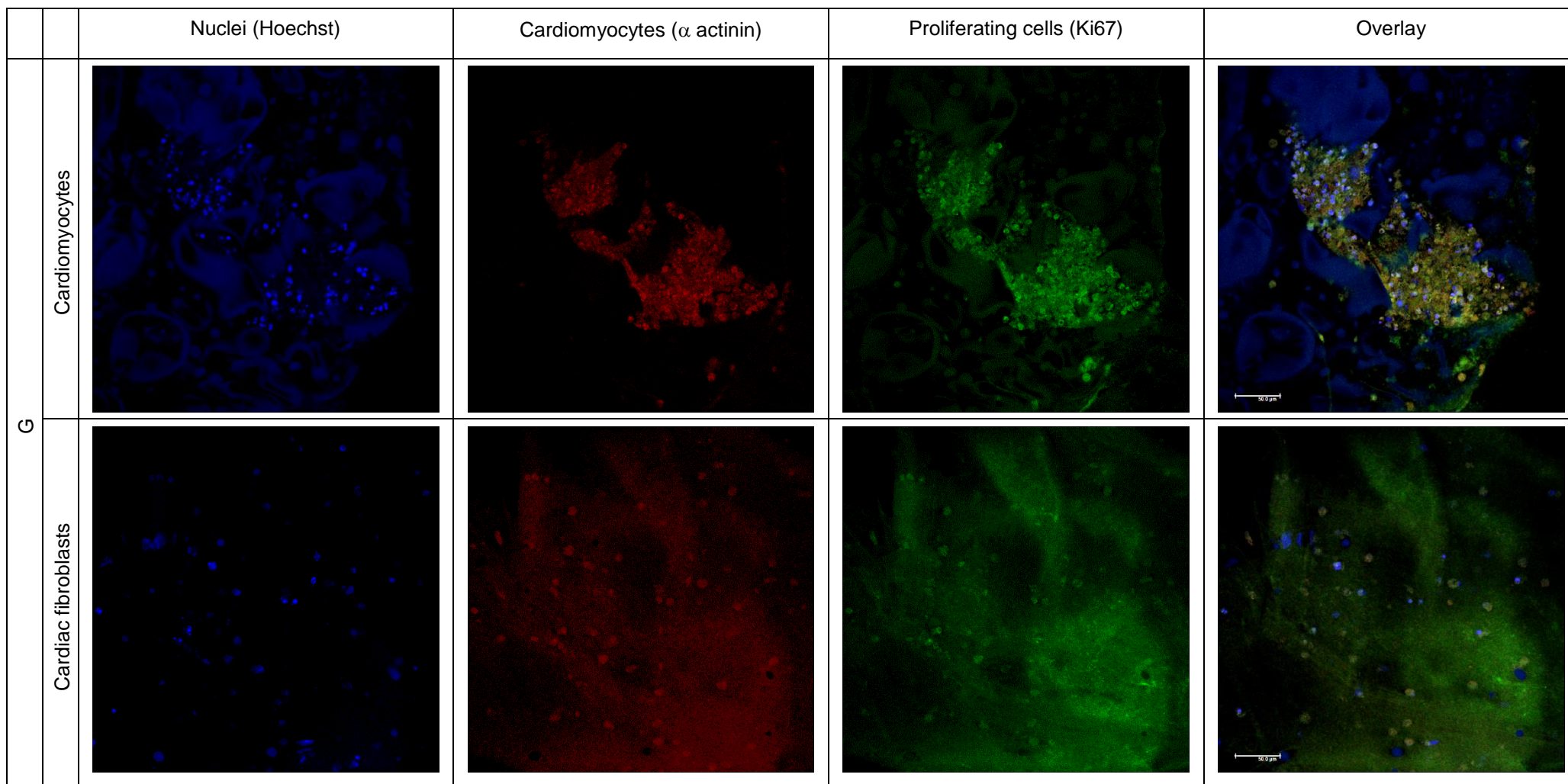


Figure 8: viability (optical density, OD) of cardiac cells (cardiomyocytes and cardiac fibroblasts) evaluated for cells grown onto G and G/CS scaffolds and in standard conditions (GM), for 3 days without or in presence of platelet lysate (w/o PL or with PL, respectively); cardiac cell growths directly on plastic well bottom without or with PL were considered as standard growths (GM and PL, respectively) (mean values \pm sd; n=8).

Cardiac cells adhered and proliferated on G/CS scaffold similar to standard conditions (GM) (one way Anova, multiple range test). On the contrary, PL embedded scaffolds demonstrated increased cell proliferation with respect to standard conditions (GM), significantly higher (one way Anova, multiple range test, $p < 0.05$) for G/CS scaffold, although it was not significantly different from cardiac cell proliferation due to PL alone (one way Anova, multiple range test). The presence of PL significantly (one way Anova, multiple range test, $p < 0.05$) increased cardiac cell adhesion and proliferation and chondroitin sulfate seems to have a synergic activity to promote cardiac cell growth.

Figure 9 shows CLSM micrographs of cardiac cells (cardiomyocytes and cardiac fibroblasts, respectively) grown on G or G/CS scaffolds in the presence of platelet lysate (nuclei in blue - Hoechst 33258; muscle fiber in red – α actinin or smooth muscle actin antibodies; proliferation marker in green – KI67). In the presence of PL, there was a marked proliferation of cardiomyocytes on G/CS scaffolds that led to confluence, while the G scaffold led to a lower degree of cardiomyocyte proliferation. Furthermore, cardiac fibroblasts adhered and proliferated to a lesser extent in comparison with cardiomyocytes in both G and G/CS scaffolds. These results suggest that the G/CS scaffold embedded with PL seems to favor cardiomyocytes proliferation rather than cardiac fibroblast proliferation, which is an important finding for future in vivo applications where cardiomyocyte growth should be promoted and cardiac fibroblast proliferation limited. ^[27]



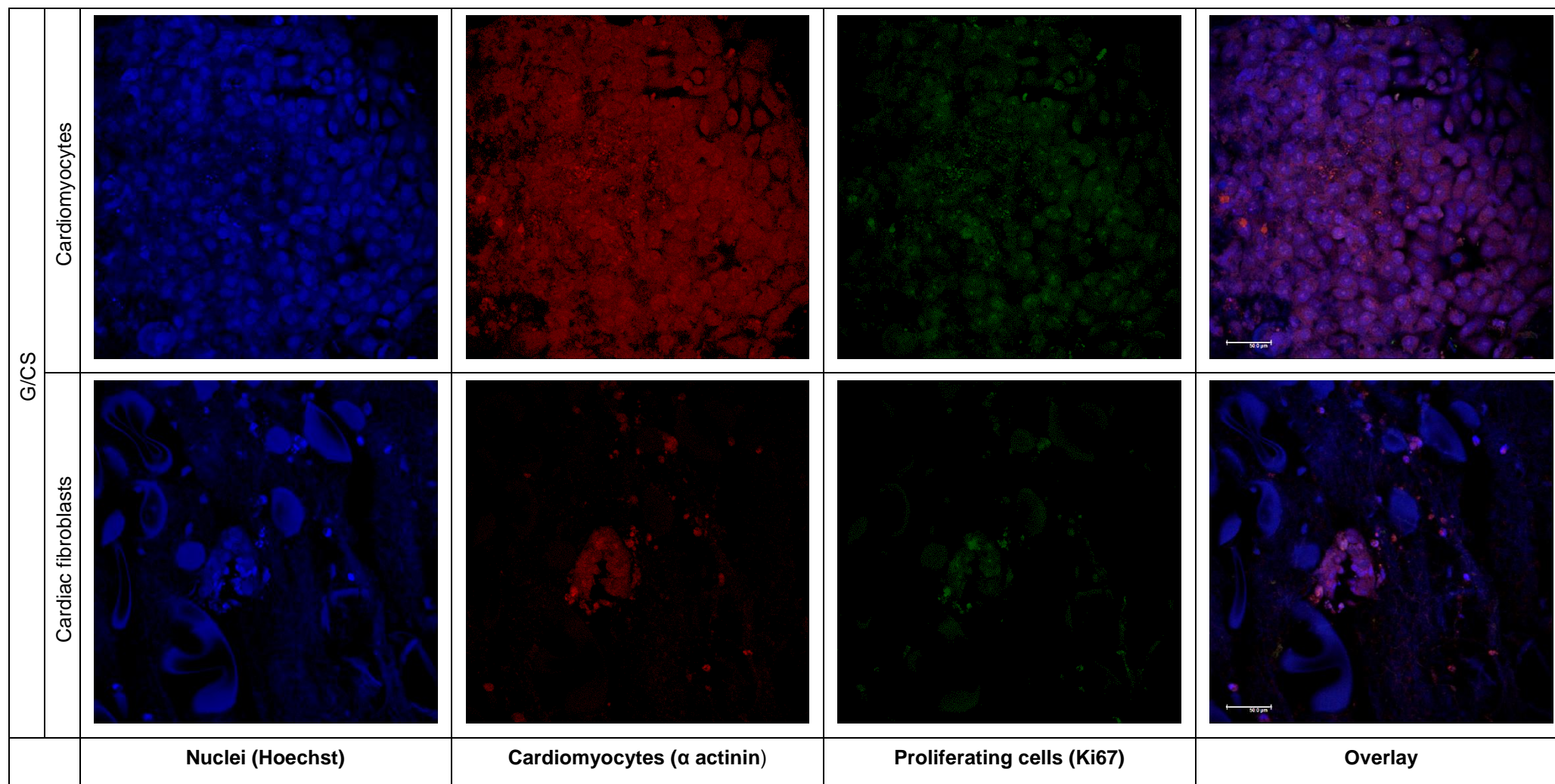


Figure 9: CLSM microphotographs of cardiomyocytes grown onto G or G/CS scaffolds in presence of platelet lysate (nuclei in blue - Hoechst 33258; muscle fiber in red - α actinin antibody; proliferation marker in green – KI67)..

Figure 10 reports SEM microphotographs of G and G/CS scaffolds embedded with platelet lysate after 3 days of culture of cardiac cells. G and G/CS scaffolds allowed the adhesion and the proliferation of cardiac cells (both cardiomyocytes and fibroblasts) to form uniform sheet with homogeneous surface.

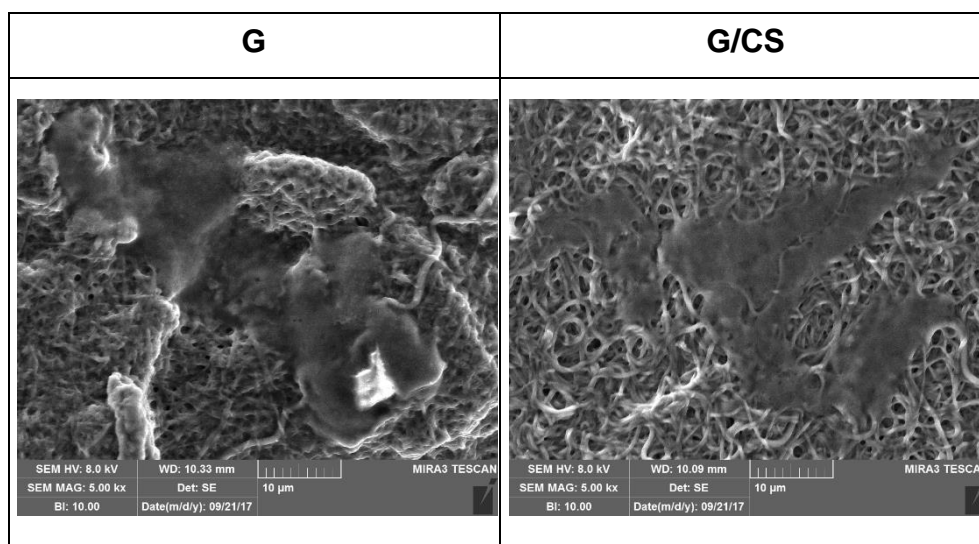


Figure 10: SEM microphotographs of G and G/CS scaffolds embedded with platelet lysate after 3 days of culture of cardiac cells.

4.5 CONCLUSIONS

G and G/CS scaffolds were prepared by means of electrospinning and were cross-linked by heating in the presence of citric acid. Nanofiber structures were not modified by the cross-linking process or by hydrating in water. Scaffolds presented good elongation (elasticity) combined with high stiffness and the presence of CS in the nanofiber structure improved mechanical properties (lower stiffness and higher elasticity), probably due to a change in the gelatin tridimensional conformation and a possible decrease in chain organization, making it more suitable for *in vivo* adaptation to heart contraction. In addition, the presence of CS improved adhesion and proliferation of fibroblasts and endothelial cells and this behavior could be related to elastic properties, which could favor cell motility.

The presence of platelet lysate and CS seems crucial for adhesion and proliferation of cardiac cells and in particular of cardiomyocytes: G/CS scaffold embedded with PL appears to selectively favoring proliferation of cardiomyocytes rather than cardiac fibroblasts.

In conclusion, G/CS scaffold system seems promising for assisting myocardial repair due to a double beneficial effect: primarily it should have a direct effect in enhancing endothelial cell proliferation and enhancing cardiomyocyte proliferation and secondly it should control fibrosis due to a reduction in cardiac fibroblast proliferation.

Acknowledgements

Dr. F Saporito wishes to thank ABOCA Società Agricola S.p.A. for her PhD grant. The authors wish to thank Dr. P. Vaghi (Centro Grandi Strumenti, University of Pavia) for CLSM, Dr. I. Tredici for SEM and FT-IR measurements and the team of housing and animal husbandry services of University of Pavia.

4.6 REFERENCES

- [1] E. Avolio, I. Rodriguez-Arabaolaza, H.L. Spencer, F. Riu, G. Mangialardi, S. C. Slater, J. Rowlinson, V.V. Alvino, O.O. Idowo, S. Soyombo, A. Oikawa, M. M. Swim, C.H. T. Kong, H. Cheng, H. Jia, M. T. Ghorbel, J. C. Hancox, C. H. Orchard, G. Angelini, C. Emanuelli, M. Caputo, P. Madeddu, *J. Am. Haert Assoc.* **2015**, e002043
- [2] C. Williams, E. Budina, W. L. Stoppel, K. E. Sullivan, S. Emani, S. M, Emani, L. D. Black, *Acta Biomater.* **2015**, 14, 84.
- [3] J. D. Drews, H. Miyachi, T. Shinoka, *Trends Cardiovasc Med.*, **2017**, 27, 521
- [4] T. Sugiura, N. Hibino, C. K. Breuer, T. Shinoka, *J Cardiothorac Surg.* **2016**, 11, 163
- [5] S. Pok, I. V. Stupin, C. Tsao, R. G. Pautler, Y. Gao, R. M. Nieto, Z.-W. Tao, C. D. Fraser, A. V. Annapragada, J. G. Jacot, *Adv. Heathcare Mater.*, **2017**, 6, 1600549
- [6] S. F. Nagueh, G. Shah, Y. Wu, G. Torre-Amione, N. M. P King, S. Lahmers, C. C. Witt, K. Becker, S. Labeit, H. L. Granzier, *Circulation.* **2004**, 110, 155.
- [7] C. Williams, K. Sullivan, L. D. Black, *Adv. Healthcare Mater.*, **2015**, 4, 1545
- [8] J. W. Yester, B. Kühn, *Curr Cardiol Rep.*, **2017**, 19: 13.
- [9] A. Elamparithi, A. M. Punnoose, S. F. D. Kuruvilla, S. Kuruvilla, *Int. J. Polym. Mater.* **2017**, 66, 20.
- [10] P. Pushp, F. Castelo Ferreira, J. M. Sampaio Cabral, M. K. Gupta, *Polymer Sci.* **2017**, 59, 515.
- [11] S. Chen, B. Liu, M. A. Carlson, A. F. Gombart, D. A. Reilly, J. Xie, *Nanomedicine.* **2017** 10.2217/nnm-2017-0017.
- [12] J. C. Deddens, A. Hossein Sadeghi, J. Hjortnaes, L. W. Van Laake, M. Buijsrogge, P. A. Doevendans, A. Khademhosseini, J. P. G Sluijter, *Adv. Healthcare Mater.* **2017**, 6, 1.
- [13] S. Gorgieva, V. Kokol, in *"Biomaterials Applications for Nanomedicine"*, Vol. 2 (Eds R. Pignatello) **1996**, pp 17-52.
- [14] A. K. Lynn, L. V. Yannas, W. Bonfield, *J. Biomed. Mater. Res. B Appl. Biomater.* **2004**, 71, 343.

- [15] D. Olsen, C. Yang, M. Bodo, R. Chang, S. Leigh, J. Baez, D. Carmichael, M. Perala, E. R. Hamalainen, M. Jarvinen, J. Polarek, *Adv. Drug Deliv. Rev.* **2003**, 55, 1547.
- [16] F. Cataldo, O. Ursini, E. Lilla, G. Angelini, *J. Radioanal. Nucl. Chem.* **2008**, 275, 125.
- [17] S. Yamada, K. Sugahara, *Curr. Drug Disc. Technol.* **2008**, 5, 289.
- [18] G. Sandri, M. C. Bonferoni, S. Rossi, F. Ferrari, M. Mori, C. Del Fante, C. Perotti, C. Caramella, *Int. J. Pharm.* **2012**, 426, 1.
- [19] G. Sandri, M. C. Bonferoni, S. Rossi, F. Ferrari, M. Mori, M. Cervio, F. Riva, I. Liakos, A. Athanassiou, F. Saporito, L. Marini, C. Caramella, *Expert Opin. Drug Del.* **2015**, 12, 525.
- [20] G. Sandri, M. C. Bonferoni, S. Rossi, A. Delfino, F. Riva, A. Icaro Cornaglia, G. Marrubini, G. Musitelli, C. Del Fante, C. Perotti, C. Caramella, F. Ferrari, *Int. J. Pharm.* **2016**, 509, 188.
- [21] L. Beer, M. Mildner, M. Gyöngyösi, H. J. Ankersmit, *Apoptosis* **2016**, 21, 1336.
- [22] G. Sandri, C. Aguzzi, S. Rossi, M. C. Bonferoni, G. Bruni, C. Boselli, A. I. Cornaglia, F. Riva, C. Viseras, C. Caramella, F. Ferrari, *Acta Biomat.* **2017**, 216.
- [23] M. C. Chang, *J. Korean Ceram. Soc.* **2008**, 45, 573.
- [24] J. Wang, M. Windbergs, *Eur. J. Pharm. Biopharm.* **2017**, 119, 283.
- [25] S. Krimm, J. Bandekar, *Adv. Protein Chem.* **1986**, 38, 181-364.
- [26] S. Mad-Ali, S. Benjakul, T. Prodpran, S. Maqsood, *Asian-Australas J. Anim. Sci.* **2016**, 29, 845.
- [27] Q. Z. Chen, A. Bismarck, U. Hansen, S. Junaid, M. Q. Tran, S. E. Harding, N. N. Ali, A. R. Boccaccini, *Biomaterials.* **2008**, 29, 47.
- [28] A. J. Engler, C. Carag-Krieger, C. P. Johnson, M. Raab, H. Y. Tang, D. W. Speicher, J. W. Sanger, J. M. Sanger, D. E. Discher, *J. Cell Sci.* **2008**, 121, 3794.
- [29] K. L. K. Coulombe, N. J. Kaiser, *Biomed. Mater.* **2015**, 10, 034003.
- [30] H. Parsa, K. Ronaldson, G. Vunjak-Novakovic, *Adv. Drug Deliv. Rev.* **2016**, 96, 195.
- [31] M. Montgomery, B. Zhang, M. Radisic, *J. Cardiovasc. Pharmacol. Ther.* **2014**,

19, 382.

This work was objected of 2 conference presentations:

1) Saporito, F., Sandri, G., Bonferoni, M.C., Rossi, S., Athanassiou, A., Perotto, G., Caramella, C., Ferrari, F.

Electrospun gelatin/chondroitin sulfate nanofibrous membranes for the treatment of myocardial infarction

Congresso Nazionale Biomateriali SIB 2017, Milano, 24-26 Maggio 2017 (ORAL PRESENTATION).

2) Saporito, F., Sandri, G., Rossi, S., Bonferoni, M.C., Del Fante, C., Perotti, C., Black, L., Ferrari, F.

Innovative therapeutic platforms for tissue repair

Advanced School in Nanomedicine, 17th edition of the Summer School for Italian PhD students in Pharmaceutical Technology, Sardegna Ricerche Scientific Park, Pula (Cagliari), 25-28 Settembre 2017 (ORAL PRESENTATION)

Conclusions

Currently tissue repairing represents one of the most important challenge and several innovative therapeutic approaches have been developed to restore physiologic functions of damage tissues and to lead orchestrated process of wound healing.

Nowadays, the attention focuses on the development of bioactive systems based on biopolymers able to interact with the injured tissue and to actively take part to the healing process: such systems have been studied to deliver active ingredients, such as natural compounds, characterized by proliferation enhancement, antimicrobial properties, hemostatic properties.

Aim of PhD project was the development of bioactive systems based on natural compounds (as matrix forming components or as functional ingredients) to achieve tissue reparation.

In particular, two different targets were considered: 1) skin: acute wounds with massive bleeding and non-healing cutaneous lesions as chronic wounds and severe burns, 2) heart: myocardial infarction.

Chapter 1 of the thesis focuses on the development of hemostatic dressings loaded tranexamic acid (TA) to be used in case of massive bleedings. The biopolymers employed were chitosan in association with glycosaminoglycans, GAGs, (Hyaluronic acid, HA, Chondroitin sulfate, CS), leading to a polyelectrolyte complex formation able to induce a better fluid absorption from the wound and higher dressing bioadhesion properties. The fast release of TA makes the dressings able to be used during massive bleeding occurring during surgery, allowing procoagulant function as quickly as possible.

Since multi-resistant bacteria represent a serious problem worldwide, a therapeutic option consists in the use of essential oils. These compounds possess an antimicrobial effect against multi-resistant bacteria but they are also extremely volatile. Due to this problem, solid lipid nanoparticles (SLN) and nanostructured lipid carriers (NLC) based on cocoa butter, as solid lipid, and olive oil or sesame oil, as liquid lipids were developed for the encapsulation of eucalyptus and rosemary essential oils (Chapter 2). NLC based on olive oil and eucalyptus essential oil allowed a high fibroblast proliferation in an *in vitro* wound healing model, confirmed also by *in vivo* application on a murine burn model. Furthermore, the encapsulation protected the

essential oils allowing the antimicrobial properties against gram-positive bacterial strain.

Chapter 3 and 4 of the thesis focus on the development of therapeutic strategies for the treatment of myocardial infarction. Two different systems were studied: in situ gelling systems and electrospun nanofibrous scaffolds. In situ gelling systems were prepared by using two different polymers: poloxamer 407, a thermosensitive material, and sodium alginate, an ion-dependent polymer. Scaffolds were obtained by electrospinning of gelatin solutions. Both systems were associated to chondroitin sulfate, a glycosaminoglycan negatively charged able to interact with positively charged molecules such as growth factors. The therapeutic use of platelet lysate (PL) as hemoderivative rich in growth factors was investigated. PL allowed to improve cardiomyocytes viability isolated from rat fetuses.

Acknowledgements

I would like to thank particularly Aboca Società Agricola S.p.A for giving me the opportunity to attend the PhD school in Chemical and Pharmaceutical Science at University of Pavia. Thanks to Aboca grant, I had the possibility to acquire a considerable experience in pharmaceutical technology research.

I'm very thankful to Cavaliere Valentino Mercati for being the major example of knowledge and excitement concerning the plants culture.

Thanks to Dr. Anna Maidecchi and Dr. Luca Rampoldi for their wide expertise and experience shown during the collaboration in the different projects.

I consider myself very lucky to have had the opportunity to “be part” of a such important company grown over the years and in the same time preserving the authenticity and family values of the past.